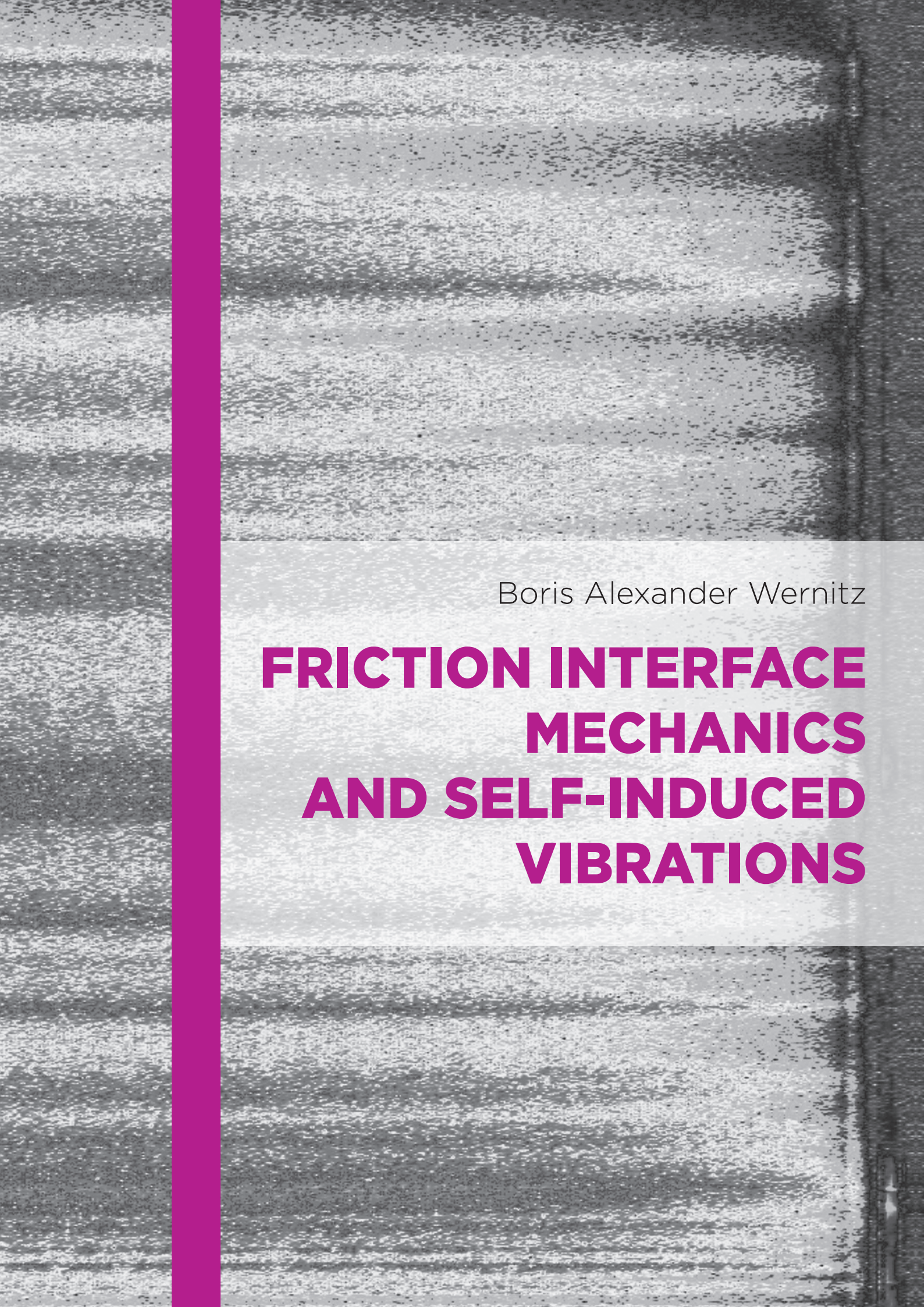

Boris Alexander Wernitz

FRICTION INTERFACE MECHANICS AND SELF-INDUCED VIBRATIONS

Boris Alexander Wernitz

Friction Interface Mechanics and Self-Induced Vibrations

Friction Interface Mechanics and Self-Induced Vibrations

Vom Promotionsausschuß der
Technischen Universität Hamburg-Harburg
zur Erlangung des akademischen Grades
Doktor Ingenieur
genehmigte Dissertation

von
Boris Alexander Wernitz

aus
Hamburg

2013

Gutachter: Prof. Norbert Hoffmann
Zweitgutachter: Prof. Michael Hanss
Tag der mündlichen Prüfung: 22. Nov. 2013

TUBdok der Universitätsbibliothek der TU Hamburg-Harburg
urn:nbn:de:gbv:830-tubdok-12462

Abstract

Vibrations in braking systems have been studied since the beginning of the last century and despite several insights, still many phenomena, particularly in the area of friction induced vibrations, are not fully understood. The objective of the actual study was the identification of the complex dynamics in the friction interface of a dry friction brake system. In this context, particular consideration was given to the generation of instabilities and brake squeal.

In work presently being undertaken, irregular vibration data of a dry friction brake in non-squealing condition were collected with sampling rates above 200 kHz. The resulting time series were subjected to linear, nonlinear and statistical analyses and in particular with regard to the involved multi-scale dynamics. At first, topological examination of the friction surfaces disclosed the microscale characteristics; visual inspections of the coating, generated on the brake disk insights in to the friction interface transformations. Secondly, linear investigations of the vibration data in the frequency domain provided first impressions of the friction interface: while the spectral frequency distribution remains mostly independent from mechanic parameters, it is essentially controlled by the pad formulation and physical and chemical interface transformations during the experiment. Thirdly, the data were explored on the basis of recurrence analysis and together with the estimation of dimensionality the phase space was reconstructed. Evidently, the irregular vibration states of friction brakes in non-squealing condition are strongly controlled both by apparently steady and disruptive phenomena (intermittency). The duration between the states was typically in the range of milliseconds. Phase space reconstruction and largest Lyapunov coefficient estimation indicated thereby that these phenomena are dominated more by low-dimensional chaotic deterministic dynamics than by high-dimensional stochastic processes. In the following, characteristic measures of the recurrence quantification analysis have been extracted which disclosed an interrelation with the noise propensity of the overall brake system.

Finally, statistical studies of the distribution of vibration increments on the basis of probability density functions concluded the evaluation of the experiments. The distribution analyses disclosed the non-Gaussian characteristic of the vibration signals under steady sliding whereby the deviation from the normal distribution depends on the corresponding scale. Furthermore, the vibration during sliding in non-squealing condition is effectively generated by dynamics on different scales. And beyond that, the difference between the measured and the Gaussian distribution suggests a correlation between the squeal propensity and the deviation under consideration.

Keywords: *Friction Contact, Friction Brake, Friction-Induced Vibrations, Chaotic Dynamics, Non-linear Time-Series Analysis, Brake Noise, Probability Density Distribution, Intermittency*

Kurzfassung

Vibrationen in Bremssystemen sind seit Anfang des letzten Jahrhunderts untersucht worden und obwohl zahlreiche Erkenntnisse über die mechanischen Zusammenhänge gewonnen wurden, sind die auftretenden Phänomene, insbesondere im Bereich der reibungsinduzierten Schwingungen, nicht vollständig erklärbar.
In der vorliegenden Forschungsarbeit wurde die komplexe Mechanik der Reibschicht einer trockenen Reibungsbremse untersucht. In besonderem Fokus stand hierbei das Entstehen von Instabilitäten bzw. Bremsenquietschen. Hierfür wurden Vibrationsmessungen an einem Bremssystem in stabil-gleitendem Zustand durchgeführt. Um die mechanischen Vorgänge in der Reibschicht im Mikrometerbereich zu identifizieren, wurden die Daten mit Erfassungsraten oberhalb von 200 kHz aufgezeichnet. Die gewonnen Zeitreihen wurden nachfolgend mit linearen, nichtlinearen und statistischen Methoden analysiert - mit besonderem Hinblick auf die beteiligten Multiskalen. Zunächst wurden die Topologie der beteiligten Reibungsoberflächen und die Filmauftragung auf der Bremsscheibenoberfläche analysiert. Dadurch ließen sich die beteiligten Skalen und Transformationen der Reibungsschicht für nachfolgende Analysen bestimmen. Spektralanalysen der Vibrationen ließen erkennen, daß die sich ausbildenden spektralen Muster weniger von den Bremsparametern als vielmehr vom Bremsbelagmaterial und der physikalischen und chemischen Transformation der Reibschicht während des Experiments abhängen.
Die nichtlinearen Phänomene wurden anhand von Rekurrenzanalysen betrachtet, wobei sich zeigte, daß die Grenzschichtmechanik in nicht-quietschendem Zustand überwiegend von gleichmäßigem Gleiten und abrupten Störungen beherrscht wird (Intermittenz). Die Dauer der Phasen zwischen den Irregularitäten lag hierbei typischerweise im Millisekundenbereich. Diese Phänomene ließen sich anhand einer Phasenraumrekonstruktion und einer Abschätzung des größten Lyapunov-Koeffizienten einordnen: die auftretenden Phänomene werden hauptsächlich von niedrigdimensionaler, chaotisch-deterministischer Dynamik, hingegen nur in unerheblichem Maß von hochdimensionalen, stochastischen Prozessen dominiert.
Darüberhinaus wurden im Folgenden charakteristische Maßzahlen anhand einer Rekurrenzquantifizierungsanalyse bestimmt und es wurde untersucht, inwieweit ein Zusammenhang dieser mit der Geräuschneigung des Gesamtsystems besteht. Hierbei wurde gezeigt, daß entsprechende Maßzahlen der Rekurrenzquantifizierungsanalyse dazu geeignet sind, die Wahrscheinlichkeit des Bremssystems, Bremsenquietschen zu generieren, zu beschreiben.
Nicht zuletzt um eine umfassendere, aus den Experimenten gewonnene Datenbasis zugrunde legen zu können, wurden zusätzlich stochastische Methoden angewendet:

eine Inkrementanalyse zeigte hierbei, daß die Beschleunigungsinkremente der Vibrationszeitreihen während des stabilen Gleitens nicht normalverteilt sind und daß die Abweichung zwischen der Verteilung der experimentellen Daten und einer Normalverteilung von den zugehörigen Skalen abhängt. Die Schwingungen im nichtquietschenden Zustand entstehen hiernach durch Dynamiken auf weit gefächerten Skalen. Eine eingeführte Maßzahl, die die Abweichung zur Normalverteilung charakterisiert, ermöglichte die Beschreibung der Wahrscheinlichkeit des Systems, instabil zu werden, bzw. die Neigung des Systems, Bremsenquietschen zu emittieren.

Schlagwörter: *Reibkontakt, Reibungsbremse, Reibungsinduzierte Schwingungen, Chaotische Dynamik, Nichtlineare Zeitreihenanalyse, Bremsgeräusche, Wahrscheinlichkeitsdichteverteilung, Intermittenz*

Contents

List of Figures

Chapter 1

Introduction

1.1 Motivation

Brakes are one of the most important parts in vehicles regarding safety and performance. From the time of their first industrial application in the nineteenth century, automotive vehicle brakes underwent several stages of design and development from simple block brakes to modern day high performance brakes. In the past century the major focus had been on braking power and reliability. However the development in recent decades has been driven more and more by comfort and economic aspects, based on a significant increase of customer awareness referring to noise and comfort aspects in general. The presence of noise often leads to warranty claims from customers, regardless of whether it is simply unwanted or unexpected, because unattended noise often creates the assumption of a defective brake although the brake is functional in all other aspects. Additionally, due to the dramatic change of the overall vehicle acoustics, noise and vibrations have increasingly gained in importance. Even before the turn of the millennium, the overall direct and indirect spend of the friction material industry had already exceeded 50 percent of the engineering budgets [1].

Brakes that squeal generally do not squeal with every brake application but rather the occurrence of noise is commonly occasional and often appears to be random. Evidently, a lot of different factors influence the vibrational behavior of a brake system. Parameters that control the dynamics are located on different scales, both

micro- and macroscopic length dimensions [1] are relevant, whereby especially the dynamics on the microscopic level are still not well understood. Obviously, friction in itself is a multiscale and multi-physics process by its very nature. Thereby, the reasons are manifold: based on the complex friction process, forces are transmitted, mechanical energy is transformed, surface topography is changed, interface material and wear may be removed or partially fed in again and even physical and/or chemical properties may change. The operational conditions, the properties of the surfaces and the interfaces, their interaction, the environmental conditions and transformations over time lead, in sum, to an unpredictable mechanical system with an erratic friction behavior. Thus, the consequential integral friction coefficient is not an intrinsic property of participating materials alone. Measurements and the identification of the above described properties are complicated, because the contact area is mostly inaccessible, or more precisely, it means that obtaining the characteristics of the friction interface is impossible without significantly manipulating them at the same time.

Even though disk brake vibration and generated brake squeal have been investigated since the beginning of the twentieth century, it still remains a challenging problem. Up to now, no valid universal theories or friction models that cover all or at least most of the general phenomena of friction induced vibrations are available. Consequently, there exists no simple or general concept of how to suppress or at least reduce brake squeal.

Evidently, general findings in the area of sliding friction which allow to combine the phenomena or, at a minimum, give a better understanding of the structural mechanics is still envisaged to be a long way ahead. Approaches which would supply insights both on different scales and comprising physical and chemical aspects, would significantly advance research and the brake industry.

1.2 State of the Art

Friction induced vibrations may appear whenever two objects are placed in contact and are allowed to slide. Frictional contact and motion becomes important in diverse

[1] In literature are found more denominations and differentiations, e.g. a *mesoscale* [65]. The classifications is not always consistent. However, the *microscale* is commonly referred to small particles of *micrometer* or even *nanometer* size in the friction interface, the *mesoscale* to compacted wear in *millimeter* size and the *macroscale* to the brake components or the complete brake system in dimensions of *centimeters* or even *meters*.

systems and the involved phenomena span vast ranges of scales from the nanometer contacts up to the geophysical scale observed in earth science. Thus, a plethora of examples are found: in the field of large scale object characteristics such as earthquake excitation generated by friction in plate tectonics, narrow-banded noises when railway vehicles run through tight curves, friction in bearings, clutches, fuel pumps, drive trains, brakes and servo-assisted steering mechanism in the automotive domain, human and artificial replacement joints, down to friction in microscales in molecular physics and friction on the atomic scale, to name but a few.

Following their major impact, of both practical and technological importance, the questions around friction have motivated progress over the centuries. Beginning with historical figures by Leonardo da Vinci which brought friction into the domain of physics, followed by the development of friction formulations known as Coulomb-Amontons' laws which have led towards a more microscopic understanding of these laws by Bowden and Tabor [9] in the middle of the 20th century: the subject of brake dynamics has generated a remarkable amount of appropriate literature and a high number of new papers are still distributed every year. Consequently, appropriate reviews and summaries of so far released papers have been frequently published, e.g. [72] in 1997, [56] in 2002, [34] in 2003, [55] in 2005, to mention but a few.

The development of friction brakes with respect to acceptable noise and vibration levels is of particular importance in vehicle design. Accordingly, the topic has been studied intensely over the years and considerable understanding and knowledge has been accumulated and documented. At present, the state of the art in this field could be summarized by saying that *in general* the *large-scale* structural dynamics of the phenomena under consideration, i.e *brake squeal*, *creep-groan* [2] , *judder* [3] , etc., seem to be understood in some degree on both a qualitative as well as a quantitative basis [34, 10, 25]. In the area of self-excited brake squeal, a large number of theories have been formulated to explain the underlying mechanisms. Numerous attempts

---

[2] Creep groan noise in vehicles brakes is a low frequency vibration problem mainly in the range of 20 Hz to 500 Hz. It appears usually at extreme low speed, in particular when releasing the brake on downhill stretches or in automatic transmission cars where there is both a transition from static to dynamic condition. The noise causing vibration is a result of the friction force gradient between sticking and sliding, generally known as *stick-slip* phenomena.

[3] Severe vibrations of the brake system or often even the whole vehicle chassis and the steering wheel are usually related to brake judder. Judder may be roughly divided into two groups: *hot* or *thermal* and *cold judder*. Hot judder vibrations are the result of uneven thermal distributions on the disk, so called *hot spots*, which lead to temporary deformations of the disk. Cold judder, on the other hand, is a consequence of permanent deformations. It is normally related to uneven disk wear patterns or *disk thickness variation (DTV)*, attributed to roughness or waviness of the disk or a possible run-out.

have been undertaken to apply the presumptions to the dynamics of disk brakes and many experiments have been completed to test them in detail, with varied apparent success.

These studies and their corresponding results have in common that the scale at which the mechanics are described, compared with the dimensions of the friction contact, is relatively large. In comparison to the variety of these large-scale investigations, the situation of research activities referring to smaller scales is different: studies with respect to interface properties and dynamics which are related to small-scales [4] seem to be just at the very beginning in friction brakes.

Nevertheless, even computer-based large-scale modeling and simulation of brake vibration and noise is not yet considered to have reached predictive power in the sense that the results would correspond reasonably to experimental testing. The reasons for this lack of predictive capability seem to be manifold; at least three important factors are: firstly, variability and uncertainty aspects concerning geometry, material and manufacturing processes play an important role. Accordingly much work in that direction is in progress [12]. Secondly, physical and chemical processes and transformations of the friction partners, e.g. due to the impacting load and environmental conditions, lead to mostly unknown material characteristics. Obviously, in-situ measurements in the friction interface and the surfaces are almost impossible and even a material characterization in laboratory conditions, even when neglecting the characteristics of *real* and *effective* contact zone, lacks the availability of appropriate measurement instruments. Hence, even the moduli of elasticity and the damping characteristics of pad materials and participating contacts in *actual operation conditions* are not available for modeling. Thirdly, and as mentioned above, an enormous lack of knowledge with respect to the small-scale properties and the small-scale dynamics of the friction contact interface is to be observed. Although it is strongly supposed as being highly relevant for the resulting large-scale friction affected or friction induced dynamics [59, 7]. There are only few experimentally validated measurements regarding the normal contact and its stiffness, while knowledge with respect to normal contact damping, or even tangential or more generalized contact properties do not seem to be available at all [3, 61, 32, 29].

Several models for examining squealing disk brakes have been postulated, however,

[4] It has been shown that the friction interface structures are reaching down below the *nanometer*-range. Hereby, the brake performance properties are supposed to be determined by the nano-structures of the interface which are formed by the wear process [49].

none of these have been prepared to attempt to include the dynamics and mechanics for all scales mentioned above. The evolved models consequently have captured some features of vibration excitation and at the same time have ignored many others. On the other hand, experimental studies have been deficient more in general, caused by the following restrictions below. Exemplarily, three experiment preparations on different configuration levels are given:

- *Pin-on-disk setups*
  So called *pin-on-disk-testers* are particular tribometers operating as instruments that measure tribological quantities, such as coefficient of friction, friction force and friction wear. Furthermore, they are also applied to examine vibrations and self-induced oscillations [64]. These setups are in general very specific, i. e. basic friction phenomena may be considered with a minimum of impact from unwanted parameters. In contrast, the dynamics are quite far away from applications and various phenomena on different scales are neglected.

- *'Minimal' or restricted experimental setups*
  Experimental setups with comparatively simple mechanical systems with less degrees of freedom but comprising brake lining material close to commercial applications. Omitting further mechanical parts helps to concentrate on the friction singularities and to understand and focus on the underlying mechanics. This more universal experimental approach is rather more capable of investigating the phenomena in consideration than the brake system setups, but in contrast, tends to have only limited applicability with its results to the application and tends to oversimplify the complex mechanics.

- *Brake application setups*
  Experimental setups with a mechanical structure which is close or equals a commercially available brake system, typically with brake and axle components of the application. Being close to the application with the advantage that findings are directly implementable, but often results in the dilemma that general conclusions dealing with friction phenomena itself are hard to derive and their results only pertain to one setup configuration.

1.3 Objectives

Regarding the progress that has been accomplished so far and based on the knowledge gaps of the current state of research regarding friction brake dynamics and friction induced vibrations (1.2), it consequently appears to be desirable to take further steps towards more insight and a better understanding of the unsolved areas of friction phenomena.

The current work is being aimed at new approaches for a better comprehension of interface dynamics occurring on small length and short time scales, including their relevance to the overall large scale mechanics. Though sub-scale effects on friction induced vibration have been dealt with in the past, e.g. [4, 6, 2, 27, 28, 22], most of the previous work has been theoretical or mainly based on computer modeling with many restrictions mentioned in the previous section. Other studies in the field of material science have focused on small scale friction mechanics without considering the overall induced large scales [65].

Even if all chemical and physical processes taking place in the friction interface and all other contacts with friction would be known and mathematically describable, its evaluation seems rather impossible: an appropriate model ought to be arbitrary fine discretized to incorporate details on smallest scales, and on the other side large enough to cover large scale dynamics of the overall system. Additionally, due to the high dimensional dynamics it would reach enormous sizes. Thus in sum, it would obviously not be computable in the near future.

In contrast to existing theoretical approaches, the objective of the present work was to describe characteristics of the experimental vibration data during non-squealing steady sliding condition. Subsequently, conclusions drawn from the observations were expected to allow estimations of the underlying dynamics. Additionally, the seemingly randomly occurring instabilities [5] were supposed to be integrated into the investigated mechanics. In summary, the present work has aimed for detailed insights into dynamical interface processes taking place on small length and short time scales, including the role they play in the overall dynamics, with respect to induced large-scale vibrations.

[5] Instabilities of brake systems are often equated with brake squeal, effectively unstable states may lead to limit cycle trajectories of the brake system with high amplitudes, which then generates squeal emission. However, Oberst and Lai [46, 47] have suggested that brake squeal may also appear in the form of chaotic dynamics; this is discussed in more detail in chapter 5.

Evidently, general findings in the area of sliding friction which combine to provide a better understanding of the structural mechanics on different scales comprising physical and chemical aspects, will significantly advance research and brake technology. The intention of this work has been to contribute to covering a distance on this path.

Chapter 2

Methodology

In the past, brake systems have usually been investigated with respect to linear stability of the steady sliding state. Although recent research in this field has been able to bring in considerable progress, the limitation of most approaches has been based both on the restricted representation of high dimensional phenomena of the friction interface [1] (see Figure 2.1) and the multi-scale characteristics which have consequently led to incomplete description of the dynamics. Additionally, the mechanics and chemical transformations of the friction interface are mostly unknown and have therefore not been considered in most approaches. On the contrary, research, development and application in the automotive industry often refer to the calculation of complex eigenfrequency analysis based on *finite element method* (FEM) simulations. The underlying models are regularly limited in terms of describing high dimensionality, friction laws, small-scale effects and damping behavior. Nevertheless they remain one of the most common methods even for developing applications with regard to brake squeal generation. Due to limited resources concerning time and computation capacity, the usual procedure is to linearize around certain system states which leads to the exclusion of nonlinearities of the friction mechanics. Furthermore, the knowledge about the friction interface, its variability and dynamics, and further participating contacts, is largely limited; thus still many questions are open about how to develop a suitable model.

To sketch just some of the appearing phenomena of the friction interface, an example of the nonlinear behavior and variability of the brake dynamics is given in Figure 2.2. In the upper part the spectral distribution of the vibrational response of a brake system is displayed. The patterns have been generated by *creep groan* [2] and

---

[1] The friction interface is also often called *third body* and, regarding the portion that is coating the disk, *boundary layer, transfer layer,* or *(friction) film.*

[2] See foot note on page 3.

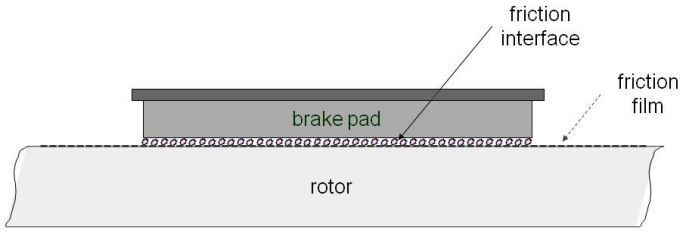

Figure 2.1: *Friction interface between brake disk and brake pads and friction film on disk surface*

squeal and have been exhibited alternatively. The epoch in which creep groan has been dominant was marked by broadband vibration with main amplitudes below 4 kHz, the squealing condition has shown tonal vibration at distinct frequencies with according harmonic oscillations. Creep groan and squeal have been related to the sinusoidal sliding velocity [3] which is depicted as the blue line in the lower diagram. Two major phenomena are noticeable. Firstly that the transition from one status to the other took place at different velocities, each marked with red and magenta colored lines. Obviously, the transition velocity between the states depends on the previous history. And secondly that the transition velocities themselves shifted from one revolution to the other: the onset of creep groan has started at ≈ 3.6 rpm during the first velocity peak and has decreased to ≈ 2 rpm at the fourth, by analogy with the velocity, at which each the squeal was initiated.

Regarding the first item, obviously, the instant of transition between the two states is related to the particular previous condition, and additionally, two completely different oscillation types may exist within the *'hysteresis-epoch'* [4] with the *same mechanical parameters* as environment. This implies that a modification must have happened to the friction interface as all other parameters remained constant. And moreover secondly and remarkably, the velocity at which the system changed each of its states, has already shifted after some ten seconds. Consequently, observations during the experiments should comprise the documentation of the disk surface as reference to the friction interface condition. For that purpose a visual method to track the interface alteration and the time scale on which it takes place was implemented

[3] Effectively, the rotational speed has been sinusoidal with 0.8 rpm at its minimum but due to the limited resolution of the rotary encoder below ≈ 1 rpm, the velocity seemingly declines to zero.

[4] Hysteresis in this case is meant in the sense that the system may, dependent on the prehistory, behave differently even with the same mechanical input. The *epoch* is supposed to be the period in which this behavior appears.

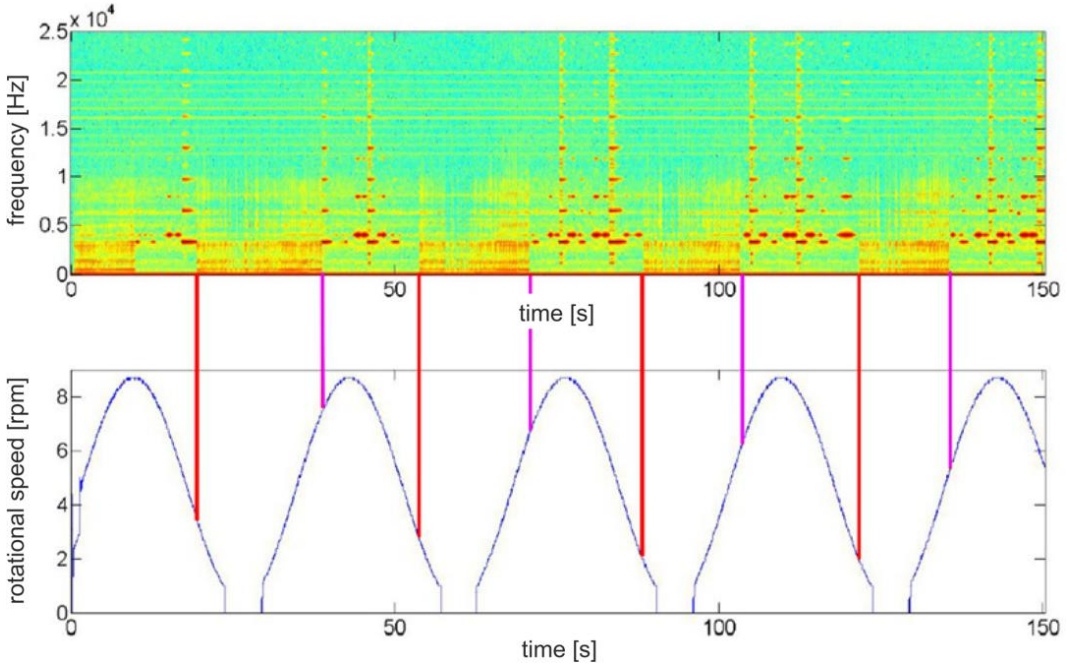

Figure 2.2: *Nonlinear dynamics: alternating low frequency slip-stick and high frequency squeal (upper part), related to sinusoidal velocity (lower part)*

at the experimental setup.

Concerning the second item, a more clearly readable representation of the phenomenon is given in Figure 2.3 which shows a record of another brake application. It includes alternating squeals two times per brake disk revolution: every yellow cross marks an observation without squeal dedicated to an angle of rotation and a rotational velocity. Green crosses represent observations with squeal and blue and red ones the onset and the termination of the squeal event, respectively. The brake application starts at the upper left corner with $\approx 47\,\mathrm{rpm}$ and ends at zero after roughly 46 revolutions in the lower middle left. Seemingly, an assumable layer or coating on the disk, or its absence, which obviously leads to squeal, has varied its shape and its location on the disk from revolution to revolution. While the squealing area around a rotational angle of $\approx 300°$ travels against the sense of rotation but keeps its width nearly constant, the surface condition around $\approx 150°$, generating squeal as well, becomes wider. Thus, the leading rotational transition angle which separates the non-squealing from the squealing state, has moved a total of $\approx 40°$ during the time of the brake application. This is equivalent to an averaged length of $\approx 100\,\mathrm{mm}$ displacement of the coating on the disk surface.

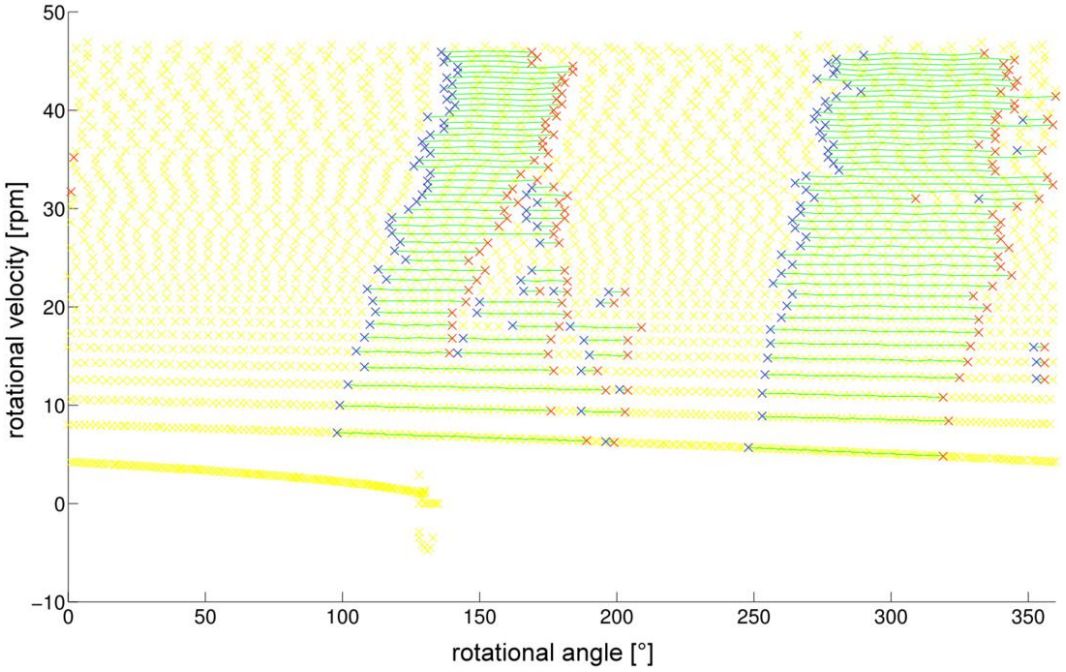

Figure 2.3: *Nonlinear dynamics: vibration generating sections on the disk move during some revolutions depending on the rotational angle and the velocity*

The above explained particularities exemplify just a fractional part of the observable phenomena around friction and friction induced vibrations: the nonlinear behavior of brake vibration excitation and friction interface mechanics, physics and chemical processes. Since the origins of these phenomena and their interaction are mostly unknown or not identified, models which comprise at least the most significant system characteristics, seem to continue to be in the distant future.

In contrast, and to overcome these uncertainties and limitations, the present study addressed the investigations from a different perspective. Instead of analyzing a given numerical model for instability or limit cycles, experimental data of the brake system in non-squealing conditions were subjected to an experimental data analysis. To cover the participating scales, the following methods were directed to this examination: firstly, techniques of linear and spectral signal analysis in the frequency domain have been applied to cover phenomena belonging to larger scales and for first inspections. Secondly, phase space reconstructions were performed as a core of an estimation of dimensionality and as a basis for the following time series analysis techniques. Thirdly, a probability density investigation was implemented to embrace all scales that the data recording provided. Finally, although the critical

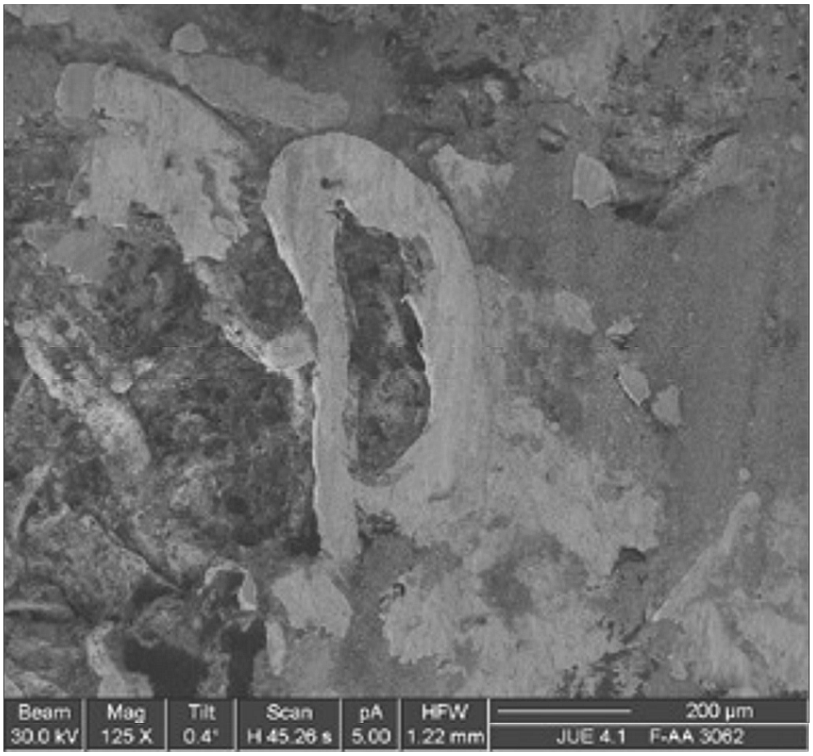

Figure 2.4: *Surface of a brake pad section (width* $= 1200\,\mu\text{m}$*), recorded with a focused ion beam (FIB) workstation. Steel fiber at pad surface (center) and plateau of friction layer (right)* [51]

uncomfortable frequencies of brake squeal are certainly limited to the audible range, the tribological and interfacial mechanics lead to broad-banded acoustic emissions at much higher frequencies. Thus consequently, all methods have been applied with particular regard to small-scale phenomena which is subsequently explained in more detail.

For the assessment of the involved frequency ranges and the identification of a suitable measurement technique, some preliminary examinations had been conducted before appropriate methodologies were identified. Regarding the interaction of wear, the involved friction surfaces and subsurfaces, a well established hypothesis has stated that the consequential friction and the tribological performance of the system is mainly determined by the growth and destruction of rigid structures in the friction interface. These formations have often been called *plateaus* [18] or *patches* [52] (Figure 2.4). Plateaus, which are formed from metal fibers or other hard materials are called *primary plateaus*. They transmit the main part of the friction performance. Wear particles flow between the primary plateaus in the boundary layer and some of them are accumulated, compacted and stacked up against the primary plateaus

and thus create so called *secondary plateaus*. Contrary to the hard primary plateaus, these plateaus are formed as a composite which represents rather elastic structures. Occasionally, the secondary plateaus break loose and are milled down in particles again. This occurs when the stability is disturbed, driven by small changes of the contact situation. In general, these mechanisms are enabled by an appropriate equilibrium of particle flow which continuously restructures the friction interface. The wear particle flow and the patches are also often called *third body*. Third bodies play an important role for balancing the tribological system in terms of abrasion, adhesion, friction and wear.
In this context it has to be considered, which scales have to be taken into account by the methods under consideration. Around friction brakes three principal categories of time and length scales seemed to be advisable:

- *Microscale*
  One of the smallest elements of the tribological system are the components of the wear flow. Additionally to the iron oxide from the cast iron brake disk, the particles contain chemical elements from all ingredients of the pad, together forming the third body. Thereby, the compound is sized on a nanoscale with grain sizes between 10 nm and 100 nm, depending on the types of the ingredients. Among others, this has also been demonstrated by [14].

- *Mesoscale*
  Fibres and wear particles with microscale sizes form the patches which exhibit an extent of between roughly 50 µm and 500 µm, depending on the pad formulation, the previous history, and the physical parameters. These structures shape the local friction.

- *Macroscale*
  The present overall mechanical system, the vehicle axle, has the largest scope regarding its dimensions on the length scale and thus spans the macro scale, comprising the brake system and the macroscopic friction interface. Accordingly, regarding the time scale, slower and more global processes such as e.g. film generation (see section 4.1.1) or pad material alteration are mapped on a macro time scale.

As a consequence, the sample rate of the conducted measurements was therefore increased to allow the investigation of spectral components even in the ultrasonic range to possibly also reveal particle and wear patch dynamics sized in microscales;

details are given in section 3.2.3. The aspect of different scales is reconsidered from other perspectives in section 3.1 and in chapter 4.
Since direct measurements or detailed observations of the dynamics in the friction interface is impossible without aggravating the overall system, the present study applies the above mentioned techniques and extracts the properties of the system directly from the measured data. Although such analysis techniques have been known and applied for nonlinear dynamical systems in a number of scientific and engineering disciplines [23, 31, 36], their application to friction affected and friction induced vibration has been rather uncommon. One of the few exceptions seems to be the recent work by Oberst and Lai [46, 47], though their work is restricted to the large-scale dynamics of friction-induced brake squeal and disregards the microscale dynamics.

Chapter 3

Experiment

3.1 Preparation

For the present study a passenger vehicle friction brake, carried by the entire vehicle corner, was assembled on an industrial *brake noise dynamometer (noise test bench)*. In industrial engineering *noise, vibration and harshness* (NVH) laboratories, brake noise investigations are typically completed by accordant setups as this approach provides a comparatively accurate simulation of the original vehicle mechanics. Additionally, in the context of examining vibrations, the original vehicle mounting suspension with axle bushings provides a more elastic interlinking to the dynamometer chassis frame. On one hand this excludes unwanted vibration from the test bench and on the other hand, and more essentially, helps to minimize the impact of the surrounding mechanics on the brake system while vibrating.

Table 3.1: Recorded signals / images

Physical and Technical Values	**Units**	**Sample Rate**
acceleration (vibration)	m/s^2	$> 200\,kHz$
rotational speed	$1/s$	$1\,kHz$
pressure	bar	$1\,kHz$
disk temperature	°C	$1\,kHz$
sound pressure level	dBA	$44\,kHz$
angle of rotation	°	$1\,kHz$
friction coefficient	-	$100\,Hz$
environmental temperature	°C	brake application average
environmental humidity	g/ml	brake application average
disk surface image	-	after each brake application

The automation unit of the dynamometer was arbitrarily programmable with regard to the operating and environmental control parameters. Additionally, the automatically controlled progression of the experiments was supported by an arbitrary chronological order of various types of brake applications. During the brake appli-

cations continuous or almost random alteration of parameters, e.g. such as pressure or velocity, was provided by freely definable shapes.

One of the most important aspects of the present work was the respective scales on which the phenomena had to be classified. Therefore, the sampling rates of the recorded signals were defined carefully: table 3.1 shows the recorded physical and technical values and the corresponding sample rates. All data were recorded with 1 kHz except the following:

- *acceleration of pad vibration*
  In contrast to other measurement channels, a supplementary but fully synchronized data acquisition system was used to synchronously record the vibration with a much higher sampling rate of $\approx 230\,\text{kHz}$ [1] . The applied vibration sensor has been of a low-mass, high frequency, piezoelectric quartz shear acceleration type. To achieve even higher frequencies, Laser-Doppler equipment with frequency ranges up to 1 GHz was evaluated as well, but due to unavoidable influences of the test bench environment, e.g. wear dust, low frequency vibrations, movements of the brake system while braking, the utilization did not turn out to be beneficial. But even though the piezoelectric transducers are typically much more robust in terms of continuous physical data flow security, measuring very small signal amplitudes with a system in close proximity of the test bench had turned out to be very difficult: strong magnetic fields originated from the engine [2] , interfered with the signals under consideration. Only a fully metallically conductive shielding of the involved measuring devices succeeded in keeping the influences sufficiently small. The purpose of the high sample rate and as a consequence, a resolution with a small temporal and spatial scale and its estimation, is given in section 3.2. By contrast, the infrasonic range and frequencies below 200 Hz have had to be cut because of the appearance of structure-borne vibrations. The vibrations in this frequency range have been attributed not to the brake system but rather to the test bench mechanics. Accordingly, the high-pass filter has therefore helped to keep the data trustworthy

[1] The data acquisition system sample rate specification of $2 \times 10^5\,\text{sample/s}$ was trimmed to obtain additional $3 \times 10^4\,\text{sample/s}$: while carefully regarding the data integrity, most data acquisition modules allow over-clocking in reasonable ranges.

[2] Due to the 220 kW high power drive engine, every acceleration of the drive shaft, even during braking and triggered by the inertia simulation, caused electromagnetic impacts at all electrical inputs.

and clean.

- *Sound pressure level*
  As illustrated later in this section and in section 4.3.3, the evaluations of the present study were constituted during periods in which the brake system was in non-squealing condition, with the exception of the noise propensity investigations, see section 4.4.3. Hence, the status was monitored continuously with a sound acquisition module providing fast algorithms for frequency and amplitude analysis and environmental noise reduction. As a result, every $\approx 50\,\mathrm{ms}$ the main frequency and its amplitude was supplied, in the case the amplitude exceeded the threshold of 60 dBA. The results of the frequency analysis below this limit value tended to be imprecise or misleading due to uncertainty where the superimposed environmental noise originated from, e.g. the engine, the brake cooling system or the local exhaust ventilation. Additionally, the structure-borne vibration amplitudes below this airborne sound threshold are small enough to fit the dynamic range of the accelerometer and thus preserve the evaluations from misinterpretation, as stated more precisely in the following.

- *Friction coefficient*
  The dynamometer was equipped with a lever arm on which the setup was mounted to measure the resulting torque when the brake was applied. Due to this mechanical assembly, the mass of the mounting, the lever arm and parts of the shaft, had to be accelerated when varying the torque. Hence, on behalf of the inertia of the mechanics, the sample rate in the hundred Hertz range proved to be adequate. The friction coefficient is calculated as follows

$$\mu = \frac{10\,M}{2\,\eta\,A\,p\,r_{eff}}\ , \tag{3.1}$$

  where M is the measured torque, η the efficiency factor of the brake, A denotes the brake piston area, p the brake pressure and r_{eff} the effective friction radius.

- *Environmental temperature and humidity*
  As it is well-known that environmental conditions such as temperature and humidity may have a considerable influence on the squeal behavior and the friction performance of vehicle brakes, it is important to monitor them. Assuming relatively slow changes of these environmental parameters allowed small sample rates and generally recording the average values of each brake application

turned out to be sufficient.

- *Disk surface image*
  One of the most important contributors to the performance of a dry disk brake friction system is the friction interface between disk and brake pad. A very thin part of this interface is the *film* or *coating* which is usually generated on the disk surface. Consequently, tracking these interface patterns helped in identifying the particular condition of the friction film. The images were recorded after each brake application. The deployed camera system held a cooled three chip CCD with a 48-bit-color resolution in total and $\approx 300\,\mathrm{pixel/mm^2}$ in the given configuration. Illustrating images and more details are presented in section 4.1.1.

The information in focus, the vibration, is developing when the pads are sliding on the disk. As mentioned above, this vibration was assessed by a piezoelectric accelerometer that was mounted on the backing plate of the outer brake pad. Thereby, the mounting base of the sensor was dimensioned for accelerations up to $\approx 2700\,\mathrm{ms^2}$ which is more than sufficient for the brake system in non-squealing condition. In addition, a number of different sensor mounting configurations were tested, and only results that were independent of the sensor mounting are presented in the following. The influence on the dynamics of the entire brake system by the mass of the sensor with $m \approx 2\,\mathrm{g}$ was supposed to be negligible. On the other hand, even if a remarkable impact would have become obvious, all observations would underlie the same influence since the measuring configuration was kept consistent at all times. Regarding the emerged amplitudes, which were relatively small, when compared with the amplitudes generated while the brake system was in squealing condition, the vibration sensory was tuned for the recording of smallest amplitudes [3] .
The analyzed lining materials were derived from the *non asbestos organic* (NAO) - type [4] and *low-Met*- type [5] with a typical spread in terms of friction coefficient and wear performance between these two formulation-families.
Each experiment progression contained roughly 2000 brake applications with a wide

[3] The upper limit of the vibration measurement chain was $a_{max} \approx 500\,\mathrm{m/s^2}$ and the lower limit remained below $a_{min} < 10\,\mathrm{mm/s^2}$ at high frequencies.

[4] The label NAO is somewhat misleading since the use of asbestos in vehicle brakes has already been prohibited by law in most countries for decades. Actually, NAO brake linings are characterized by low wear, low dust emissions and a typical slightly lower friction coefficient.

[5] Low-Met pads means *low metallic* overall contingent which is typically < 30 %.

spread of parameter combinations [6] . And each exhibited a duration of about one and a half days and the recorded vibration data during the brake applications comprised in total more than 10^9 samples per experiment. All samples of all the vibration records were synchronized with all other measurements and operating conditions and could therefore be related to them.

3.2 Techniques

3.2.1 Friction Surface Visualization

Friction is a multi-scale and multi-physics process by its very nature: mechanical energy is transferred, forces are transmitted between scales and components, surface topographies change, interface layers may form, physical and chemical properties of the friction partners can be modified and additionally other details are involved [19].

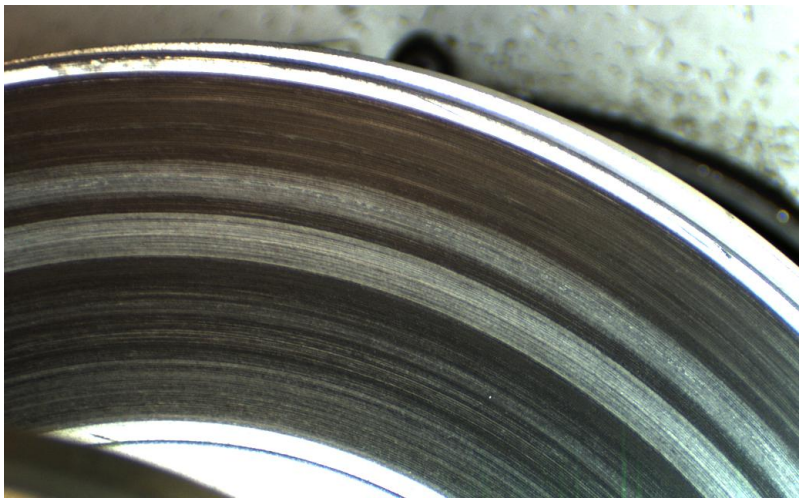

Figure 3.1: *Disk surface friction film example*

One of the most important contributors to the dry friction system is the friction interface layer between the disk and the brake pad. It is a compound of both the wear of the gray cast iron and the wear of the brake pad consisting of the ingredients according to the pad formulation [49, 50]. As a result of varying system parameters, the friction interface may change significantly. This can affect for instance the

[6] Controlled parameters were in the following ranges: disk temperature 50 °C to 300 °C, sliding velocity 0.2 m s^{-1} to 9.6 m s^{-1}, brake pressure 0 bar to 52 bar.

thickness of the film [7] and its consistency, both integral or partial.

However, the experimental identification of properties related to the above outlined processes is complex because the contact area is difficult to access without significantly changing it or its dynamics at the same time. To obtain an impression nonetheless, a picture of the disk surface and the adhered layer was taken directly after each step. Consequently, tracking the interface patterns on the basis of these images helped in identifying the particular conditions of the friction film. An example picture is given in Figure 3.1. Photographing reflecting metallic disk surfaces with only a very thin layer is problematical: the illumination has to be well balanced both in terms of the angle of incidence and brightness control, and the camera has to provide a very high color resolution [8] . Additionally, the optical system has to be placed far enough from the brake system to make sure that the wear dust will not influence the photographing.

3.2.2 Friction Surface Roughness

In most cases, roughness of participating surfaces is considered to be of high influence on the friction and wear performance. Abrasion is an indicator for roughness which forms together with the adhesion forces the overall friction value [9] . It is also considered to influence both the self-excitation behavior and the acoustic emissions. Consequently, the observation of the roughness adds important information to the friction dynamics investigation. A first approach for a visualization is the use of

---

[7] For example, in standard vehicle friction brakes a friction layer of 1.4 nm thickness can be formed during ≤ 50 ms [5].

[8] The applied camera system supplied a 48-bit color resolution and the disk surface was illuminated by a dedicated passive reflecting lamp unit with diffuser which provided a soft and constant stream of continuous lighting. Various preliminary tests had to be performed to identify an appropriate brightness so that the maximum of contrast fitted the dynamic range of the camera and kept the signal-to-noise-ratio high. The presetting had to cover the disk both at the beginning of an experiment with high reflectance of the unused metallic disk and later in the experiment with a possibly dark surface after thermal load.

[9] Usually the peaks of the roughness profile do not necessarily constitute the points of contact because the shapes of both partners have to be considered. Admittedly, in case of the contact between brake pad and disk, the friction partners have quite different characteristics in terms of their surface contour. The magnitude of the heights of the disk are much smaller than those of the pad (see Figure 3.3(a) and Figure 3.3(b)). Furthermore, the roughness of both friction partners may also promote adhesion.

appropriate *kernel image processing* techniques with *convolution filters* [10] . An example of a 3 x 3-point kernel, developed in particular for enhancing the dimension perpendicular to the disk surface, is given in Figure 3.2: some asperities with a diameter $\ll$ 1 mm are visible, leaving trails to the right of the disk surface as the sense of rotation was counterclockwise. The convolution filtering helps to identify the roughness of the surface by reconstructing the out-of-plane extent on the basis of the two-dimensional video data, presupposed, the video processing is applied carefully with specific observance and prevention of artifacts and misinterpretation.

Figure 3.2: *Disk surface asperities: image processing with convolution filters*

This qualitative technique which characterizes the roughness of disks, was supplemented by a quantitative calculation of the surface as a result of image data from a bifocal microscope, which is introduced in the following section.

3.2.3 Vibration Investigation

Following the remarks of a previous section, the vibration recording has been tuned to provide more insight in described mechanics. Regarding the time and length

[10] The effects provided by convolving a suitable kernel and an image are commonly used e.g. for enhancing hidden or covered information. The mathematical implementation of a convolution algorithm is based on the multiplication of each kernel value by the corresponding image pixel value.

resolution, it has had to cover the expected frequencies of elementary events in the friction interface. This assumption had been motivated by the wide-spread ideas of asperity or plateau destruction and formation in the contact interface [18, 44]: assuming e.g. an asperity or friction plateau of about 3 µm in size, and assuming vehicle speeds of about 3 km h^{-1} [11] , corresponding frequencies have to be taken into account by measurements, which are discovered only with sampling rates at about or above 200 kHz.

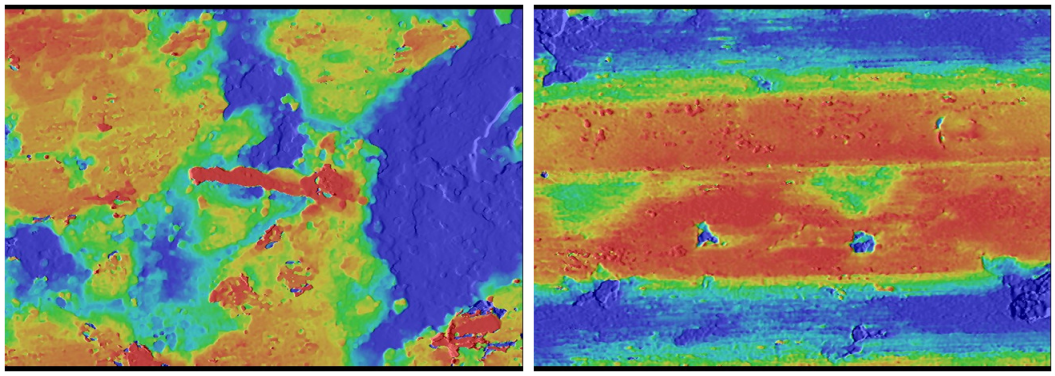

(a) Pad surface, scale: −25 (blue) to 25 µm (red)

(b) Disk surface, scale: −1.5 (blue) to 1.5 µm (red)

Figure 3.3: *Topographies of a brake pad (a) and a brake disk (b), scanned with a bifocal microscope* [54]*, dimension each* 510 µm × 694 µm*, blue areas are in direction into the according material (gaps), red areas mark contact zones*

Since at present there seems to be no truly well-based idea on the highest relevant frequencies in the interface dynamics under consideration, the present limit of maximal ≈ 230 kHz was somewhat *ad-hoc*, but also, from a more practical perspective, related to available and suitable sensory equipment. This resolution limit is typical for the applied piezoelectric sensors. However, a big advantage is the robustness of this sensor type regarding the influence of brake dust and the strength against vibrations in the infrasonic range. This is an important advantage in contrary to optical devices. Furthermore, another weak point of optical devices with higher frequency limits in this context is the relatively high propensity of data disruptions due to the alteration of the properties of the vibrating reflection surfaces. In contrast, piezoelectric ceramic transducers tuned for acoustic emissions above 100 kHz typically fail

[11] Friction induced noise appears typically at small vehicle velocities as e.g. 3 km h^{-1}.

in the low frequency range. However, for all results presented in the following, the experiments were conducted with respect to the influence of the sampling rate: in many cases reasonable results have been obtained only for high enough sampling rates (see sections 4.3.1, 4.3.2, 4.3.3 and 4.5), at least beyond the audible range [12] .

Figure 3.3(a, b) give an idea of the microscale asperities and an indication of even smaller scales which are not represented due to the optical resolution of the bi-focal microscope. In sum the surfaces lead to very low amplitudes during steady sliding that have to be resolved by the accelerometer. Hence, due to the observed small amplitudes, a *signal-to-noise ratio* (SNR) estimation has been relevant: an error estimation on the basis of both the sensory and measurement device specifications was completed and is described in the following. It was accomplished with particular regard to the SNR, since noise plays an important role, which is discussed in more detail in section 4.3.2. The accelerometer is specified by a typical spectral noise of $628\,\frac{\mu m s^{-2}}{\sqrt{Hz}}$ above 1 kHz that leads to a signal noise of $\approx 0.2\,\mathrm{m\,s^{-2}}$ regarding the bandwidth of 100 kHz and $\approx 0.02\,\mathrm{m\,s^{-2}}$ regarding the bandwidth of 1 kHz, respectively.

The resulting signal-to-noise ratio is then

$$SNR_{acc} > 88\,\mathrm{dB} \tag{3.2}$$

In the measurement chain the digitizing unit contributes to the parasitic errors in terms of noise and quantification error as follows: the single point and the average deviation in the operating voltage range are specified as 84 µV and 7 µV, respectively. This leads to a signal-to-noise ratio of

$$SNR_{ADC,\,singlepoint} \approx 80\,\mathrm{dB} \tag{3.3}$$

and

$$SNR_{ADC,\,average} \approx 100\,\mathrm{dB}, \tag{3.4}$$

respectively.

Summarily, the measurement precision estimation resulted in a high enough SNR in

[12] A further increase of the sampling rate for some additional experiments apparently did not change the qualitative result, which would suggest that the relevant dynamical processes in the considered frequency range predominantly have been resolved. However, it has to be considered that the observations *above* 230 kHz within this study used undocumented equipment, which still left some question marks over the results, concerning the reliability of the measured data. For this reason, these observations were abandoned.

the sense that the mechanics have not become hidden behind measurement noise. However, the overall noises comprising the impact of the sensory, the measurement chain and other sources, e.g. related to parasitic electromagnetic influences which have been neglected in the estimation, appeared in subsequent analysis. And this not at least by reason of the enormous dynamic measurement range regarding smallest vibration scales up to high vibration amplitudes appearing shortly before the system transits to a limit cycle. Nevertheless, the resulting errors due to the included noises were small enough to reconstruct the phase space and to identify the dynamics (see section 4.3.2). And, moreover, the linear spectral analyses revealed a sufficient preciseness of the recorded data (see section 4.2). In this context it should be highlighted again, that this study intentionally omitted conditions in which the brake system emits squeal. Prior accomplished examinations of appearing acceleration amplitudes in squealing conditions suggested to stay below a threshold of

$$a_{max,th} < 5\,\mathrm{m\,s^{-2}}, \tag{3.5}$$

which indicates a squeal occurrence [13] . This threshold allows small harmonic fractions, e.g. a state in the phase space somehow with a distance to a fixed point but far enough away from a limit cycle. Investigations of these system conditions somewhere between the states, turned out to promote the system characterization: the delineation between the harmonic and the broad-banded mechanics helped to understand the underlying dynamics. In section 4.3.3 some analyses of such traverses between the dynamic states are given.

[13] The appearance of squeal is detected by the microphone signal and the distinct harmonic peaks in frequency analyses of the acceleration.

Chapter 4

Data Analysis and Evaluation

4.1 Friction Surface Investigation

4.1.1 Friction Surface Visualization

The friction surface was visually analyzed on the basis of photos taken during the experiments; each brake application was followed by an image of the disk surface. It turned out that as a result of varying system parameters, the friction interface, or its according traces, left on the disk surface, often changed significantly. Regarding the temperature, for instance, the greasing of particular lubricants failed at low temperatures; some formulations showed this effect appearing below $T_{disk} < 80\,^{\circ}\mathrm{C}$. Failing lubricants may lead to very high wear and leave distinct appearances on the disk surface.

Beside the impact on wear, friction value and vibration excitation, the transformation of the friction interface also affected the thickness and the consistency of the friction film, both integral or partially.

Consequently, tracking the interface patterns on the basis of these images has helped in identifying particular conditions of the friction film. Some pictures are given exemplarily in Figure 4.1. At the beginning of the experiments, the friction layer developed very rapidly when the pad slides on the disk. Even after the very first brake application a film coating became visible (Figure 4.1(a)). The applied experimental procedure, similar to the *SAE2521* [1] [11], provided a friction couple preconditioning at the beginning of each experiment after which in general, a smooth interface layer developed (Figure 4.1(b)) [2] . Equally, thermal load usually led to a smooth layer, but, depending on the applied lubricants of the pad formulation, the film had

[1] The applied test procedure was following for the most part the SAE2521 which comprises huge varieties and ranges of temperatures, pressures and velocities.

[2] The preconditioning, also called *bedding* or *running-in* comprises approximately 70 brake applications and is intended to adapt the surfaces to each other.

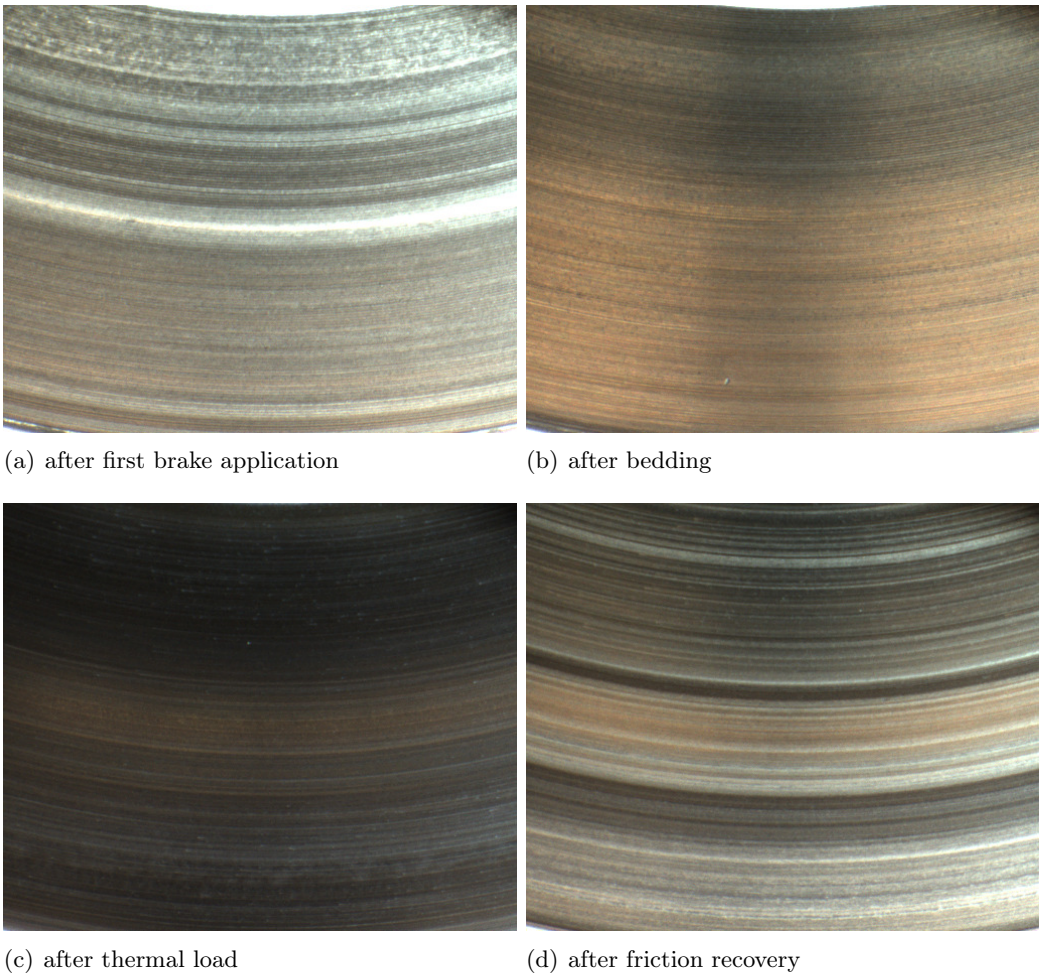

(a) after first brake application

(b) after bedding

(c) after thermal load

(d) after friction recovery

Figure 4.1: *Transformation of a brake disk surface during an experiment*

a different chemical and physical texture. The visual inspection then often revealed a darker and more colored friction film in the case of particularly tuned lubricants (Figure 4.1(c)). However, in contrast to the condition of the film in Figure 4.1(b), the layer generated after thermal treatment, e.g. the so called *fading* [3] , was repeatedly weaker and therefore more rapidly damaged in subsequent brake applications. The section following the thermal load portion within the procedure is applied for friction recovery. This is intended to, and usually does, even in case of a sometimes significantly high decrease of friction performance, restore the overall friction value and leads back to a friction coefficient in the range of the nominal value. In contrast, this friction value recovery, as a rate of the entire contact area, is mostly indepen-

[3] The fading section applies a high thermal load and amounts to temperatures at $\approx 650\,^{\circ}\mathrm{C}$.

dent from the partial damaging of the friction layer. Considerably, in most cases the squeal propensity increases drastically after the fading and recovering section as well. The damage of the film becomes obvious by uncoated sections of the disk (Figure 4.1(d)).
In general, if the parameters do not change drastically, the film pattern remains steadily or changes only slowly from one brake application to the next. Nonetheless, regarding longer time scales with varying conditions in between, even with then recurring identical parameters, the accumulation shape has often changed drastically.

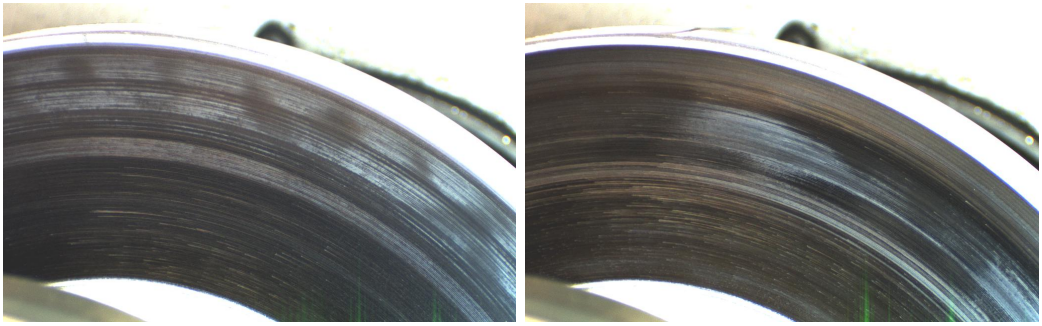

(a) Disk surface: periodic coating

(b) Disk surface: periodic removal of friction film

Figure 4.2: *Periodic accumulation and extraction of friction film on the disk surface*

Further phenomena which have been observable in some experiments refer to occurrences on comparatively smaller scales: Figure 4.2(a) demonstrates periodic coating and removal of the friction film. Assuming, the disks rotates with a rotational velocity that matches a slow vehicle speed (with typically higher noise propensity), the frequency of the disk inhomogeneities is in the range of 5 Hz to 20 Hz. Remarkably, the distribution of the coating patterns is not related to any geometric characteristics, for instance the alignment of fins in ventilated disks does not match the distribution structure of the coating.

To which extent these particular phenomena control the friction coefficient and the impact on self-induced vibration has not been measurable, not only because the overall friction value belongs to the total surface which the pad covers, but also because the consequential rotational torque variation is much too small to be observable at the test bench which has been used (see also section 3.1). A further phenomenon regarding the disk surface has been observed: some pad formulations exhibited accumulations on the disk at the position the brake was clamped. Obviously, the very

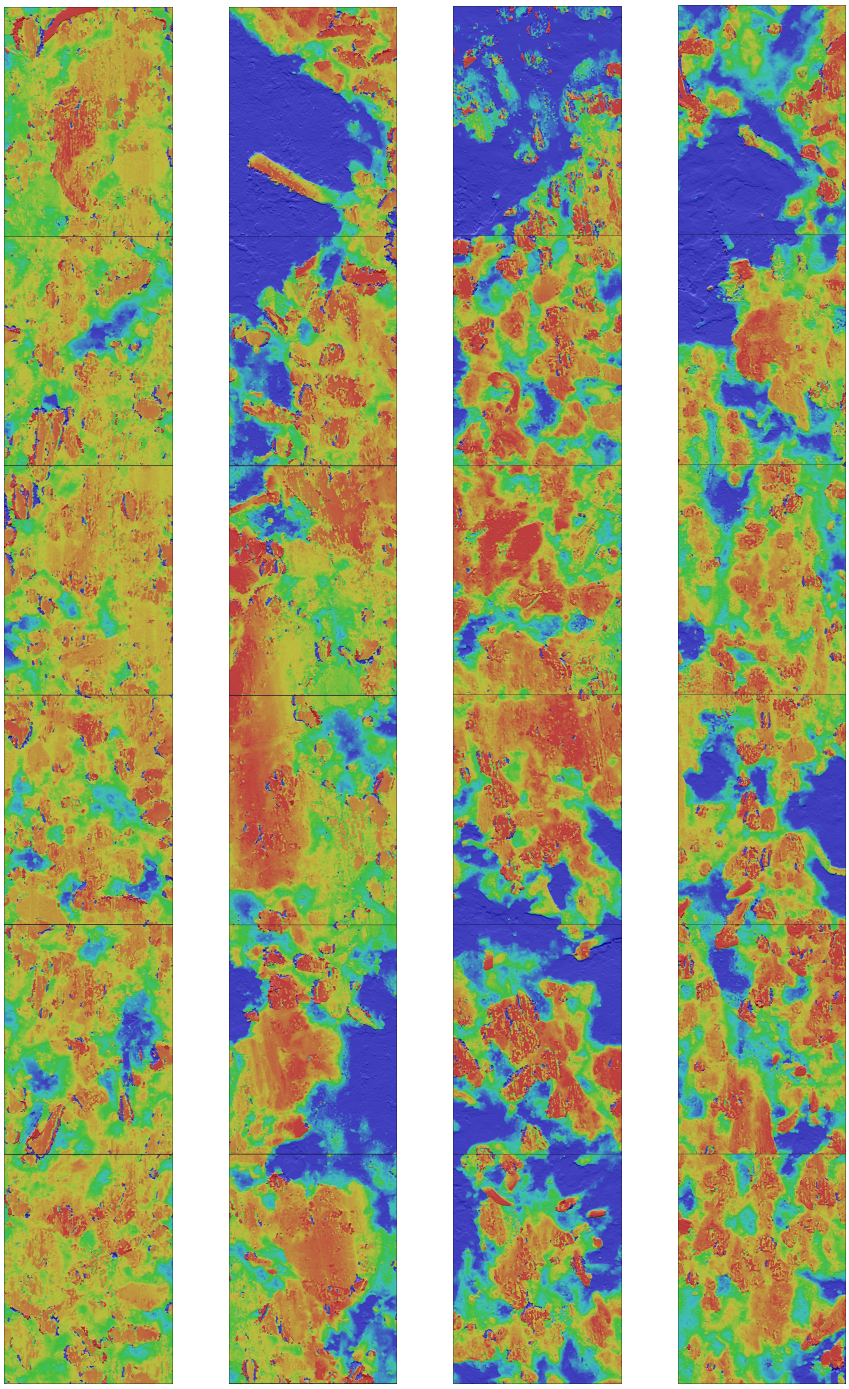

(a) (b) (c) (d)

Figure 4.3: *Pad surface topography with dimensions each* $510\,\mu\text{m} \times 4.16\,\text{mm}$*, color range* $-25\,\text{um}$ *(blue) to* $25\,\text{um}$ *(red); (a) and (b) surface parts of a pad with low squeal propensity, (c) and (d) with high squeal propensity, accordingly* [54]

short moment the pad made contact with the disk at the very beginning of each brake application, the transient static friction left a mark. When the pads encounter the position after one revolution again, the system, if the conditioning of the friction and its noise related noise propensity is high enough, has a tendency to exhibit vibrations at that position. Evidently, the occurring instability at that particular location hints at a significant friction variation which leads to subsequent displacements.
Regarding the wear behavior, a clear correlation between a robust film and low wear is observable. In contrast, the correspondence between film presence and squeal propensity seems much weaker. This is in particular remarkable as the coating is in general supposed to organize the friction interface in a sense that abrasion and adhesion are balanced in a sustained manner. Ergo, a seemingly smooth circular flow of wear particles is expected to keep the sliding steady and thus promotes the prevention of instabilities. Consequently, and to resolve the apparent contradiction, further investigations were completed and are described in the following.

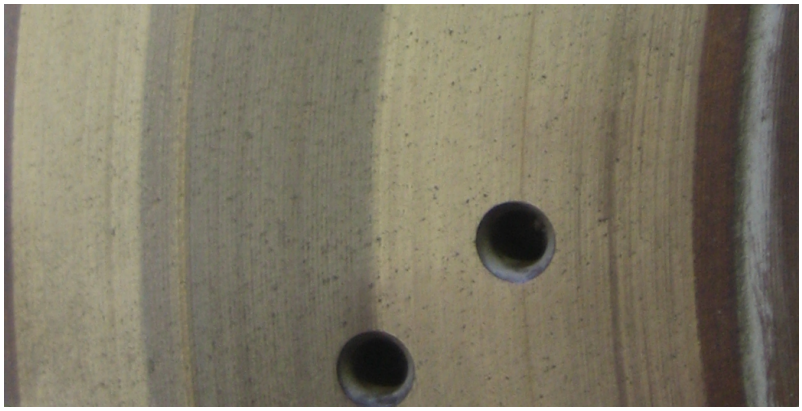

Figure 4.4: *Disk surface image, both with (darker patch) and without (brighter patch) friction film*

Based on the macroscopic observations of the friction film which became visible on the disk, the surfaces have been examined additionally with a bifocal microscope to reveal the corresponding topographies and structures on a micrometer scale. Therefore, three different experiments were executed: firstly, the surface of a pad which has been identified as exhibiting low noise occurrence and secondly, the surface of a pad, participating in an experiment which showed plenty of noise events, was examined. The third experiment was conducted to characterize the topography of a disk surface both with and without visible interface layers at the same time.

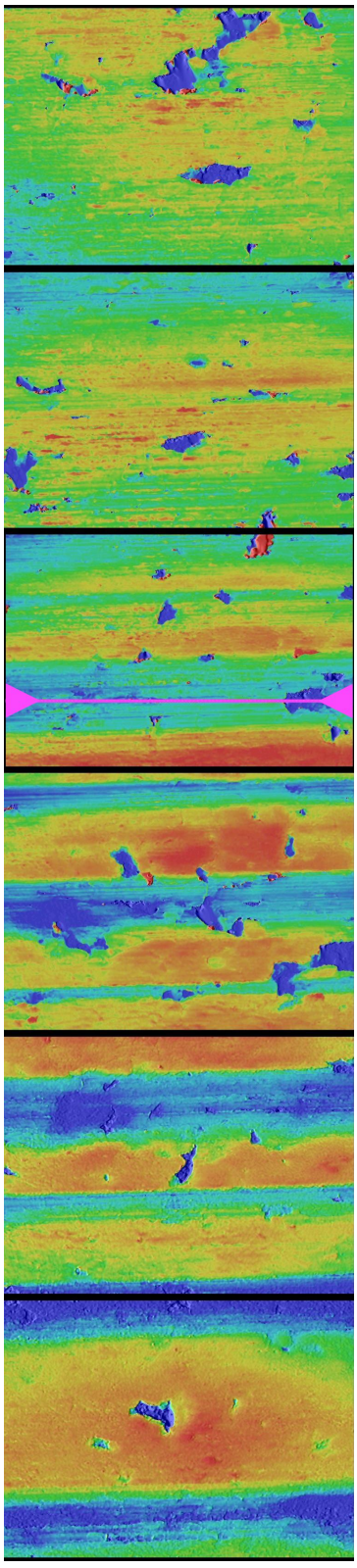

Figure 4.5: *Disk surface topography; above the magenta colored line with friction film, below without,* 694 µm × 3.06 mm [54]

For the evaluation of the first (Figure 4.3(a) and 4.3(b)) and second experiment (Figure 4.3(c) and 4.3(d)), optical measurements shown by two photo strips each at the outer pad shape and near the effective radius were made. Hereby, each photo stripe was composed of six single-shot exposures, identifiable by thin vertical lines between them. Due to measurement errors, small deviations at the borders are noticeable, however, without disturbing the whole picture. At a first glance and when regarding the topographies zoomed with the high original resolution, a tendency appears that the noisier the friction couple appears to be, the rougher, or to be more precise, the smaller and more pronounced the contact areas constitute. On the other hand, quite a few converse observations have made it difficult to draw a clear picture so far.

The third experiment in this section gives an idea about the disk surface characteristics and differences between both a fraction with and without film: Figure 4.4 presents friction rings with layers in the center and without a friction film both at the inner and the outer side of the brake disk. Quite clearly, the experiment offered a

film related investigation with both film / no film presence, with identical environmental conditions. Along a radial line transversing the statuses with present film layer to the uncoated area, the disk surface was inspected by a bifocal microscope again. The dimensions of the imaged areas were 694.41 um in width and 3060.5 um in height and the color was in the range of -1.5 um (blue) to 1.5 um (red).
Figure 4.5 puts the surface of the disk on a microscale view: above the magenta colored line the friction film was present and below no visible layer could be observed: manifestly, the surface or topography of the portion with film is more evenly distributed and the averaged depth differences are less expanded. Even though this characteristic appears as strong tendency, it still remains a qualitative observation. A quantitative and more robust description is provided in the following section.

4.1.2 Friction Surface Roughness

While the topographical attributes of a brake disk surface with and without film layer have been investigated qualitatively in the prior section, the same experimental data were directed towards a quantifying roughness estimation. With data points at the location x_m, x_n and M, N as the total number of data points in the two directions and z as the height dimension, the two-dimensional average roughness R_a is given by

$$R_a = \frac{1}{(M-1)(N-1)} \sum_{m=1}^{M} \sum_{n=1}^{N} |(z(x_m, y_n) - \langle z \rangle|, \tag{4.1}$$

the root mean squared roughness R_{RMS} by

$$R_{RMS} = \sqrt{\frac{1}{(M-1)(N-1)} \sum_{m=1}^{M} \sum_{n=1}^{N} [(z(x_m, y_n) - \langle z \rangle]^2} \tag{4.2}$$

with

$$\langle z \rangle = \frac{1}{(M-1)(N-1)} \sum_{m=1}^{M} \sum_{n=1}^{N} z(x_m, y_n), \tag{4.3}$$

respectively.

The roughness R_a, based on the data of the bifocal microscope which are represented in Figure 4.5, is illustrated in Figure 4.6. Every dot stands for the according roughness calculated on a particular subfigure [4] . According to the quadratic term in Equation 4.2, the root mean squared roughness R_{RMS} delivers for larger outliers from the average, both huge heights and deep gaps, higher roughness values than R_a. Obviously, the roughness R_a stays almost equal following the calculations in radial direction, both with or without film coating. The roughness R_{RMS} in contrast apparently varies significantly with the presence of the friction film, the value of R_{RMS} is more than doubled in segments without friction layer. That means in consequence, the outliers from the average, visible in Figure 4.5 as deep blue troughs and red regions that are presenting contact areas, dominate the surface in portions without

[4] In contrast to the six sub-figures in Figure 4.5, the calculation in Figure 4.6 is based on a larger number of sub-figures: the presented six pictures are a selection of the seventeen images that where available in total.

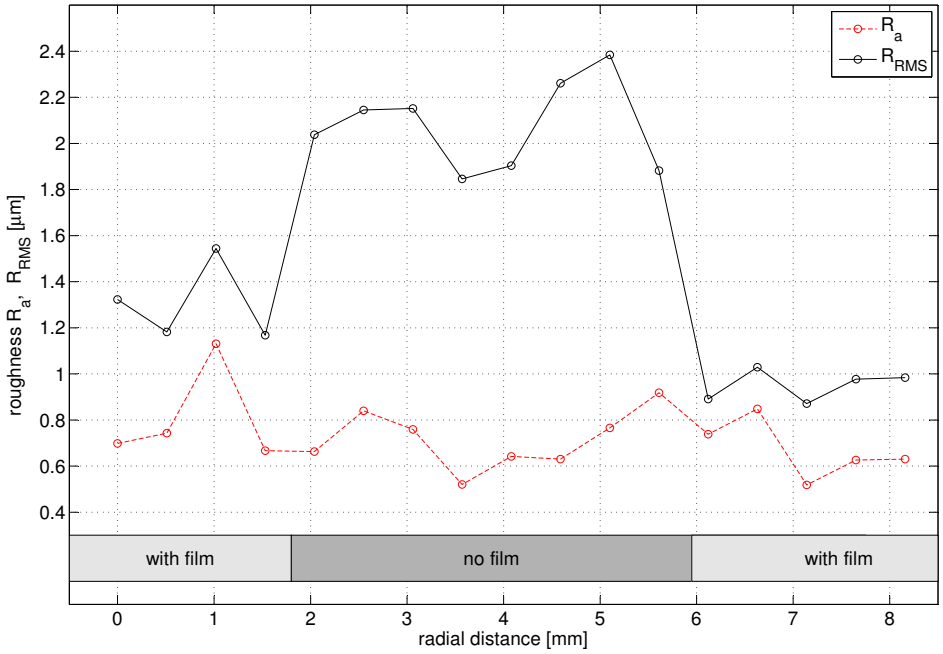

Figure 4.6: *Disk surface roughness, both with and without friction film.*

film or more precisely, dominate the surface *more* than in regions with film. As the visual inspection in section 4.1.1 already suggested with this trend, the roughness estimation substantiates the statement.

Figure 4.7: *Disk surface with applied convolution filter, original dimensions* 15 mm × 15 mm

On the other hand, as also already mentioned in section 4.1.1, the correlation between a comprehensive film and the tendency of the system to generate noise appeared more or less weak. Accordingly to the results of the roughness estimations, indicating that a film leads to a smoother disk surface but at the same moment does not predominantly supply better noise performance, contradicts the assumption that rough surfaces would automatically more easily trigger brake squeal. What is appropriate, on the other hand, is that the film promotes better wear performance; an elevated roughness apparently leads to a more pronounced abrasion.

Additionally, there is also the fact that no robust statistical connection and much less a direct link between considerably asperities, generated visibly on the disk surface, and the noise generation has been observed. Figure 4.7 illustrates an example of a 15 mm x 15 mm disk surface fragment, recorded within an experiment. The picture was computed with the aid of convolution filters (introduced in section 4.1.2): interestingly, even distinctly shaped asperities did not seemingly influence the vibration characteristics. Conceivably firstly because of the quite uniform distribution over the disk surface and secondly due to the relatively soft pad material, the peaks did not lead to remarkable irregularities of the vibration state. The same applies to the friction coefficient which is almost unaffected by the asperities [5] . But it has also to be considered that the recording of the overall friction value on the basis of the calculated ratio of applied pressure and resulting torque according to Equation 3.1, with a comparatively high unresponsiveness of the torque sensory, is barely supposed to leave high-frequency traces in the recordings.

To consolidate the findings: if even smoother surfaces, expectedly resulting in decreased vibration amplitudes during sliding, do not automatically result in less noise propensity, then well-established assumptions dealing with self-induced vibrations have to be reconsidered and expanded. Friction dynamics apparently are complex; for a more comprehensive description evidently further or complete other parameters and mechanical behavior have to be included.

Consequently, in the following sections new approaches and techniques will be introduced to achieve a better understanding of the underlying friction dynamics.

[5] As the experimental setup did not provide the measurement of local friction values, the mentioned friction value belongs to the overall friction value of the pad surface.

4.2 Linear Analyses in the Frequency Domain

Even though the recorded data of the brake vibration are supposed to be strongly nonlinear, a preliminary inspection of the data through linear analysis has helped to identify behaviors on longer time scales. For this reason the records of the accelerometer have been subjected to a *Short-Time Fourier Transformation* (STFT). A typical spectral distribution of the vibration data during a stop brake application is depicted in Figure 4.8. The given picture is representative insofar as the following enumerated characteristics are somehow typical, even if the spectral distribution itself is unique for every particular brake application. Following peculiarities are observable:

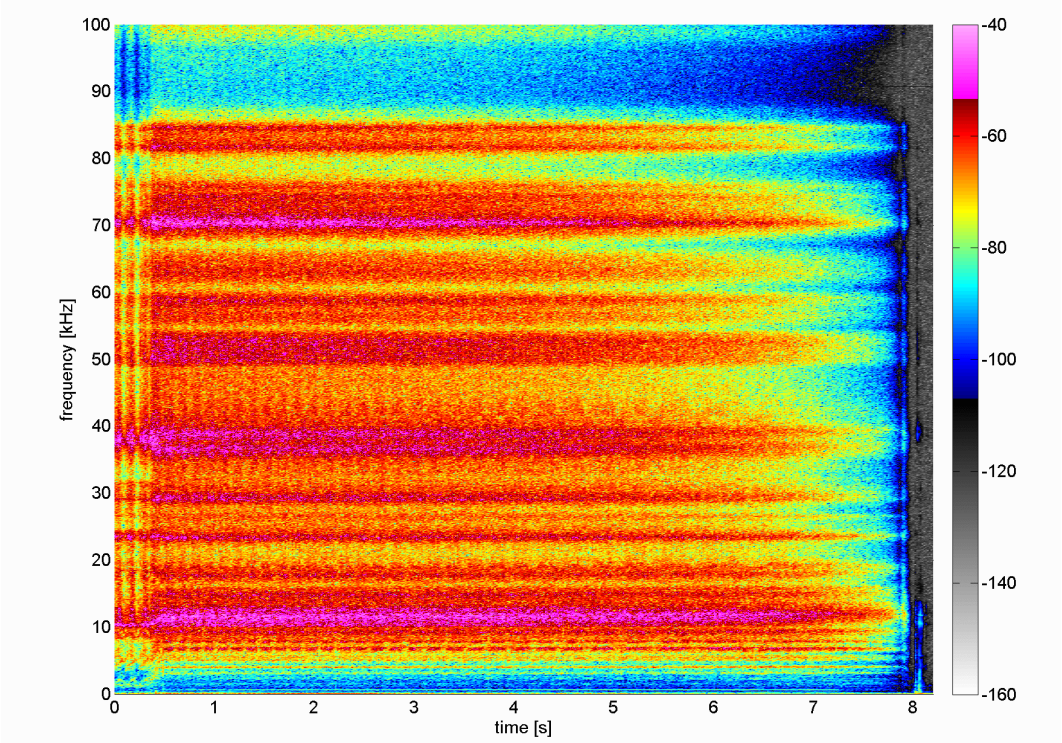

Figure 4.8: *Spectral density vibration distribution of a brake application with velocity deceleration from* 50 km/h *to* 0 km/h

- As already anticipated in section 3.2 it is not surprising that the audible range up to 16 kHz covers only a small portion of the acquired signal. In the range between 16 kHz and 100 kHz considerable spectral frequency bands are revealed. Hence, beside the audible frequency range, the main information of the signal and accordingly the involved mechanics are evidently found in the ultrasonic range.
- The spectral distribution of the vibration data is predominantly broad-banded.

Even rather narrow bands with higher amplitudes cover some hundred Hertz. Evidently, no squeal, other tonal events or distinct natural harmonics of participating parts appear in the spectrum (in contrast to the spectral characteristics of a squeal event in Figure 4.17)

- Although the vehicle speed is in the span of 50 km/h to 0 km/h, which corresponds at its maximum with a sliding velocity of $\approx 6\,\mathrm{m\,s^{-1}}$ at the effective friction radius, the distribution over frequency obviously reflects almost steady-state behavior. The µm-structure of the friction surfaces is evidently not revealed by the present linear analysis. Otherwise, and in regard to the static sample rate, one would assume a change of the patterns when coming from higher speeds to lower sliding velocities, due to the fact that the relative length resolution increases with lower rotational and the related sliding velocities. On the other hand, the Fourier transformation is averaging over a certain time span so short variations might get lost. But however, evidently the distribution during braking does not change significantly. Consequently, this particular attribute of seemingly steady sliding has been subsequently analyzed with nonlinear methods in the following sections.

- In the very left part of Figure 4.8 two distinct characteristics appear:

  - The frequency distribution does not show significant differences between the clamped and the non-clamped state of the brake. The transition from non-clamped to clamped condition is thereby clearly readable from the significantly increasing amplitudes, approximately after the first 400 ms of braking. Evidently, the predominant frequencies do not change between the states. In contrast, as the modal properties of the system differ measurably (as a consequence e.g. of the tensioning or force impacts) between these two cases, it suggests that the measured broad band signals do depend more strongly on the contact interface dynamics than on the modal properties of the whole structure. This supports the requirement of the vibration sensory setup that was supposed to predominantly examine the friction interface even when it is mounted in a rather complex, in terms of the entire dynamic structure, vehicle corner. The idea of 'cutting free' the friction interface while keeping the influence of the surrounding mechanics small, evidently operates accordingly.
  - The vibration amplitudes are strongly correlated to the brake pressure, or, to be more precise, to the contact force between disk and pads. Con-

sequently the amplitudes are higher in the clamped state, but also the non-clamped state at the beginning of the brake application shows a force impact. In this case it is pulsating, due to the unavoidable run-out of the disk. The run-out effects that the pads make intermittent contact to the disk, which is originated by and related to the clearance between disk and pads [6] .

- The frequency range above $\approx 85\,\text{kHz}$ indicates lower amplitudes, but effectively the sensitivity of the accelerometer declines above this threshold.

The pattern in Figure 4.8 characterizes exemplarily a particular state of the friction interface within an experiment. It remained more or less stationary from braking to braking when the conditions remain unchanged [7] . Additionally, considering the variation of the spectral distribution from one brake application to the next, it appeared, in general, that it did not change substantially even if parameters were changed. Figure 4.9(a) illustrates a brake application with 20 bar and Figure 4.9(b), which displays a brake application that immediately succeeded the previous, presents a brake application with 10 bar brake pressure, while other parameters remained unchanged. This suggests the assumption that the emerged patterns, and therefore, the distribution of the vibration in the frequency domain, are mainly related to the dynamics of the friction interface. However, this particular investigation assumes linear behavior and reflects only processes on comparatively large scales, given by the STFT. The suggestion that the dynamics may stay unchanged on the time scales under consideration is also supported by the optical inspection of the disk surface which changes or remains unchanged in a similar way, see Figure 4.1. However, the potential picture that underlying (micro-) dynamics may behave similar, is substantially modified in subsequent sections in that nonlinear techniques are applied.

---

[6] The clearance of typical passenger vehicle brakes, both fixed and floating calipers, result in practice in off-brake forces on principle. In this case the intermittent frequency at the beginning of the brake follows the rotating speed of approximately 700 rpm which leads to roughly 12 contacts per second.

[7] An exception to this trend demonstrate repeatedly applied drag brake applications, e.g. brake applications with constant and low speed. In contrast to stop and snub brake applications, analyses showed that drag brake applications alter the frequency patterns even if conditions are unchanged. It is commonly known that multiple reapplications of drag brake applications lead to an 'artificial' friction interface structure. This usually increases the friction value and noise propensity. In industrial noise performance testing, stop brake applications are therefore typically introduced after a certain number of drag brake applications to restore the friction couple.

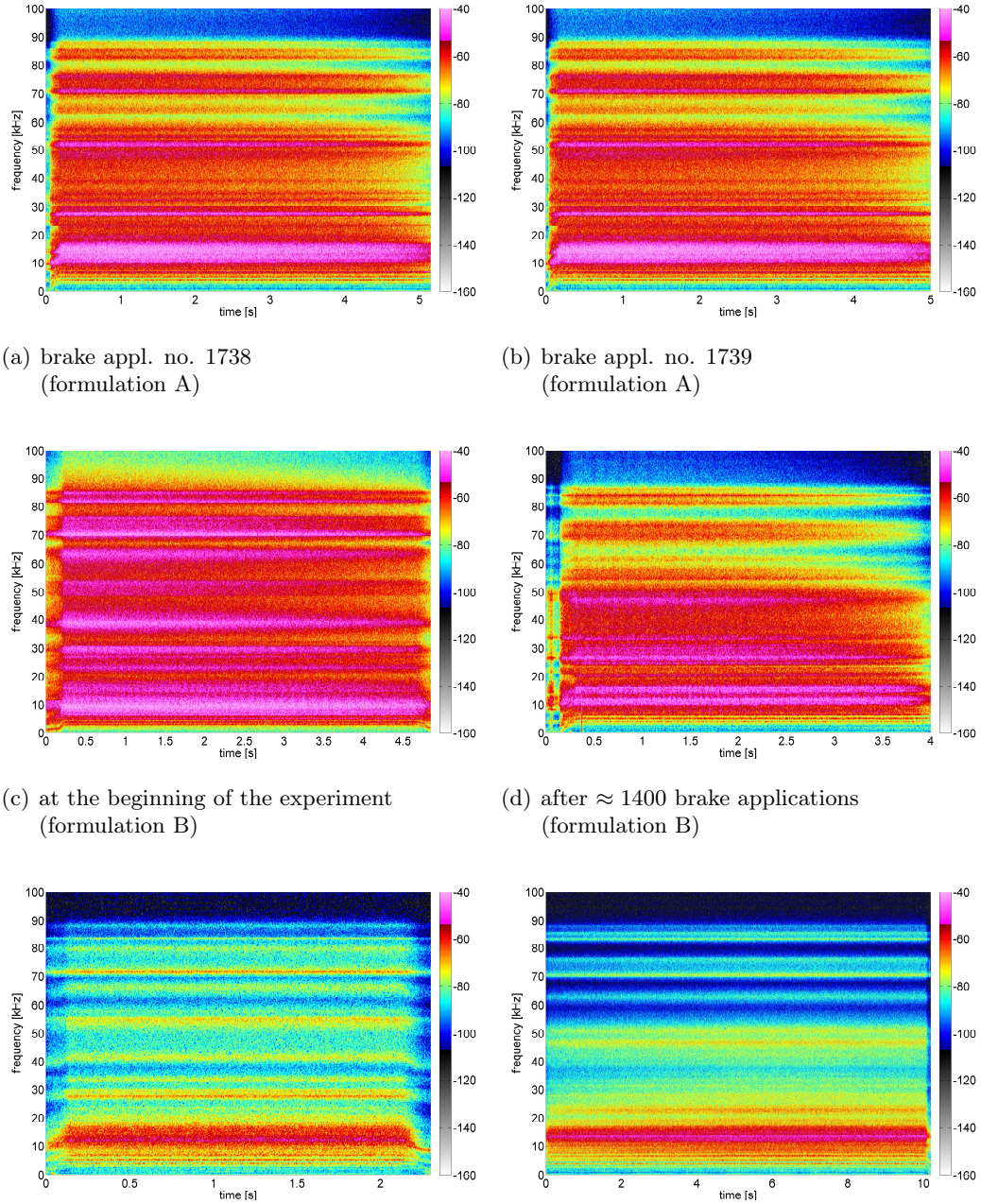

(a) brake appl. no. 1738 (formulation A)

(b) brake appl. no. 1739 (formulation A)

(c) at the beginning of the experiment (formulation B)

(d) after ≈ 1400 brake applications (formulation B)

(e) at the beginning of the experiment (formulation C)

(f) after ≈ 1300 brake applications (formulation C)

Figure 4.9: *Spectrograms of vibrations in different brake applications and states*

In contrast to these broadband frequency distributions that did not change their patterns due to varying parameters, at least not immediately [8] , the tonal resonance

[8] Immediately in this case means that external mechanical modifications of the brake system may certainly influence the friction dynamics *on larger time scales*. But this is rather not a direct impact on the underlying dynamics but more related to the alteration of the friction contact after a sufficient sliding distance with according reorganization of the interface.

frequencies of the system however, altered significantly as a result of mechanical system modifications. The natural frequencies, exhibited when self-induced vibrations led to mode coupling as the system response, adjusted themselves according to mechanical parameters. That means in particular, when reducing or increasing e.g. the brake line pressure, the elasticities of the brake system change and lead therefore to a an eigenfrequency shift, easily measurable for instance by modal analysis (see also item 4 on page 38). Further explanations about the interaction between broadband frequencies, multi-dimensional friction interface, and distinct limit cycle frequencies are given in the section 4.4.3.

However, the frequency distribution may, and typically did, change completely after hundreds or thousands of brake applications in between, and a varying load history, hence, the patterns were modified significantly. This means in particular that some frequency ranges may lose energy gradually or may completely disappear, while other frequency bands may develop or move to other ranges. While the pattern in Figure 4.9(c) reflects the dynamics of a brake application at the beginning of the experiment with pad formulation B, Figure 4.9(d) illustrates the friction interface condition after roughly 1400 brake applications within the same experiment. Evidently, some characteristics of the distribution have remained while at the same time other frequency bands have shifted. In comparison with the alteration during the same experiment, the difference from one pad formulation to another is often even more prominent: Figure 4.9(e) shows the frequency distribution of formulation C, again at the beginning of the particular experiment, and Figure 4.9(f) after roughly 1300 brake applications, respectively.

Following the findings so far, the patterns may change case-by-case from brake application to brake application, but seemingly the alteration during a braking remains minor. But as the dynamics *do actually* lead to seemingly stochastically occurring instabilities and in contrast to the apparently regular behavior, the spectral vibration distribution must contain information about the friction interface and dynamics of the friction couple. However, the mechanisms that trigger these instabilities do not become visible. In this context it has to be considered as already indicated above that the applied short-time Fourier transformation naturally averages over a certain duration. Thus some details, in particular nonlinear and transient phenomena, will barely leave footprints or might completely get lost.

In this way, since the preliminary findings have dealt with medium- and long-term scales in the range of hundreds of milliseconds to periods of hours and days, underlying short-term phenomena have not been taken into account in this context. Consequently, investigations that consider dynamics on microscales and that complement the analyses accomplished so far, are presented in subsequent sections.

4.3 Time Series Analysis

Analytical friction models have been developed on the basis of observations and often have been able to mathematically represent an appropriate system. In the case of the present dry friction system the involved processes are complex and they and their dimensions are mostly unknown. Hence, modeling by means of physical observations is delicate and moreover, the unawareness of the nature and the behavior of the underlying dynamics may lead to inadequate assumptions.
A model-free approach, e.g. a study on the basis of analyses of experimental data, may by contrast describe a system without prior knowledge of causal relations. This applies certainly similarly when regarding a physical system which dynamic equations are generally unknown (see also chapter 2). But in many cases only one physical parameter $x(t)$ as a function of time can be measured. Nevertheless, it is often possible to draw a picture of the chronological development of the entire system on the basis of one-dimensional *time series* $\{x_i\}_{i=1}^{N}$. These one-dimensional records allow reconstruction of the higher-dimensional, original phase space which is equivalent with regard to the same topological characteristics [62]. One of the most important techniques for the reconstruction of dynamical system is the method of *delays*. From time delayed values of the scalar measurements, vectors are formed in a new space - the embedding space:

$$\vec{\mathbf{x}}_n^d = (x_{n-(m-1)\,\tau},\, x_{n-(m-2)\,\tau},\, \ldots\,, x_n), \tag{4.4}$$

where m is the embedding dimension and τ the time delay. Moreover, these are the key factors in the context of phase space reconstruction. If the embedding dimension and the time delay are selected too large, the phase space reconstruction will be poor. A too large τ will bring areas close to each other which are far apart from each other in the original phase space. On the other hand, when selecting τ too small, the chronological distances will become dominant and the phase space will not be

sufficiently unfolded and therefore remain too small which inhibits the identification of its structure [62].

A tool to determine a reasonable delay was suggested by Fraser and Swinney [21]: the *mutual information*. It also takes nonlinear correlations into account, unlike the autocorrelation function. The delay can be heuristically estimated from the mutual information by

$$S = -\sum_{ij} p_{ij}(\tau) \ln \frac{p_{ij}(\tau)}{p_i p_j}, \tag{4.5}$$

where p_i is the probability to find a value of the time series in the i-th interval and the common probability $p_{ij}(\tau)$ that an observation is contained in the i-th and after the observation time τ is in the j-th interval. Several investigations have proven that if the time delayed mutual information S exhibits a marked first minimum at a certain value of τ then this value is supposed to be a proper applicant for a realistic time delay [31]. Equation 4.5 will be used to characterize the dependency between the appropriate time series and the phase space and will be applied to the estimation of delays in section 4.3.1 and subsequent sections.

4.3.1 Phase Space and Attractors

Generally, nonlinear time series analyses of deterministic systems demand the existence of a phase space or state space in which each state defines the prospective chronological development of the system. Phase space trajectories compose the phase space in which all observations are contained in an invariant quantity; the *attractor* and its dimension characterizes the overall dynamics. Whilst usually rather scalar measurements are observed in an experiment than the phase space trajectories, the starting point of a nonlinear time series analysis lies in the reconstruction of the vector phase. This then represents the phase space of the unknown dynamical system, which is entitled as the *embedding*. And if this system is defined by a scalar time series and has d degrees of freedom, the combination of $m > 2d$ consecutive observations allows representation of $m-$dimensional vector-valued interpretation of the dynamics [62].

In this context, it has to be considered that the phase space of rather low-dimensional experiments in laboratory environment with specific preparations and low noise and observations of analytical models, may, in general, predominantly be successfully re-

constructed by nonlinear time series analysis tools. As opposed to this, 'open area experiments' posses often unknown stochastic fractions, generally higher dimensions (typical for open systems), noise, and sometimes even only small data sets are available. These considerations are continued in section 4.3.2; a discussion about the applicability of the present techniques with regard to the present experiments is addressed there as well.

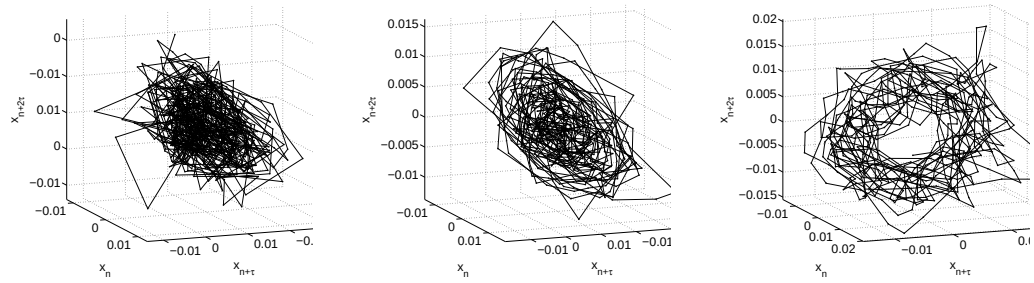

(a) 50 kHz sample rate, brake appl. no. 65

(b) 100 kHz sample rate, brake appl. no. 65

(c) 200 kHz sample rate, brake appl. no. 65

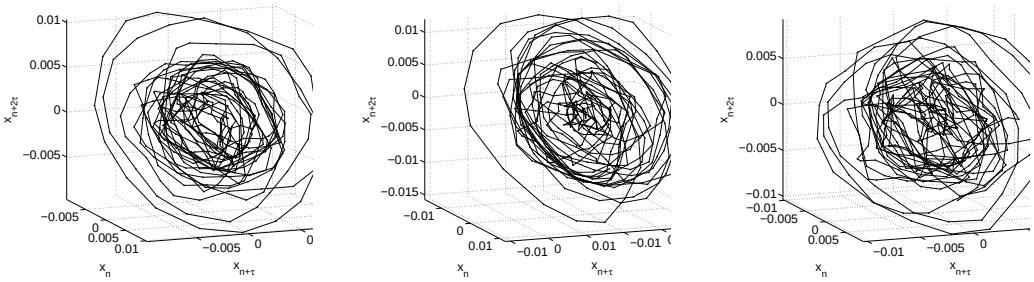

(d) Beginning of brake appl. no. 77

(e) Center of brake appl. no. 77

(f) End of brake appl. no. 77

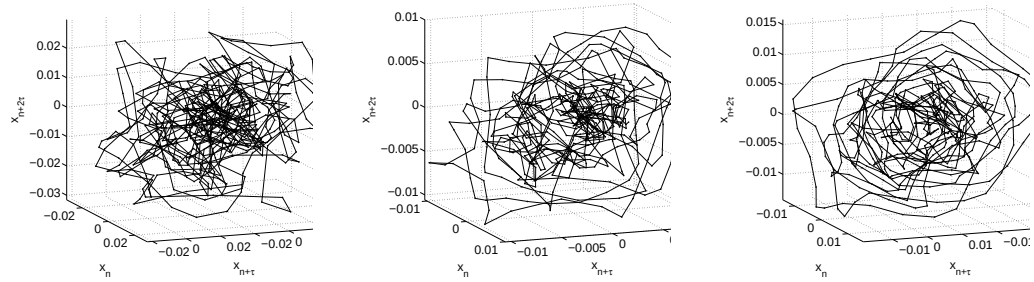

(g) brake appl. no. 1

(h) brake appl. no. 2

(i) brake appl. no. 3

Figure 4.10: *Phase space trajectories of delay vectors*

Added to these possible obstacles, the validation of the attractor reconstruction is often made worse by another reason: the dynamical system may not evolve toward a low dimensional attractor which can consequently not be visualized in two or three dimensions. However, even as the depiction of more than three dimensions is not possible, a low-dimensional representation of a higher-dimensional system may nevertheless deliver insights into the overall dynamics of the system. Consequently, in Figure 4.10 some delay vectors according to Equation 4.5 with 500 elements each of the formulation B pads are displayed. All observations are completed with a measurement frequency of $\approx 230\,\text{kHz}$ except the first row: it represents a brake application [9] with 50 kHz (Figure 4.10(a)), 100 kHz (Figure 4.10(b)) and 200 kHz (Figure 4.10(c)) sample rate. As already discussed in section 3.2.3 and reviewed from another perspective in section 4.3.2, the resulting phase space of the dynamics of the microscale asperity characteristics of the sliding friction surfaces requires a time resolution that is high enough to be unfolded: only the observation sampled with 200 kHz reveals a kind of structure [10] (Figure 4.10(a) to 4.10(c)).

The second row illustrates the phase space reconstruction of a brake application, just after the *running-in* at the beginning of an experiment (brake application no. 77) and with constant speed, at the beginning (Figure 4.10(d)), in the middle (Figure 4.10(e)) and near the end (Figure 4.10(f)) of the brake application. Seemingly, the trajectories of the section at the beginning of the brake application is slightly more structured even down to smaller values than those from the center and the end of the application. The observations illustrated in Figure 4.10(d-f) are the basis of the largest Lyapunov coefficient estimation in section 4.3.3.

Finally, the last row demonstrates how the friction couple develops from being unadapted to adjusted: Figure 4.10(g) displays the phase space vectors at the beginning of the very first brake application within an experiment. Evidently, the brake disk surface and the pad surface are not yet aligned to each other [11] which obviously leads

[9] The observations are made at the beginning of the brake application number 65 of the applied test procedure SAE2521 [11] at $v \approx 80\,\text{km/h}$. The sampling starts at the same time stamp but due to the different sampling rate the delay-vectors are stretched differently, within the concerned observing time the velocity decay is $\Delta v \approx 1.2\,\text{km/h}$.

[10] Due to a better comparability, the delay is kept constant in all graphs. Adapting the delay was supposed to promote a better unfolding of the observations with lower sampling rates but evidently even with modified delays no clear picture of any structure became visible.

[11] The surfaces of the friction couple strongly depend on the load history of the brake system. Without the *friction film*, a thin film formed of the wear of the cast iron disk and the pad ingredients, the dry friction contact is still inoperable or, to be more precise, the friction coefficient has not yet developed and is significantly lower.

to an unsystematic or stochastic structure. This characteristic is confirmed by the visual inspection of the surfaces, examples are given in section 4.1.1. In contrast, the structure of the dynamics of the subsequent brake application displayed in Figure 4.10(h) seems to be more ordered and conclusively the phase space trajectories of the brake application following the first two, depicted in Figure 4.10(i), exhibit an even more structured formation. The three discussed brake applications were hereby carried out one after the other with identical parameters.

Obviously and actually expectedly, the phase space trajectories of the observed vibration in the ultrasonic frequency range are evidently strongly correlated with the characteristics of the nonlinear friction dynamics and the processes at the friction interface. The high dimensional mechanics of the tribological system, mainly consisting of the sliding partners and the particles and patches between them, at the beginning acting seemingly stochastically or randomly, but after a period become increasingly more and more arranged in a physical or even chemical manner. And as a consequence they apparently operate organized or synchronized together. The dynamics in this case of proper coordination potentially should have less active dimensions, since the three-dimensional reconstruction is hardly applicable to unfold processes with significantly higher dimensions. Thus, a system with high number of degrees of freedom would leave a less structured picture of phase trajectories as that in Figure 4.10(d), or, less succinctly, in Figure 4.10(i). But again, the presentation of higher dimensional systems in a three-dimensional figure naturally underlies limitations.

The attributes of the trajectories, in particular the consideration of dimensionality is researched in greater depth in section 4.3.2. Other ways of describing the trajectories e.g. with *Poincaré maps* [12] had not enhanced the representation of the state space, on the one hand because canceling just one dimension did not improve the unfolding significantly and on the other because the noise of the data blurred the image. Other and in this context more useful techniques to represent the states of the system have been applied in section 4.4.1 on the basis of *recurrence plots*.

In summary, the phase space visualization even only with three dimensions has turned out so far to be a useful method for detecting roughly the existence of any

[12] Poincaré maps illustrate the intersection of a continuous dynamical system orbit with a lower dimensional subspace, transversal to the flow of the system. It is one dimension smaller than the original system but preserves many features of it. A Poincaré map differs from a *recurrence plot* (see section 4.4.1) in such a way that *space* determines where to plot the intersection point and not the *time* of recurrence.

dynamical structure of the systems under consideration. As a type of diagnostic modeling, it uncovers structures in the apparently random data. In contrast, the visualization of the time series in strictly chronological order, thus a one-dimensional row without any embedding or reconstruction, would lead to the assumption that the friction interface vibration records would be purely random.

4.3.2 Estimation of Dimension

In the previous sections the data analysis raised the question of how many (active) degrees of freedom play a role in the friction interface dynamics. Evidently, to describe the system, the estimation of dimensionality is essential. Therefore it must be ensured that the embedding dimension, which has to be determined, is sufficiently large to cover most of the mechanics and the particularities [60]. In this section, the estimation of dimensionality was supplied by the method of *false nearest neighbor* counting, introduced by Kennel et al. [33]. According to this method, the identification of the embedding dimension is based on the computation of the distances between each point in the time series in an m-dimensional phase space and its nearest neighbor. As the embedding dimension increases, the distance should not change if the points are truly nearest neighbors in an unfolded phase space. The criterion for a point to be a false neighbor, due to an embedding dimension chosen too low, is then

$$\frac{|x_{n+1} - x_{k+1}|}{||\vec{x}_n - \vec{x}_k||} > D_{th}, \tag{4.6}$$

where D_{th} is a heuristically determined threshold value and $||\vec{x}_i - \vec{x}_j||$ denotes the Euclidean distance in the m-dimensional embedding space between point x_n and its nearest neighbor x_k under consideration. When the fraction of points being false nearest neighbors has become sufficiently small, the embedding is considered as to be successful. The same concept but with some modifications which avoid certain spurious results for noise, was suggested by Kantz and Schreiber [31]: based on Equation 4.4 and with σ as the standard deviation of the data and Θ as the Heaviside function it reads

$$X_{fnn}(r) = \frac{\sum_{n=1}^{N-m-1} \Theta\left(\frac{\left|\mathbf{x}_n^{(m+1)} - \mathbf{x}_{k(n)}^{(m+1)}\right|}{\left|\mathbf{x}_n^{(m)} - \mathbf{x}_{k(n)}^{(m)}\right|} - r\right) \Theta\left(\frac{\sigma}{r} - \left|\mathbf{x}_n^{(m)} - \mathbf{x}_{k(n)}^{(m)}\right|\right)}{\sum_{n=1}^{N-m-1} \Theta\left(\frac{\sigma}{r} - \left|\mathbf{x}_n^{(m)} - \mathbf{x}_{k(n)}^{(m)}\right|\right)}, \tag{4.7}$$

where $\mathbf{x}_{k(n)}^{(m)}$ is the closest neighbor to $\mathbf{x}_n$ in m dimensions, i.e. $k(n)$ is the index of the time series element k different from n for which $|\mathbf{x}_n - \mathbf{x}_k| = \min$.

It has to be noted that for systems with a certain amount of noise, i.e. basically for all experimental systems, the system dynamics can often still be unfolded to a large extent, as long as the effects of noise are rather weak in comparison to the deterministic component of the dynamics. However, if very large embedding dimensions are needed, noise may also strongly shadow the deterministic dynamics of the system. In the present study, effects of noise are not considered explicitly; it has been seen from the results that this purely deterministic approach works surprisingly well. Apparently, stochastic aspects seem to play only a secondary role for the present analysis [13] .

Figure 4.11 illustrates the results of calculations applying the false nearest neighbor method to recorded time series. Three different brake applications were divided into six equally spaced sections and the first 5000 samples of each are exploited in Figure 4.11(a, b, c). Evidently, the fraction of the false nearest neighbors as a function of the embedding dimension decreases rapidly for embedding dimensions up to about 10 to 15. Then either the number of data-points becomes too small for the analysis or the false nearest neighbor count increases again, due to the influence of measurement noise. In case of Figure 4.11(a), the underlying data belong to a pad formulation with moderate squeal propensity. Figure 4.11(b) depicts again six different data sections but in this case from a friction couple that tends to generate more squeal in general. Evidently, the necessary embedding dimensions are even lower, roughly in the span of six to ten.

According to the previous considerations and estimations concerning further parts of brake application data, the present results suggest that the deterministic part of the system's dynamics could be described in a phase space with only about (roughly) 6 to 15 dimensions. In parallel, noise is superimposed on the deterministic dynamics. Nevertheless analyses of several data records have shown that even with varying con-

[13] Other studies analogous to the current one have been conducted by [20, 73]. But in opposition to the present work, computer based simulation data has been used. Since computer modeling does typically however, not include sub-scale dynamics and corresponding complex vibration components, the specific questions related to the role of noise did not appear there.

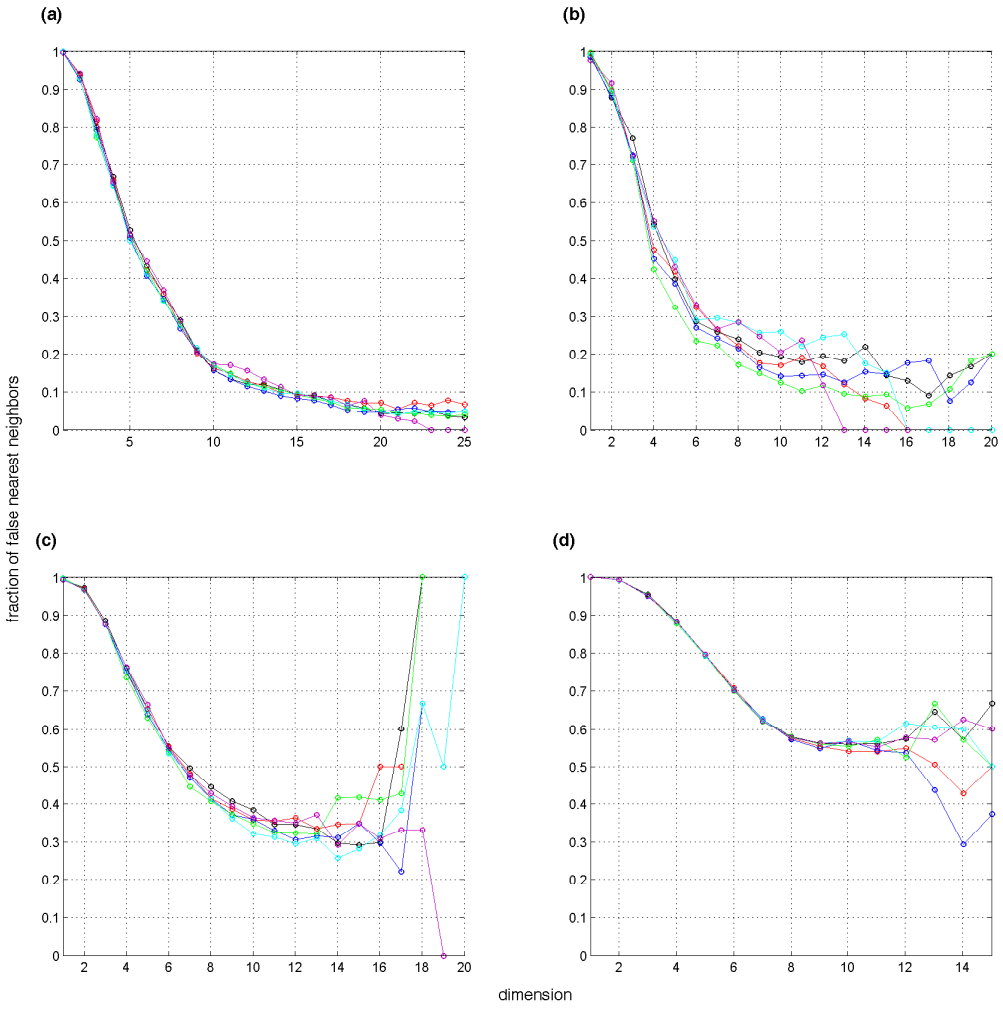

Figure 4.11: *Phase space reconstruction: the fraction of false nearest neighbors as a function of the embedding dimension for each six different sections within a brake application. The time series data originate from time series data of pad formulations with moderate squeal behavior (a) and with a generally high noise propensity (b). Fractions of an under-sampled series depicted in (c) and the dimension estimation for white noise in (d).*

ditions in terms of brake system parameters [14] , the aspect of a rather low embedding

[14] The velocity within the break application in Figure 4.11(a) decreases from $v = 80$ km/h to $v = 30$ km/h while the temperature increases from $T = 100°C$ to $T = 160°C$. Figure 4.11(b) shows the result for a drag brake application with a constant velocity $v = 3$ km/h and temperature $T \simeq 60°C$, while the friction coefficient increases from $\mu = 0.38$ to 0.48. Similar to the data in Figure 4.11(b) but with a temperature of $T \simeq 100°C$ the estimation of dimension is depicted in Figure 4.11(c). The delay in these examples is $\tau = 4$.

dimension persists.

In addition it has to be noted that in case of too low sampling rates the estimation of the dimensionality fails. E.g., Figure 4.11(c) shows a sampling rate of only about 40 kHz, which corresponds roughly with the beginning of the ultrasonic range of about 20 kHz when reconstructed, according to the Nyquist-Shannon sampling theorem. The fraction of false nearest neighbors remains still rather high, between 0.3 and 0.4, and does therefore not yet allow a reasonable estimation of the embedding dimension. In turn this suggests that sampling with 230 kHz in fact seems to capture the relevant dynamics for reaching a successful embedding. For completeness and to compare the dimension estimation of the experimental system with a pure stochastic one, the results of the approach at hand in the case of random white noise time series data is analyzed and contrasted in Figure 4.11(d): then the ratio of false nearest neighbors does not fall below a limit of about of 50 %.

Additionally, and to improve the assessment of estimations of suitable embedding dimensions, further systems have been compared. As the *Lorenz attractor* [15] is a pure deterministic, chaotic system, it provides a basis for the estimation of preceding calculations. In combination with added stochastic noise it supplies an estimate for the reliability of the assumptions made so far. Figure 4.12 illustrates the fraction of false nearest neighbors as a function of the embedding dimension for the Lorenz system. Evidently, in case of the noise-free deterministic system (black curve), the assessment shows that the fraction equals zero with an embedding dimension of $m = 3$, naturally, because the Lorenz system is three-dimensional. When only 10 % of white noise is added to the deterministic time series (blue curve), the picture is much less clear. The estimation tends to propose a higher embedding than the deterministic portion alone would need. Remarkably, the comparatively small amount of corrupting noise alone leads to a fraction of false neighbors of ≈ 60 % for a three-dimensional embedding. And the estimation performs much worse in the case of 50 % added noise: in this case no clear picture appears (red curve). This is similar to pure noise in Figure 4.11(d).

The outcome is even more surprising when viewed in comparison to the high-dimensional experimental time series under consideration: the estimations in Figure

[15] The Lorenz attractor is a linked system of three ordinary differential equation with real numbers and real-valued, time dependent functions. It is discussed more in detail in section 4.4.

4.11(a+b) already suggest appropriate embedding dimension roughly in the range of ten with much smaller fractions of false neighbors, in contrast to the three-dimensional Lorenz system with 10 % noise. Obviously, the experimental data contain less amount of stochastic processes than it has been assumed. From this it seems reasonable that false nearest neighbor ratios below values of 10 % or 20 %, as they result for the presently measured vibrational data, strongly indicate dominant deterministic dynamics.

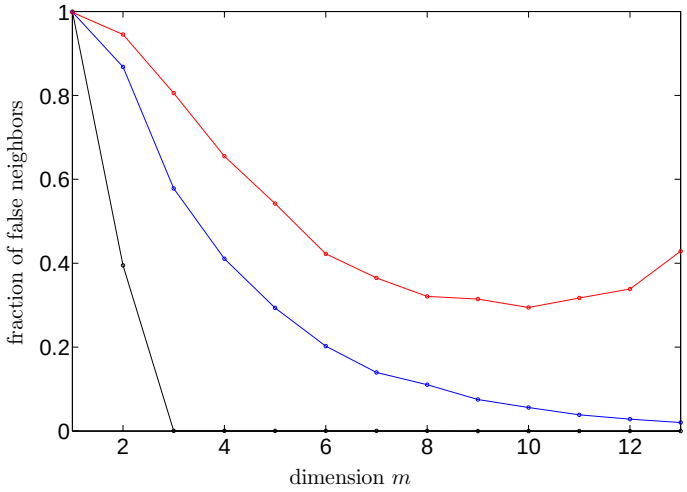

Figure 4.12: *Phase space reconstruction: the fraction of false nearest neighbors as a function of the embedding dimension of a noise free Lorenz time series (black), Lorenz system corrupted with* 10 % *(blue) and* 50 % *(red) white noise. Control parameters are* $\sigma = 10$, $\rho = 28$, $\beta = 8/3$.

The low-dimensional characteristics are quite surprising, reconsidering the friction interface system: a large number of dynamical processes is active at the interface of a brake pad when sliding over a brake disk. A huge amount wear particles flow and form a third body, acoustic waves such as bulk waves or surface waves may be excited, relaxation processes take place, possibly synchronization appears, to name just a few. Thus, to capture all these dynamically active and relevant effects, it should likely be considered that a large number of degrees of freedom have to be taken into account. In view of this and the overall complexity of a complete braking system, the apparently low embedding dimension during non-squealing condition is quite a surprising result. Also, the system does not seem to be in a state that is just randomly excited by interface processes: the embedding analysis suggests that the nonlinear structural dynamics seem to select a rather small number of active degrees

of freedom responding to the processes at the friction interface.

4.3.3 Estimation of Lyapunov Exponents

The investigations discussed in the preceding section indicated that rather low-dimensional dynamics hiding behind the steady sliding than high-dimensional stochastic processes dominate the mechanics in friction brakes. It now appears quite consequent to consider, if possibly a strange attractor is involved and if this is proven to be true, to further characterize it. A widespread procedure for characterizing a dynamic system concerning its type, which means conservative, dissipative or divergent, is based on the calculation of *Lyapunov* exponents. This classification is made possible by the fact that the Lyapunov exponents of a dynamical system describe the temporal change in separation between adjacent points in phase space. They jointly form the Lyapunov spectrum [16]. A positive exponent corresponds to a direction with phase space expansion and indicates a strange attractor. Negative exponents are related to phase space contraction in the corresponding directions. In most cases however, only the largest exponent is considered, since in deterministic systems a single positive Lyapunov exponent is already a sufficient criterion for chaos. In the following is correspondingly always meant *the largest* exponent when referring to *the* Lyapunov exponent.

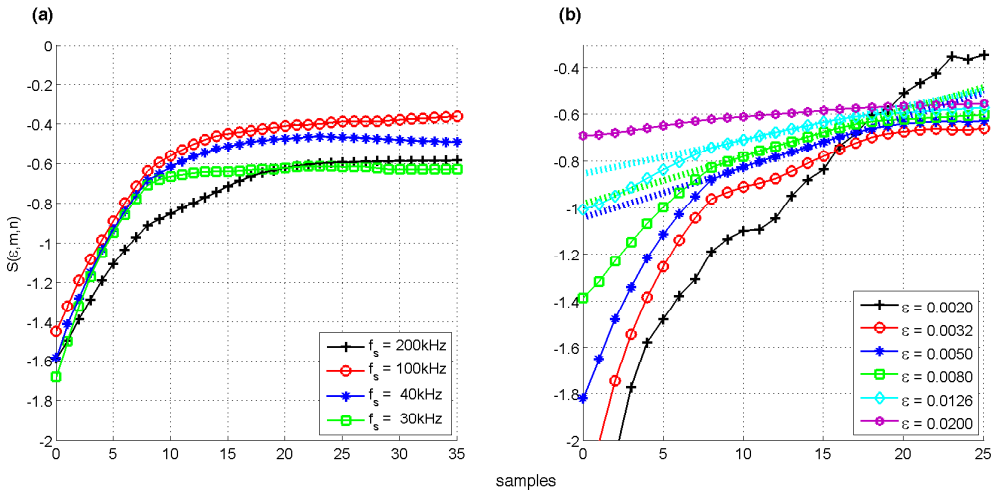

Figure 4.13: *Lyapunov estimation for different sampling rates (a). Evolution of the distances between nearby trajectories of brake vibration data over time subjected to different neighborhood diameters ϵ (b).*

The Lyapunov exponent was determined, after an appropriate embedding, by the following well-established approach [31]: for a given reference point of the embedded time series, the average of all distances to neighboring points within a neighborhood of radius ϵ is computed. Then all the so selected points are followed forward in time and the time-evolution of the averaged distances is recorded. The slope of the natural logarithm of the resulting function then gives the maximum Lyapunov coefficient. To obtain a global measure, the procedure is applied to a large number of reference points, and the local results are averaged. Formally the procedure can then be denoted as

$$S(\epsilon, m, n) = \frac{1}{N}\sum_{n_0=1}^{N} \ln\left(\frac{1}{|\,\mathcal{U}(x_{n_0})\,|}\sum_{x_n \in \mathcal{U}(x_{n_0})} |x_{n_0+\Delta n} - x_{n+\Delta n}|\right), \tag{4.8}$$

where x_{n_0} are the N reference points, $\mathcal{U}(x_{n_0})$ stands for the neighborhood of x_{n_0} with neighborhood size ϵ and Δn denotes the discrete time variables, due to the data acquisition.

The procedure can be applied successfully if the resulting function S shows linear scaling behavior for a substantial range of time. Of course scaling cannot be expected for too short times, since then the exponentially growing part of the flow does not yet dominate the other components. And also for too large lengths of time, scaling has broken down, since the idea of a Lyapunov exponent as a local measure did not apply any more. Hence, only if S shows reasonably linear scaling for a substantial interval, the maximum Lyapunov exponent can be determined from the slope in that interval.

Before the approach can be applied, one has to make sure that the sampling rate is high enough to catch the relevant dynamic phenomena. Figure 4.13(a) shows S for different sampling rates. One may see that for too low sampling rates, i.e. even for rates at about 100 kHz, a scaling range cannot be clearly identified. For larger sampling rates a scaling range shows up (black curve). This suggests that firstly the sampling rate is then high enough to include the significant interface processes, and secondly that the calculation approach for the largest Lyapunov exponent has then become self-consistent. In compliance with previous investigations, again, this is an indication that the dynamics in focus need to be acquired with a high enough sampling rate.

Another important issue in this context is the estimation of the neighborhood size ϵ (an Euclidean norm is assumed). Obviously, too small values of ϵ would render

the analysis highly erroneous, since then a too small a population of states follows to evaluate the Lyapunov exponent and measurement noise plays an overlarge role. Contrariwise, when ϵ is too large, nonlocal effects grow in importance and the approach should also fail [31]. Figure 4.13(b) gives the actual behavior of S for different ϵ. It shows that for $0.003 \lesssim \epsilon \lesssim 0.013$ the results yield about the same slope for $8 \lesssim$ n $\lesssim 18$.

This slope can be taken as an estimation of the maximal Lyapunov exponent λ when the slope indicates a linear increase with identical gradient for all dimensions m larger than some m_0 and for a reasonable range of ϵ [31]. Evidently, the characteristics of the present time series comply with the given requirements.

From the data which are used to determine the neighborhood size ϵ in Figure 4.13(b), Lyapunov exponents can thus directly be read off the slope within the linear scaling range of S. In the present estimation the largest Lyapunov exponent yields $\lambda = \emptyset$ 0.021 ± 0.004. In this result the error has been estimated from the linear regression used to obtain the slopes and is given as a measure of uncertainty or error due to the arbitrariness of selecting ϵ within the described range. The calculation was accomplished for a series of $n = 1000$ samples in non-squealing condition with a dimension $m = 8$ and a delay $\tau = 4$.

Concerning the estimation of the Lyaponov exponent in this section so far, the underlying records contain exclusively data of states in which the brake has been running in a non-squealing state. To reveal interrelations between the deterministic chaotic dynamics and the squeal behavior of the overall system, if indeed there even are some, the transition from non-squealing to squealing states has been examined in the following [16] . Therefore, a record of roughly one minute duration under unchanged external conditions has been used as a reference. Compared with the observations displayed in Figure 4.13, the only modification in terms of external brake parameters and conditions, was in the preceding load history; the observations derive from the same experiment.

Figure 4.14(a) gives results for a number of different sections while each is based on data records within early phases of this total measurement. Again a reasonable

[16] According to the restrictions concerning the dynamic overhead due to focusing on a wide dynamic range on the microscale, comprehensive analyses of squealing states were limited, see also section 3.2.3.

scaling region becomes evident. The deviation of the estimated Lyapunov exponent in comparison of that described in Figure 4.13(b) is relatively small, in this instance it yields $\lambda = \emptyset\ 0.027 \pm 0.003$. The environment size ϵ was set to the fixed value of $\epsilon = 0.005$ and the embedding parameters again were determined as dimension $m = 8$ and delay $\tau = 4$. Apparently, the underlying time series fragments are quite similar regarding their resulting slope, thus the velocity with which states in phase space diverge. After about 30 seconds within this measurement the brake did however, start to squeal [17] . Thus, within the present context the estimation of the largest Lyapunov exponent has been repeated when the brake was in a state just before squeal and after the squeal had set in (Figure 4.14).

When the brake is still non-squealing, but a posteriori it is known that squeal will appear within a short period, the behavior (Figure 4.14b) is rather similar to what was seen before. There is still a scaling range pointing to a positive Lyapunov exponent yielding $\lambda = \emptyset\ 0.029 \pm 0.004$ which is in the range of the non-squealing state, and obviously distant enough in time from the transition. However, the length of the scaling region seems to have become markedly smaller. In contrast, when squeal has set in, the scaling range disappeared (Figure 4.14(c)). From analyzing this 'approach to squeal' for a number of different measurements, the conclusion becomes evident that the length of the scaling range continuously decreases when the system comes closer to the squealing state. Squealing and non-squealing states thus seem to differ substantially with respect to their largest Lyapunov exponents: the non-squealing state has a positive exponent, which points towards underlying chaos-like dynamics, while the squealing state does not manifest positive exponents.

In part the findings correspond well with the usually accepted picture of generation of squeal: typically squeal is thought to be related to the occurrence of a limit-cycle oscillation of the brake, possibly initiated through an instability of the steady sliding state. The present finding of non-positive Lyapunov exponents in the case of squeal corresponds well to this picture, since the largest Lyapunov exponent during limit cycle oscillation should just be zero. However, the finding of positive Lyapunov exponents during steady sliding, contradicts assumptions in state-of-the-art modeling and the widespread idea of steady sliding which corresponds to a fixed-point, or

[17] The phenomenon of a brake system changing from a non-squealing to a squealing state, or vice versa, is actually quite often observed and typically attributed to the change of unknown inner or underlying variables which control unknown excitation mechanisms. E.g. the interface temperature which may influence the contact situation; or the wear state. In sum, it is assumed to be exhibited due to friction interface modifications, both local and integral.

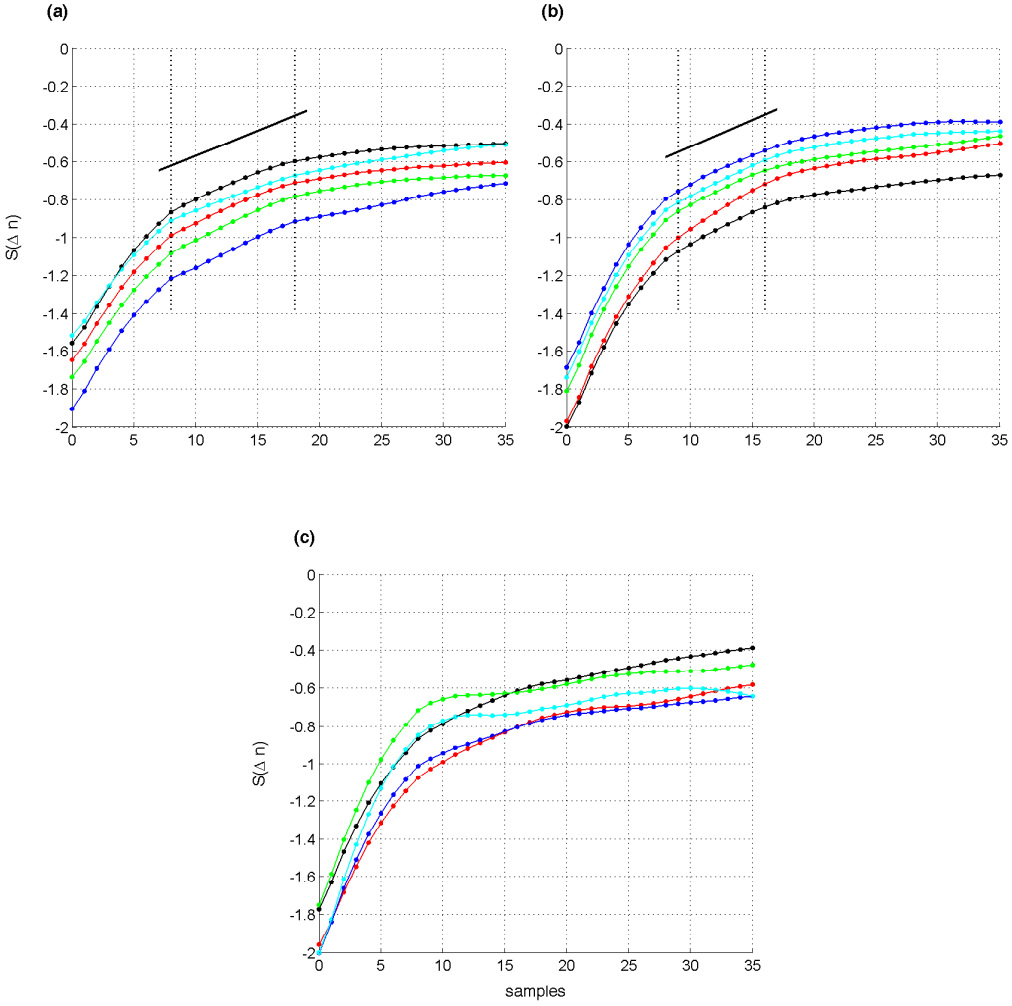

Figure 4.14: *Lyapunov exponent estimation of brake vibration data of five different sections each: in non-squealing condition (a) and in transition from non-squealing to squealing condition (b). Attempt to estimate the maximum Lyapunov exponent in squealing condition (c).*

equilibrium solution of the system. Together with the dimension estimation in the previous section, it suggests that the resulting irregular dynamics of the friction-excited system during steady squeal-free sliding are in fact based on a more or less low-dimensional strange attractor which is only slightly affected by superimposed noise. The present analysis rather indicates that the seemingly steadily sliding and non-squealing system is in fact in a state of irregular chaos-like dynamics; of course it has, on long time and large length scales, appeared stationary (see also section 4.2). But when taking into account the faster time and shorter length-scales, this

seems not to be an adequate picture.

And it corresponds well with the findings concerning the intermittent behavior during sliding which is investigated with other techniques in the succeeding section 4.4.1.

4.4 Recurrence and Intermittency

Recurrence, i.e. the state of a system coming arbitrarily close to a previous state after some time, is a very widespread phenomenon of many complex systems and is especially well known from natural systems [37, 39, 40]. The recurrence of states e.g. in nature has been known for a long time in various sciences. Some examples of phenomena at different scales are the *Milankovich Periodic Seasonal Cycles* [18] of the earth on a time scale of tens of thousands of years, irregular cycles such as the *El Niño Southern Oscillation* [19] with a cycle duration of some few years, or the recurrence phenomena in *Cosmic-ray Intensity* [20] with a periodicity of about one month.

According to the discussions about the scales that are applicable to the processes in friction interface in preceding sections, they are obviously much shorter than the above mentioned examples. Nevertheless, the techniques which are appropriate for the description of recurrences are independent from where the scales of the phenomena under consideration are located. To visualize recurrence phenomena, a usually high-dimensional state-space has to be taken into consideration [27, 28], which basically means that low-order models do fail in capturing essential properties of the arising system dynamics. Eckman et al. [17] however, first introduced a technique that overcomes the difficulty of spanning the high-dimensional state-space by introducing the approach of building up what is now typically called a *recurrence plot:* a square matrix is considered, where each axis corresponds to a time-axis. If a state

[18] Milankovitch theory, firstly presented 1924, describes large scale effects of changes in the earth's movements upon its climate: one full cycle of the earth's axis precession lasts roughly 26 000 years. Additionally, the angle between the rotational axis and the normal to the plane of its orbit exhibits a 41 000 years cycle.

[19] The El Niño Southern Oscillation is a complex, coupled system which describes the interrelation between variations in the temperature of the surface of the tropical eastern Pacific Ocean and the air surface pressure of the tropical western Pacific. It is assumed that the cycle time is twofold, a shorter cycle of about 7 years and a larger one with roughly 30 years are somehow coupled.

[20] Recurrences phenomena in the daily mean cosmic-ray intensities have shown a cycle periodicity of around 28 days; 1939 discussed by Monk.

recurs after a certain time-interval, the corresponding point in the matrix is marked, such that formally the components R_{ij} of the recurrence matrix can be specified by

$$R_{ij}^{\epsilon} = \theta(\epsilon - ||x_i - x_j||), \tag{4.9}$$

where a (possibly high-dimensional) state at a certain time t_i is denoted as x_i, ϵ is a threshold parameter, and θ stands for the Heaviside step function. If only a time series of scalar values is available, the phase space can be reconstructed by using a time delay embedding [21] , see also section 4.3.
Instead of using a threshold value, the distance between each state at a given time and the state at a later time can also be plotted directly:

$$D_{ij} = ||x_i - x_j||. \tag{4.10}$$

The resulting plot displays the distances between the states and in this way it also characterizes the recurrence behavior. This representation is usually called *distance plot* and sometimes also *global recurrence plot* [30].
The recurrence characteristics of the phase space trajectory of dynamical systems often contain single dots and / or lines which are vertical or horizontal and others run parallel to the mean diagonal, named the *line of identity* (LOI). Hereby, the diagonal lines represent fragments of the trajectory which run parallel for some time in phase space and the vertical lines symbolize sections which remain in a similar phase space region for a certain time. Single, isolated recurrence points may occur in case when states are rare or if they do not persist for any duration. They may also hint towards processes which fluctuate heavily or that are uncorrelated random.
The attributes of a chaotic, analytical system without noise, as comparison to the experimental records under consideration with noise and possibly other statistical processes, is explained using a clear example: according to the applied control parameters, Figure 4.18(a) shows a part of the time series based on the *Lorenz attractor* [22] . Obviously, in the case of appropriate control parameters, the Lorentz attractor

[21] However, it was found and has to be considered that delay embedding in some cases may produce spurious structures in recurrence plots [63].

[22] The Lorenz system is a linked system of three ordinary differential equation with real numbers a, b, c and real-valued, time dependent functions

$$\frac{dx}{dt} = \sigma(Y - X), \qquad \frac{dy}{dt} = X(\rho - Z) - Y, \qquad \frac{dz}{dt} = XY - \beta Z.$$

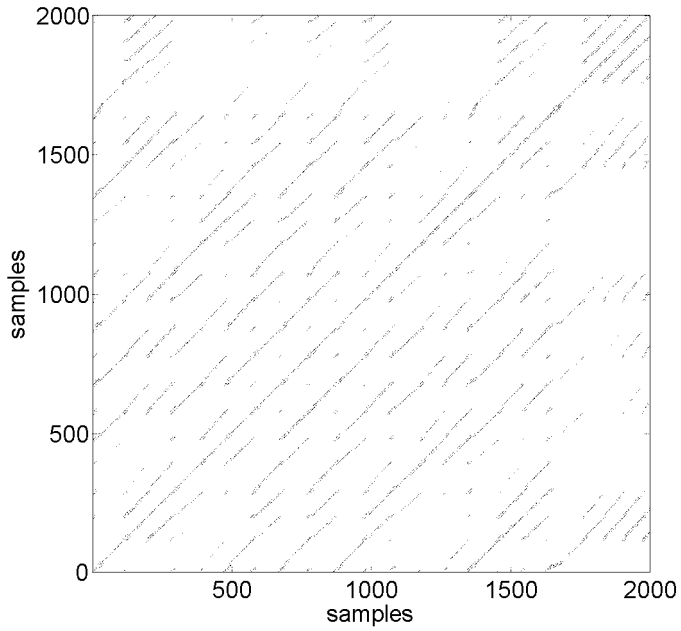

Figure 4.15: *Recurrence plot of a segment of the phase space trajectory of the Lorenz attractor with parameters* $\sigma = 10$, $\rho = 28$, $\beta = 8/3$

itself performs discontinuous: the system spends long periods close to the periodic orbit, but occasionally moves away for phases of chaotic dynamics that cover the rest of the attractor. This scenario, usually called *intermittency*, was firstly described by Pomeau and Manneville [58]. According to this characteristic, the corresponding recurrence plot manifests the intermittent behavior: Figure 4.15 depicts recurrences of a fragment of the phase space trajectory of the Lorenz system. Many short diagonal lines with a rather homogeneous distribution represent epochs in which the phase space trajectory progresses analogous to precedent or subsequent trajectories, stating that states and dynamics are similar in these periods. The discontinuous diagonal lines reveal hereby the unstable orbit of the chaotic and fully deterministic Lorenz system. In contradiction to a harmonic oscillator, the distances between the diagonal lines are not constant. The differences represent therefore the irregular periods of cycles which is characteristic for intermittent systems.

The resulting time series is displayed in Figure 4.18(a) and discussed in section 4.4.2.

To allow a thorough evaluation of the present experimental observations, again by means of recurrence analyses, the known characteristics of the Lorenz system have been rediscovered for comparison purposes. This is illustrated in the next section.

4.4.1 Recurrence Analysis

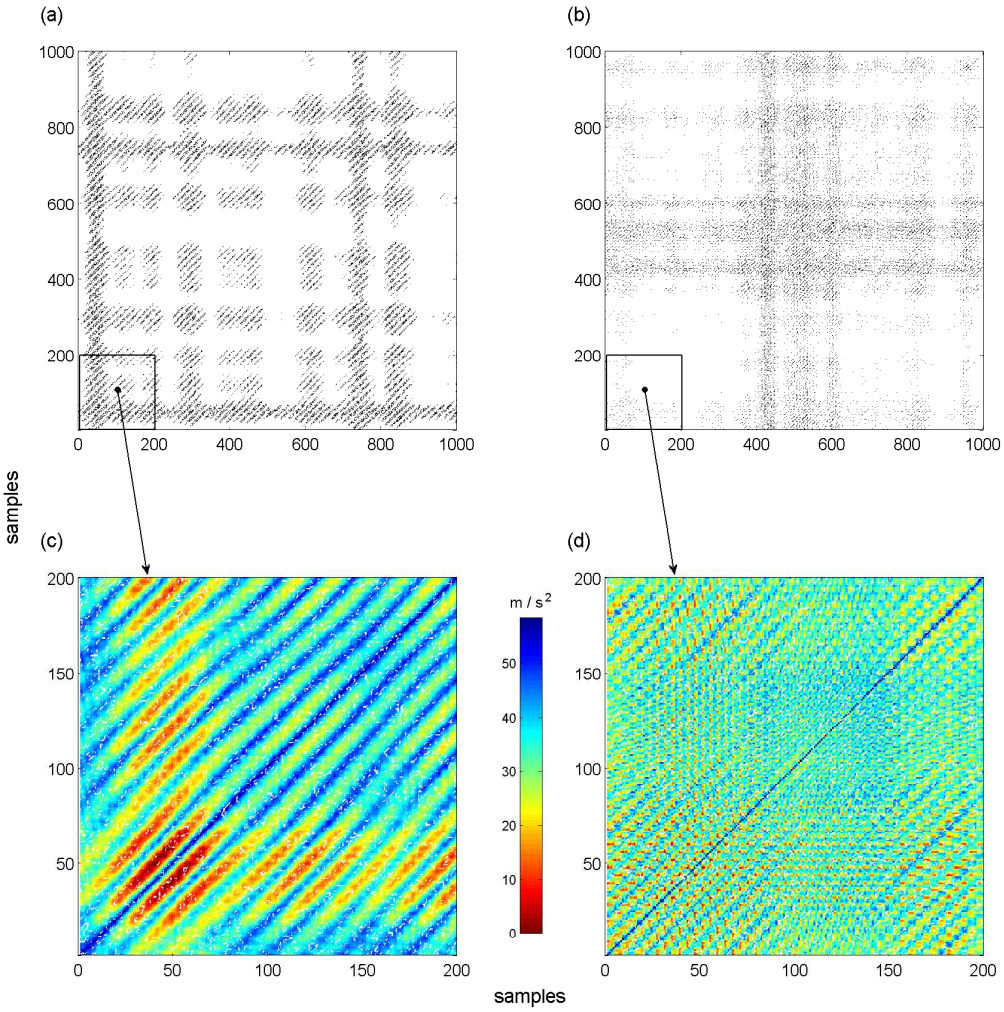

Figure 4.16: *Recurrence plots of* 5 ms *brake application at the beginning of an experiment (a) and after thermal load (b), distance plots (c, d) corresponding to the first 200 samples of (a, b)*

Unlike the *recurrence plots* of differential equation systems such as the Lorenz attractor, the recurrence plots of experimentally measured data evidently imply in addition both noise and errors of measurement. But undoubtedly, they are helpful when in-

vestigating systems without an established model, if only the impact of parasitic influences is sufficiently small. In the present context, the phase space reconstruction in section 4.3.2 suggested that the resulting dynamics are largely deterministic in the sense that remaining stochastic components seem weak.

Consequently, the recurrence plot technique, in particular developed for nonlinear deterministic dynamical systems, has been applied. Necessary for this technique is the estimation of the embedding dimensions (see section 4.4). The assessment of the dimensionality of the friction interface mechanics was described and carried out and in section 4.3.2, accordingly. For all subsequent computations thus consequently, unless otherwise indicated, a dimension of $m = 10$ has been applied.

Figure 4.16 shows typical recurrence plots of the time series friction vibration records during a drag brake application, i.e. a brake application with constant sliding speed. During this brake application the system did not exhibit squealing noise or any other low-frequency vibration, such that the vibration signal equals the broad-band background signature of steady sliding. Figure 4.16(a) represents the recurrence plot of a brake application for the duration of 5 ms at the beginning of an experiment. In contrast, Figure 4.16(b) contains the data of a brake application after roughly 1400 brake applications and a *fading* module in which the friction interface has been heated up beyond 650 °C [23] . Figures 4.16(c, d) expand the first 200 samples of Figures 4.16(a, b) on the basis of distance plots, respectively.
The recurrence plots show a number of marked features. Firstly, in Figures 4.16(c, d) there is a fine-structure of parallel, diagonally oriented lines. They basically indicate that after a state has recurred to a certain region in state space, both the original, as well as the recurring state evolve pretty much in parallel for a while, and also resemble each other again after a certain interval in time, which is a sign for (stable or unstable) periodic solutions underlying the overall dynamics. The diagonal fine-structure also shows that for most times, there does not seem to be a truly strong stochastic influence, which would lead to quick random separation of trajectories after recurrence. Interestingly, the fine-structure seems much weaker after thermal loading, which suggests that the thermal treatment provides some sort of randomizing of the resulting dynamics.

[23] Drastic load in vehicle brake testing such as the so called *fading* is a wide-spread procedure to explore the behavior and performance, both braking power and noise, of a friction brake after thermal load.

In addition and secondly, in Figures 4.16(a, b) is also a checkerboard structure in the plot: there are darker regions indicating that the system is somehow trapped in the momentary state, and there are brighter regions where trapping or recurrence is less pronounced. In analogy to fluid dynamics the states within the darker regions are sometimes called *laminar states* [39], while the states in brighter regions correspondingly might be called *turbulent states*.

Interestingly, the present visualization suggests that after about 1 ms (corresponding to about 200 samples) darker regions are disrupted, which means that on this time-scale the underlying evolution of the states deviates strongly from the previous laminar evolution. It seems plausible that these disruptions should be caused by processes in the contact interface, like e.g. break away of asperities or plateaus. Although the analysis cannot give mechanistic explanations on the specifics of the underlying processes, it does however allow to extract quantitative measures characterizing them.

Summarizing the findings: seemingly the vibration dynamics appear to be strongly deterministic and dominated by periodic processes on short time-scales and random influences do not seem to be marked. For longer time-scales of about 10 ms the system shows however, strong disruptive behavior between regular laminar and turbulence-like behavior. The conclusion in this section, that random, stochastic and parasitic influences play only a minor role in the overall dynamics, was already supported by the outcome of the estimation of dimensionality (see page 50).

Although recurrence plots allow basic inspections and deliver first essential information about the dynamics of the system under consideration, no quantitative measures are supplied. For a more comprehensive characterization, quantifying measures have been developed; this is discussed in the next sections.

4.4.2 Recurrence Quantification Analysis

Figure 4.16 represents recurrence plots in two different conditions of the brake system under consideration. In view of the enormous number of resulting patterns and features as a consequence of the large amount of corresponding states the friction interface may assume, a more comprehensive analysis and classification for consolidating the recurrence descriptions seems desirable. Hence, the concretion of the visual inspection of recurrence plots leads from the qualitative examination to a quantification of the time series. The heuristic approach to quantify recurrence plots is called *recurrence quantification analysis* (RQA). The RQA is a conceptual method

of quantifying the statistics of recurrences, therefore mainly the number and the duration of states are counted. From a chronological view it means to follow the state space trajectory of a dynamical system and to remember each state and compare it with all subsequent states. One of the main advantages of the RQA is its application for quantifying the small-scale structures of recurrence plots even for short and non-stationary data. Related efforts were firstly developed by Zbilut and Webber Jr. [74]. Subsequently the presented measures were extended with further quantifications by Marvan [41].

The particular characteristics of recurrence plots, e.g. lines , their orientation and interruptions, periodic structures and unstructured accumulations of points, all that attributes correspond to a typical behavior of the phase space trajectory (see also section 4.4). To quantify these specific features, several measures have been established [24] and some of them will be discussed in the following.
The most straightforward measure is the *recurrence rate* (RR) which reflects the density of recurrence points in a recurrence plot. With the Recurrence $\mathbf{R}$ of all points N at the according recurrence point with indices i, j it yields

$$\mathrm{RR} = \frac{1}{N^2} \sum_{i,j=1}^{N} \mathbf{R}(i,j). \tag{4.11}$$

RR hints the recurrence probability of a particular situation.
Since deterministic processes show long diagonal lines in recurrence plots, quite obviously the estimation of the percentage of recurrence points that form diagonal lines with length ℓ is a measure for the deterministic behavior and the predictability of a dynamical system. With $P(\ell)$ as the frequency distribution and ℓ_{min} as the minimum length of diagonal lines, the *determinism* (DET) can be calculated by

$$\mathrm{DET} = \frac{\sum_{\ell=\ell_{min}}^{N} \ell \; P(\ell)}{\sum_{i,j=1}^{N} \mathbf{R}(i,j)}. \tag{4.12}$$

[24] In parallel, network-based concepts have been applied within the last decades, in particular in the case of spatially extended systems to describe network dynamics. Typical measures for network-based concepts are e.g. the *link density, degree centrality, average path length* and the *local* and *global clustering* [35]. In fact, the recurrence matrix of an enclosed mechanical system and the adjacency matrix of an extended network such as neural, computer, social and transportation networks or even the global climate system are quite similar: the recurrence matrix represents the neighbors in phase space and the adjacency matrix represents the links in a network [38].

Accordingly, information about the *average* predictability of the systems is given by the *averaged diagonal line length* (L):

$$\mathrm{L} = \frac{\sum_{\ell=\ell_{min}}^{N} \ell \; P(\ell)}{\sum_{\ell=\ell_{min}}^{N} P(\ell)}. \tag{4.13}$$

As the friction interface under consideration shows significant intermittent characteristics with typical *laminar* phases (see section 4.4.1), the question of how often the dynamical system recurs in this state becomes a focal point. The answer is delivered by the measure *laminarity* (LAM): the quantity of recurrence points that shape vertical lines with length v and a minimum length v_{min} can be estimated by

$$\mathrm{LAM} = \frac{\sum_{v=v_{min}}^{N} v \; P(v)}{\sum_{v=1}^{N} v \; P(v)}, \tag{4.14}$$

where $P(v)$ is the frequency distribution of the vertical lines with length v. Evidently, LAM represents the occurrence of laminar states of the system while neglecting their length. A more informative value, in terms of the time length the system persists in a certain phase, is given by the *trapping time* (TT):

$$\mathrm{TT} = \frac{\sum_{v=v_{min}}^{N} v \; P(v)}{\sum_{v=v_{min}}^{N} P(v)}, \tag{4.15}$$

which simply computes the average length of the vertical line structures, again with length v and the minimum length v_{min}.

For the analysis of transitions within the actual friction interface time series, e.g. from laminar phases to limit cycles, the mentioned measures allow the time dependent characterization of the friction interface when windowed calculations are applied. This will be implemented in the subsequent section. Additionally, some of the RQA measures that were introduced have been consulted to characterize the dynamics and the vibrational behavior of the present brake system and will be discussed

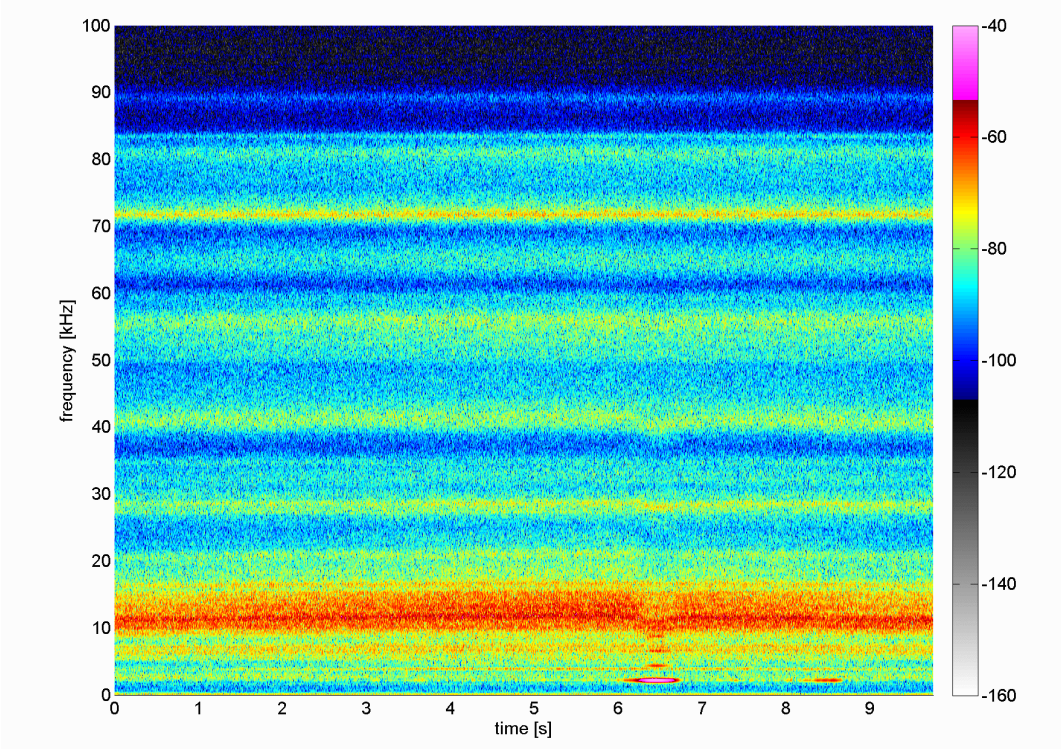

Figure 4.17: *Spectral frequency shift caused by a squeal event*

there in more detail.

4.4.3 Recurrence Quantification Analysis and Squeal Propensity

As already indicated in the introduction of this study, the causal relationship between the mechanics in non-squealing state, i.e. mechanics progressing at microsecond-scales and below, and the propensity of the system to pass into a limit cycle, thus, the squeal propensity, is still mostly unknown. Consequently, examining the corresponding states and applying describing and quantifying measures accordingly, even without knowledge of the direct causal relation, would nevertheless help to describe the systems behavior. Such describing attributes for first estimations have been already introduced in section 4.4.2.

The investigations of the precedent chapters concerning the analyses of time series characteristics have been mostly limited to measurements of the system in non-squealing states. These states have allowed a detailed view at the microscale mechanics: tuning the dynamic measurement range has permitted a high observation

accuracy even at very low amplitudes (see section 3.1). Evidently, too high (tonal) amplitudes, induced by squeal, have led to records with significant distortion. However, the present brake system has emitted brake squeal in certain preparation setups in the audible range of 2 kHz to 8 kHz. Corresponding data sections have been omitted, consequently, in preceding investigations.

Nonetheless and more detailed, squeal events with low enough vibration amplitudes that have not exceeded the dynamic range of the signal amplifiers, have been used for analyzing the system being in transition to the limit cycle and in squealing condition. In this context, squeal events with lower amplitudes have had in general only a small influence on the broad banded vibration and this impact has decreased from lower to higher frequencies. However, even though the impacts have been quite small, the squeal event displayed in Figure 4.17 at $f_{squeal} \approx 2\,\text{kHz}$ [25] between the 6th and 7th second of the recording, influenced the entire underlying dynamics. Although the influence has been somewhat small, a slight shift of the distribution is notable, e.g. close to 40 kHz. In contrast, the squeal event with the same frequency between the 8th and 9th second with a lower amplitude has had nearly no visible effect on the energy distribution in the frequency domain. This marks the threshold which decides if an examination is still reasonable: as the objective of the present work has been focused on the small-scaled underlying friction interface dynamics, the observations have only made sense so far, when guaranteeing that the influence of the surrounding (instable) brake system and signal distortion did not invalidate the evaluation. This is important in so far as the appearance of harmonics may have various sources and the shift of the high frequency content has not been adequate clarified.

Moreover, when a squeal has reached even higher amplitudes, the small scale dynamics of the friction interface have become hidden and the applied analysis techniques have not delivered further insight in the dynamics [26] . Consequently, all records have been reviewed concerning the above mentioned threshold and according observations have been rejected [27] . This has in no way harmed the study, because, as already

[25] The equidistant horizontal lines above the fundamental tone but below 10 kHz mark the harmonic components as no overtone filtering has been applied.

[26] Following the precedent considerations regarding the measurement range, foregoing experiments with higher vibration amplitudes and less sensitive amplifier inputs had revealed that that configuration had made it impossible to capture strong squeal events and the microscale dynamics in parallel. Hereby, it could not be established with certainty whether this was related to possibly completely changed mechanical behavior or simply due to the measurement setup restrictions.

[27] As it would be inappropriate to just omit some observations with too high amplitudes within a time series, in this case the entire brake application has been discarded.

revealed in section 4.3.3, there is much more information in the non-squealing condition and the dynamics in transition from this state to a limit cycle. In that context it became apparent that the deterministic dynamics in non-squealing condition, prior to their transition to the limit cycle, inherit some of the information of the very near future.

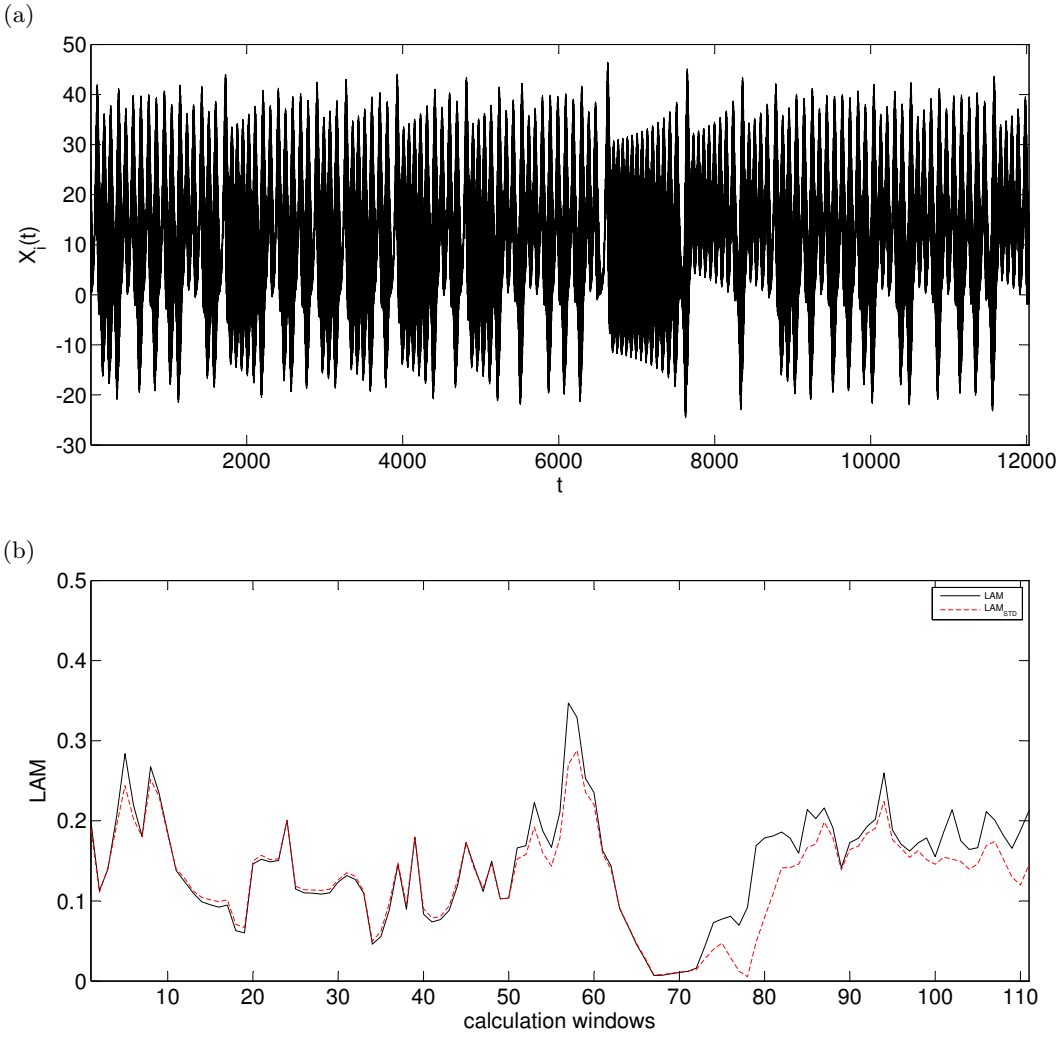

Figure 4.18: *Time series segment of the Lorenz attractor (a) and the correspondent laminarity (b); control parameters* $\sigma = 10$, $\rho = 28$, $\beta = 8/3$

Although various RQA measures, including those that are described by the Equations 4.11 to 4.15, have been tested to quantify the condition of the friction contact, especially two attributes in particular have turned out to carry most of the infor-

mation in focus. Accordingly to the flow of fluids in pipes, as an example, the flow of wear particles in the friction interface has been similarly characterized as either a more laminar flow or a stream with turbulences [19]. Vertical lines in recurrence plots have hinted in section 4.4.1 at the presence of laminar states. Based on that, the *laminarity* (LAM) and *trapping time* (TT) have been computed according to Equation 4.14 and 4.15.

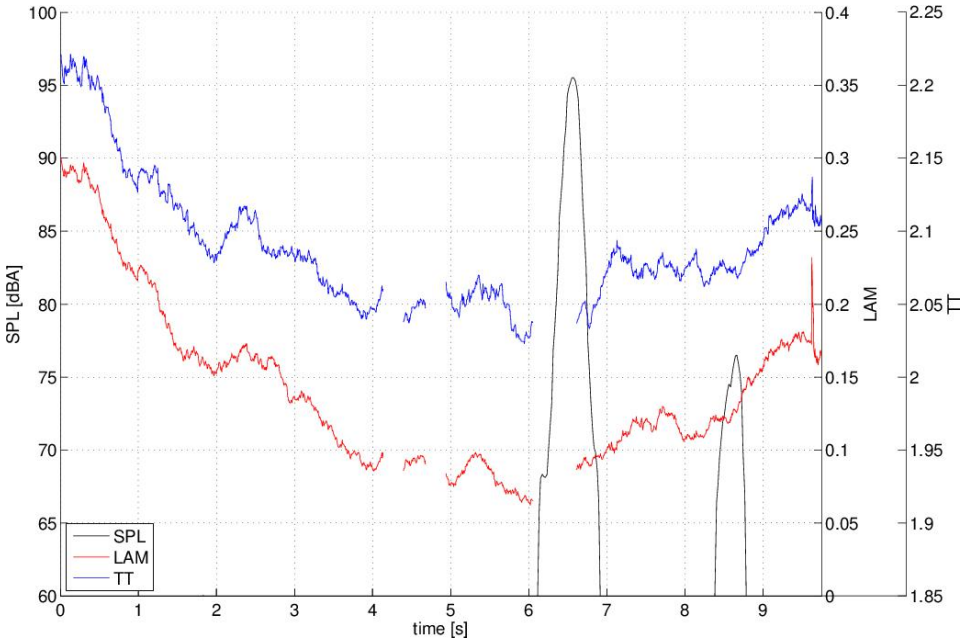

Figure 4.19: *Recurrence quantification analysis and squeal*

But firstly and for easier interpretation of the estimations concerning the experimental data, the *Lorenz attractor* with known deterministic dynamics has been considered: the correspondence between LAM (Figure 4.18(b)) and the one-dimensional time series values over time (Figure 4.18(a)) of the Lorenz system (see section 4.4) are depicted in Figure 4.18. Evidently, the intermittent behavior of the system, revealed by the related time-wise progress in Figure 4.18(a), namely, the irregular disruptions between quasi-periodic orbits, are reflected by the LAM. Values near zero indicate either disruptions or non periodic behavior or other processes quickly followed one after each other. In contrast, higher values point towards a more laminar development. In this context has to be considered that a direct and evident relationship between the time series and the laminarity cannot be expected since each LAM value is a result of computation windows comprising multiple data points. For the calculation of Figure 4.18 1000 data points have been applied, with a shift of ten samples from

window to window. Following this, the LAM does not reach higher values because one calculation window includes multiple disruptions.

As every deflection [28] of the sliding brake pad leads to an oscillation, the assumption that larger LAMs and TTs are more likely to decrease the squeal propensity, has seemed natural at first glance. Figure 4.19 displays the LAM, the TT [29] , and the squeal *sound pressure level* (SPL) exemplarily for a brake application containing a squeal event [30] . The discontinuance of the LAM and the TT parallel to the onset of the squeal with an amplitude $> 80\,\mathrm{dB}$, originated from the high vibration amplitudes which overexcited the data acquisition (see chapter 3.2 and foregoing discussion), however, in the case of the second squeal with lower amplitude, it has become obvious that the LAM and the TT have not or only slightly been affected by the presence of squeal with a low enough amplitude. Moreover, although no direct relationship between the RQA measures and the onset of instabilities has been found, the squeal has occurred when the LAM and the TT have been comparatively small. Due to many more parameters and dynamic phenomena which influence the behavior of the brake system, the context between RQA measures and the squeal propensity has not been in evidence for every state and every detail, but nevertheless, a significant trend has been observed.

Consequently, to obtain a more general idea of the interrelationships, three experiments based on *SAE2521* [11] brake test procedures were executed (details are given in chapter 3.2). Two modules each, the *bedding* and the first *noise matrix* [31] , delivered time series data for a comparison (Figure 4.20). The upper graph (Figure 4.20(a)) underlies a friction couple with a very low squeal propensity while the data depicted in the middle (Figure 4.20(b)) descend from brake pad formulations with a medium probability of squeal events. The lower chart represents an experiment with

[28] Deflections of the brake pad are supposed to have various sources, e.g.: local or global friction variations, surface inhomogeneities of the brake pad or the disk, mechanical force impacts or, more generally, modifications of the contact situation dedicated to various causes.

[29] The calculation of LAM and TT has been based on the following phase space reconstruction values: embedding $dimension = 8$, $delay = 4$, $norm =$ Euclidean, $blocklength = 1000$ samples.

[30] In contrast to the before mentioned data processing which would have omitted this brake application due to amplitudes over the threshold, in this case it is applicable since the data is not part of an overall view and the distorted parts are clearly identifiable.

[31] The bedding contains brake application starting at 80 km/h and 100 °C, ending at 30 km/h, with alternating brake pressures; the noise matrix holds drag brake applications at 3 km/h and 10 km/h with varying temperatures and brake pressures. Velocity specifications are related to vehicle speed, therefore the vehicle speed of 1 km/h equals ≈ 113 mm/s sliding velocity of the pads on the brake disk.

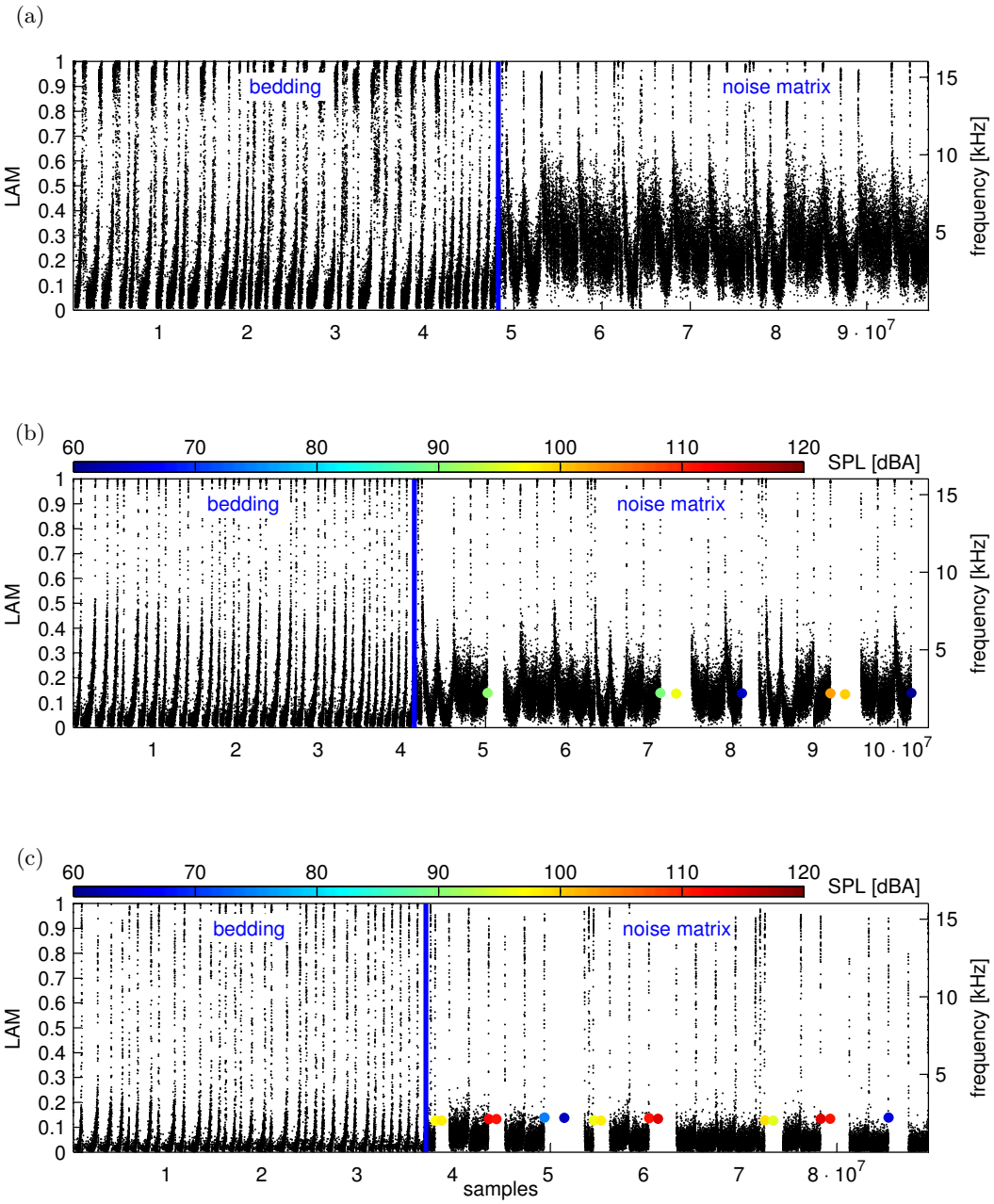

Figure 4.20: *Laminarities of three different brake pad formulations with corresponding noise events: (a) Laminarities of an almost quiet brake pad formulation, moderate quiet brake pad formulation (b) and of a noisy brake pad formulation (c); colored dots mark noise events with sound pressure levels according to corresponding colorbar.*

a comparatively high accumulation of noise (Figure 4.20(c)). Each black dot is the outcome of a laminarity calculation from 1000 samples each and the colored points reflect squeal events with the given frequency and an amplitude corresponding to the given color bar [32] . In the presence of squeal amplitude above the threshold, the laminarities are not plotted as indicated above. Regarding the calculation of the depicted laminarities, the phase space was reconstructed with an eight-dimensional embedding and the Euclidean norm was used to compute the distances between all possible vectors (Equation 4.14). Regarding the threshold cutoff ϵ that determines if a vector pair is said to be recurrent, the identification has turned out to be crucial. Various static alignments of ϵ have been examined but the correlating results then suggested to apply dynamic values. Since the system state changes, regarding the three experiments, from large to small accelerations on a scale of more than 100 dB, the most meaningful outcome was derived by adapted thresholds. In this context, the standard deviation of the analyzed time series data frames appeared as the most meaningful limit. It has to be considered hereby that on the one hand, evidently, the dynamic repositioning of the threshold impedes the comparableness of separate modules within the experiments themselves, but on the other eases to match them amongst each other.

Obviously, the shape of the laminarities in the bedding section differs significantly between Figures 4.20(a), 4.20(b) and 4.20(c). While the upper time series exhibits laminarities over the full scale from zero to one [33] , with a higher concentration in the range of zero to 0.3 and 0.8 to one, the picture at the bottom represent LAM's up to one as well but with a significantly lower quantity and most of the values stay below 0.1. The estimation of the experiment displayed in the middle shows values in between the two in a medium range, respectively. Regarding the LAM's in the *noise matrix* module, the dissimilarities are even larger. The laminarities of the

[32] Each squeal event is represented as one SPL per brake application; the highest amplitude of the recorded air-borne noise with the corresponding frequency is thereby depicted.

[33] In theory, when the laminarity equals one, it means that 100 percent of the 1000 observations within a data frame are considered to be located in the same area of the phase space. Conversely, if no laminar phases appear, the lamanarity yields zero. In this context, it must be noted that all estimations regarding the phase space and necessary heuristic values certainly play a role. The applied parameters may have in certain cases led to not-perfect adapted thresholds as the relevant values have been a compromise to cover an enormous amount of data. If the laminarity equals a value near 1, the threshold might be too large and as a consequence, observations below this threshold are regarded as being close to each other in phase space. However, in consideration of the reproducibility and comparability it has manifested that in keeping the algorithm for the threshold estimations constant, the outcome resulted in more expressive answers, when neglecting some minor inaccuracies.

quiet formulation in Figure 4.20(a) are much more pronounced than in the case of the medium and the fully noisy experiment. Seemingly, the occurrence of noises in (b) and (c) and the absence of squeal in the first case are well corresponding with the estimated laminarities: the friction couples with less squeal propensity show a higher LAM in their sliding state.

Seemingly, as a matter of fact, the detail that the characteristics of the system, namely the squeal propensity, are measurable even in non-squealing condition, is quite remarkable. Expressed in other words, this means that the low-dimensional and deterministic friction interface dynamics on a microscale, which characteristic is friction contact inherent, possess information about the probability of instabilities.

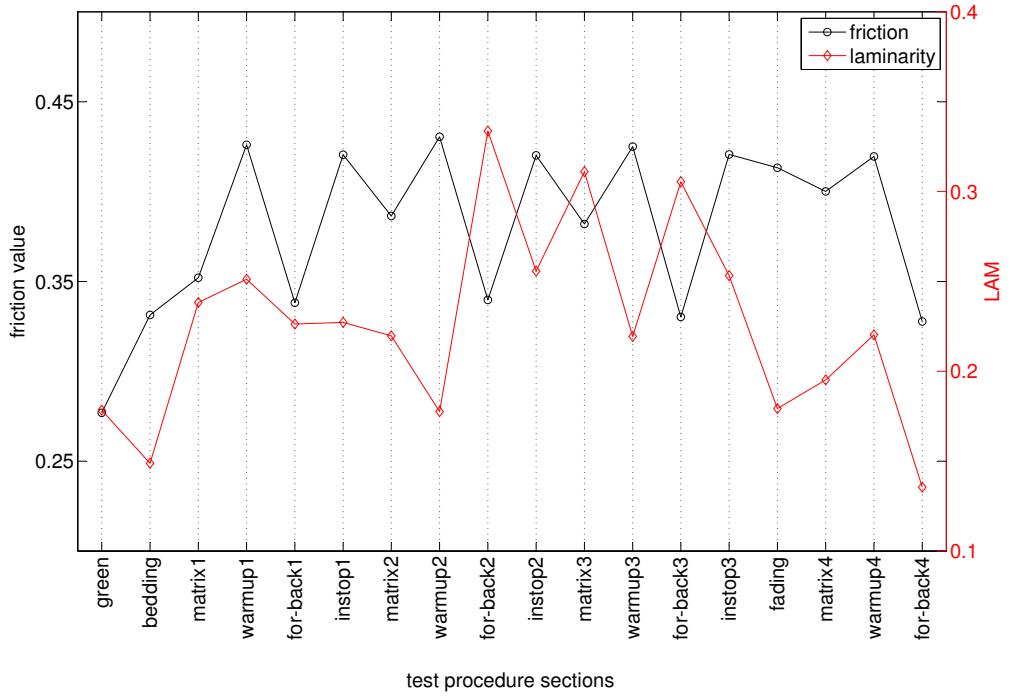

Figure 4.21: *Friction and laminarity*

Important in this context is the question whether the LAM is predominantly a reproduction of the integral friction coefficient: assuming that a high friction value, probably based on a friction interface with higher abrasive characteristic, and probably accompanied from more mechanical disruptions, would automatically lead to a lower laminarity. If so, the information retrieved from the LAM would not reveal new and independent characteristics of the dynamics.

For clarification, the LAM and the friction value, each averaged over each brake

application, was computed for a comprehensive experiment, containing an entire SAE2521 procedure with all modules.
It turned out that, contrariwise, the LAM and the overall friction value are not associated; the results are illustrated in Figure 4.21. Obviously, in some sections the laminarity follows the friction value [34] , in others its evolution moves oppositional.

4.5 Probability Density Distributions

Regarding the different scales the phenomena are located on, it has yielded that the examinations on the basis of *recurrence quantification analysis* (RQA) (section 4.4.1) have reached their limit when all scales have been included. Even in the case of a rather low dimensional embedding, for unfolding the phase space the computational costs already reached a remarkable amount. Firstly because of the high sample rate necessary to allow observations on microscales and allocate the belonging micro-mechanics, that has led to enormous high data volumes. And secondly, in consideration of the slow macroscale-mechanics, thus longer time episodes: an observation time of roughly 10 s, as a typical brake application duration, has led, together with some data-overhead, to an allocated memory size of about 40 MByte which means approximately 80 GByte of compressed data per experiment. For example, a relatively simple parameter study regarding the laminarity estimation leads to a considerable effective calculation time. On closer examination, then for this example, a single data-block with length of 1000 samples spans a memory size of about ≈ 1 GByte and applied $1e6$ times for the entire experiment culminates in a computation time, even without overlapping of data windows, of weeks for each experiment and just one parameter variation. With high-performance computers in parallel it takes still multiple days.

Other approaches that have been relevant to identify the dynamics of friction and wear in disk brakes on the basis of numerical simulations, have been completed by applying *movable cellular automata* (MCA) [44, 48, 53] or *finite element analysis* (FEA). Although the techniques have advanced significantly, the limitation of these and other approaches lies in the complex conflation of the particle flow and its dy-

[34] The friction value progression is quite typical for this kind of procedure, after establishing a nominal value, it fluctuates according to the past history and the present load.

namics on a microscale and, conversely and in combination, the necessary length scale for the description of the entire system. A simple mapping or expanding up to a macroscopic behavior seems likely to fail. And again, as indicated in previous discussions, the description of the microscale-dynamics is still not available and thus the assumptions of how the systems behave have often seemed weak concerning the simulation of real systems, especially their long-term behavior.

These considerations have guided towards an alternative and rather more on a stochastic methods based approach. Since the different length scales and their behavior in particular have played a decisive role in preceding examinations, it appeared to be meaningful to investigate the increments between the data samples for a description of the friction system. Then, the investigation of the distribution of these increments on different scales, has significantly decreased the complexity and the time required for computing and has therefore eliminated the restrictions due to the high quantity of data.

Studies from other areas dealing with different scales and their distribution, e.g. wind turbulences analyses, have described the characteristics of the air flow velocities on small, meso and large scales. In this context, the wind turbulences on small scales have been associated with statistics of anomalous large scale phenomena [57]. Further examples of time series increment examinations have dealt with stochastic analyses of the earth's vertical velocity data time series [35] [36] and the behavior of the daily increment distribution of the stock market index.

Accordingly, estimations of *probability density functions* (PDFs) that characterize attributes of the brake friction vibration have been conducted and are portrayed in the following. The distribution of discretely sampled but continuous random variable leads to a histogram which represents a discontinuous probability density distribution. The time series leads to the i-th acceleration increment Δa_i with

$$\Delta a_i = a_{i+\tau} - a_i, \tag{4.16}$$

where τ is the given sample time. The acceleration increment series then yields

$$\overrightarrow{\Delta a_i} = (\Delta a_i,\, \Delta a_{i+\tau},\, \Delta a_{i+2\tau},\, \ldots,\, \Delta a_{i+n\tau}). \tag{4.17}$$

[35] Investigations of fluctuations have reported on the correlation between the scale distribution transitions of long-range characteristics and inspections shortly prior to an earth quake and has therefore provided a precursor for earthquake detection.

The following sum counts the total number of observations n falling into each of the disjoint class with numbers k; the histogram then meets the following conditions:

$$n = \sum_{i=1}^{k} \Delta a_i, \quad \text{with} \quad a_j^l \leq \Delta a_i \leq a_j^u \tag{4.18}$$

and a_j^l, a_j^u, $(j = 1, 2, ..., k)$ as lower and upper class threshold. In general, the empirical, discontinuous distribution can be approximated by a continuous PDF through a kernel density estimator. However, for the reason that most measured values range in the interval around the mean value, or else, categories with higher increments contain data with only a few samples, continuous functions that have been applied have not been suitable in terms of insufficient converging. And precisely because the outliers have been of particular interest, the investigations have been limited to the distribution histograms of empirical data and, what is more, the underlying intervals have been kept small.

An example of a distribution of acceleration increments of a rather noisy pad formulation is given in the semi-logarithmic Figure 4.22(a). The underlying data were retrieved during a stop brake application with a brake pressure of 25 bar and pad initial sliding velocity of $\approx 5.6\,\mathrm{m/s}$ which is in accordance with a vehicle speed of 50 km/h. For comparative purpose, the curve is related to the standardized normal distribution, represented by the red dotted line, with the same standard deviation σ as the measured data. The calculation of this reference curve can be expressed as follows

$$f\left(x, \mu, \sigma^2\right) = \frac{1}{\sigma\sqrt{2\pi}} \exp -\frac{1}{2}\left(\frac{x-\mu}{\sigma}\right)^2, \tag{4.19}$$

where σ^2 is the *variance*, σ the *standard deviation* and μ the *mean* or *expectation*. Evidently, the experimental data are largely congruent with the standard distribution. Most of the difference between both curves in the neighborhood of the lower ends of the increment distribution is caused by smaller quantities of measured increments which escalate the measurement and statistical errors.

In contrast, with the same brake parameters and the same load history, a different pad formulation which has shown in general a low squeal noise propensity, demonstrates a significantly different distribution in Figure 4.22(b): above $|\sigma| \gtrsim 2.3$ the measured distribution of increments is explicitly higher than the standard deviation which means in other words, the amount of large acceleration increments is higher

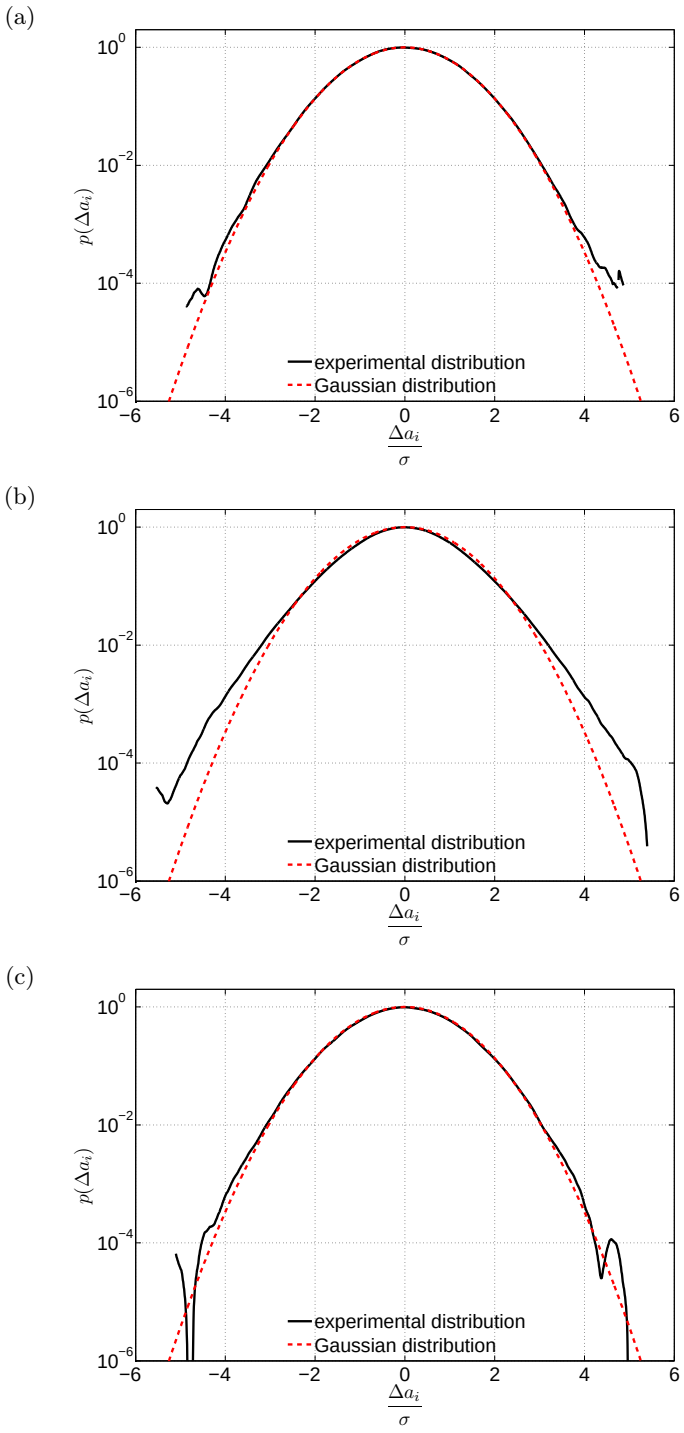

Figure 4.22: *Experimental increment probability distribution of (a) pad formulation A (noisy), (b) formulation B (quiet), (c) with the same data as (b) but under-sampled, and (a, b, c, red dotted) appropriate Gaussian distribution*

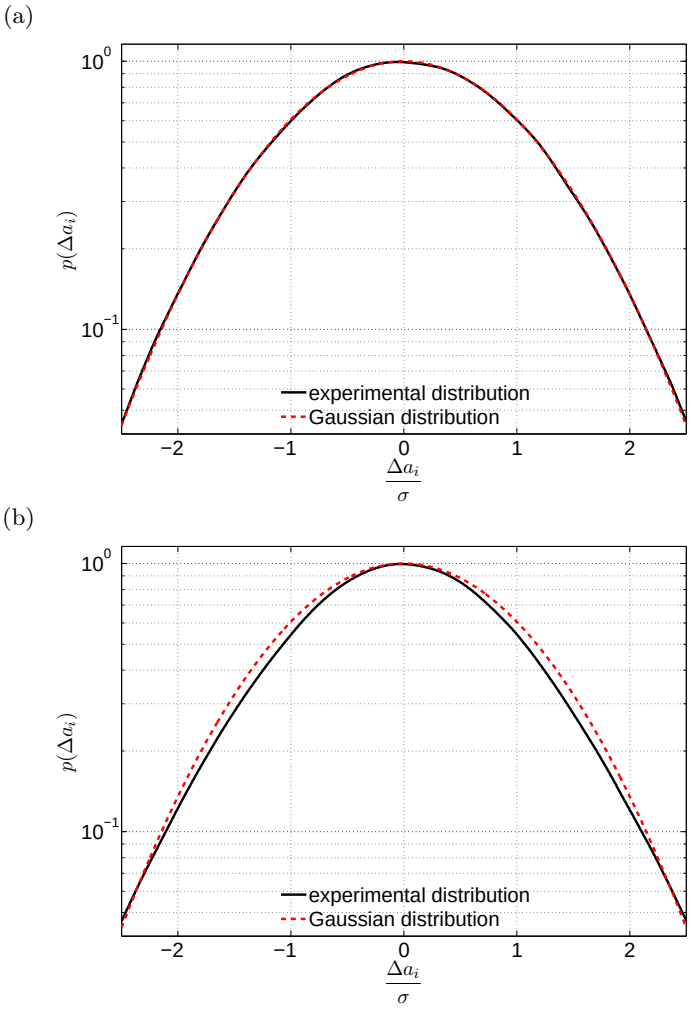

Figure 4.23: *Detail of experimental probability density distribution of increments (a) pad formulation A (noisy), (b) formulation B (quiet) and (a, b; red dotted) appropriate Gaussian distribution*

than the Gaussian propensity would propose. In parallel, because the standard distribution is aligned to the measured data by the same deviation, the propensity below $|\sigma| \lesssim 2.3$ is lower than the distribution of the standard deviation. Figure 4.23(b) displays this detail using another axes scaling. Similarly, Figure 4.23(a) displays the deviation to the Gaussian distribution for the noisy formulation and small values. In this case, the experimental data are aligned again with the standard distribution as for larger values. Evidently, in case of the low-noise formulation, two distinct acceleration ranges or scales are present: large increments occur relatively frequently, compared with the Gaussian bell curve, and small oscillations are underrepresented, in contrast. As already outlined in previous sections, the sampling rate plays an

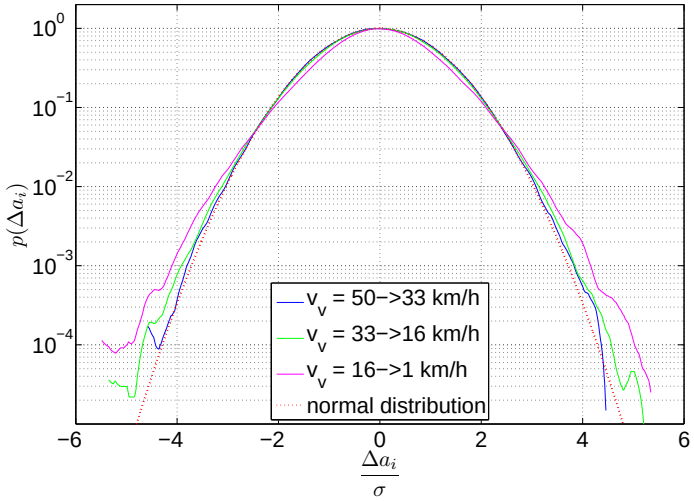

Figure 4.24: *Increment probability distribution of a stop brake application classified into separate sliding velocity classes with the given vehicle velocity v_v*

important part in terms of the system identification. Figure 4.22(c) illustrates the same data as in Figure 4.22(b) but with an under-sampled rate of $\approx 80\,\text{kHz}$. Again, the characteristics which become evident at a sample rate of $\approx 230\,\text{kHz}$ in Figure 4.22(b) are hidden in case of an inappropriate recording rate.

In the field of fluid mechanics, the alternation between phases of non-turbulent, i.e. laminar motion, and turbulences is called *intermittency*. This scenario was first described by Pomeau and Manneville [58] and termed *intermittent transition to turbulence in dissipative dynamical systems* (see also section 4.4). An intermittent mechanical system, hence, in this context, describes the characteristic of a nonlinear, dynamic system with a basically regular sliding behavior which is interrupted by short phases of chaotic dislocations.

The present distributions evidently feature the same characteristic: a high number of small increments presenting longer phases of laminar flow on the one hand, only few large increments on the other, hinting at very rarely occurring bursts. The nonlinear chaotic characteristic of the sliding motion has already been revealed by the estimation of a positive largest Lapunov exponent in section 4.3.3 and the intermittency has been accordingly examined in more detail by the recurrence investigations in section 4.4.1. Moreover, the non-normal distribution of the data supports the results, as a non-Gaussian distribution often both hints at and is essential for intermittent behavior.

Additional to the techniques in previous sections, the analyses on the basis of PDFs suggests the differentiation in multi-scale phenomena. Hence quite consequently, further investigations concerning the time scale have been accomplished. Since the friction surface dynamics are supposed to be somehow controlled by the sliding velocity, the division of the experimental observations in velocity classes seemed promising. Accordingly, the velocities [36] were split in velocity decelerations section of $v = 50 \dashrightarrow 33\,\mathrm{km/h}$, $v = 33 \dashrightarrow 16\,\mathrm{km/h}$, and $v = 16 \dashrightarrow 1\,\mathrm{km/h}$ [37] . A first approach that was undertaken, located the histogram edges at thresholds in such a way that the number of samples were evenly distributed among the velocity-classes [38] . On one hand it did not change the results significantly, but on the other hand, the edges and classes were not comparable between separate brake applications any more. Consequently, the investigation has been completed with fixed velocity thresholds as mentioned above. Figure 4.24 displays the distribution of the measured data in relation to the velocity, again associated with the Gaussian distribution. Surprisingly, the class containing the accelerations recorded at higher velocities is almost distributed in accordance with the standard deviation and the class of slower velocities shows the highest amount of large increments.

In view of the fact that the noise propensity definitely increases with decreasing velocity in general, this seems somehow contradictory to the previous findings that rather quiet formulations lead to larger deviations from the normal distribution. Possibly, additional parameters not covered by the present work, impact the increment distribution notably. Another consideration that helps to resolve the apparent contradiction deals with each of the absolute value of the standard deviations: since the actual calculations are normed to σ, its influence, regarding its absolute value, becomes hidden. In view of the standard deviation range between different brake application data of $\sigma_{max}/\sigma_{min} > 6$, additional future investigations appear necessary. Since the conducted experiments do hardly supply sufficient data for stop braking

[36] For practical purpose and to link the results to the application, the velocity indications apply to the belonging vehicle speed and not the sliding velocity (Figure 4.24).

[37] The data recording was finished at 1 km/h so that the large and abrupt accelerations emanated from the stoppage did not distort the measurement.

[38] The friction coefficient has been different in general between the pad formulations and is strongly velocity related. Consequently, every single observations features a unique friction value. According to the idea of evenly distributed quantities of data within the velocity classes among the experiments themselves, the histogram edges would have had to be aligned individually.

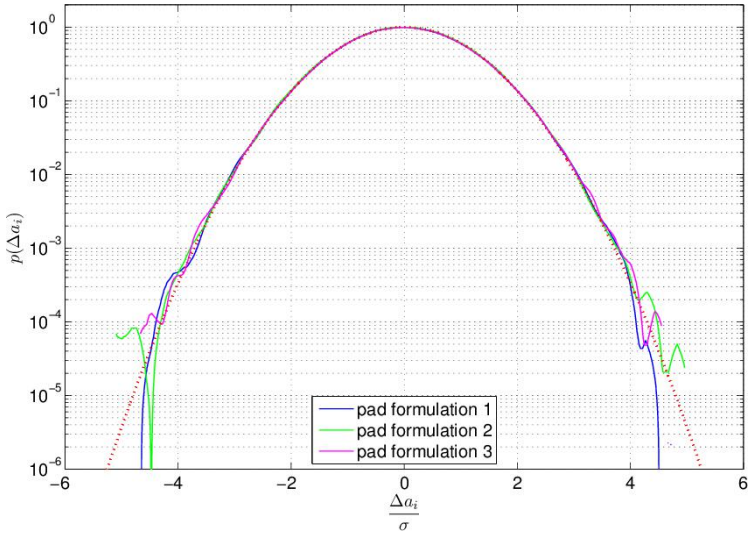

Figure 4.25: *Increment distribution of a drag brake application*

applications [39] , down to zero velocity, and with the same configurations exceptionalness without squeal in parallel for experiments under consideration, further experiments, tuned to pronounce the connection between velocity and distribution, are supposed to bring more light on this questioning.

However, with regard to low velocity drag brake applications that showed significantly smaller σ values, accordingly Figure 4.25 reflects the characteristics of the increment distribution concerning steady braking without rotational velocity change. The data are seemingly normally distributed in this case, regardless of the pad formulation.

Following the examination of the data, a further characteristic of the friction interface has been pronounced. Based on the development of distributions during the experiments, the transformation of the friction interface has become apparent. What the visual inspection of the very first brake applications in section 4.1.1 and the delay vectors in section 4.3.1 already confirmed, namely, that the friction interface has constituted rapidly from the very beginning of the sliding, the increment distribution

[39] Due to the fact that vehicle brake squeal issues predominantly occur at small velocities, the attention is focused on this range. Therefore most commonly, bench tests for noise investigations provide drag brake applications by operating the brake against the drive train. The applied *SAE2521* [11] is a bench test designed for brake noise investigations. It comprises brake applications that do not end at 0 km/h, stop and drag brake applications while the latter accounts for more than 75% of the total brake applications. Even though the drag brake applications are rather rare in the technical application, except in mountainous areas, they are known as being more critical in terms of searching unwanted noise behavior.

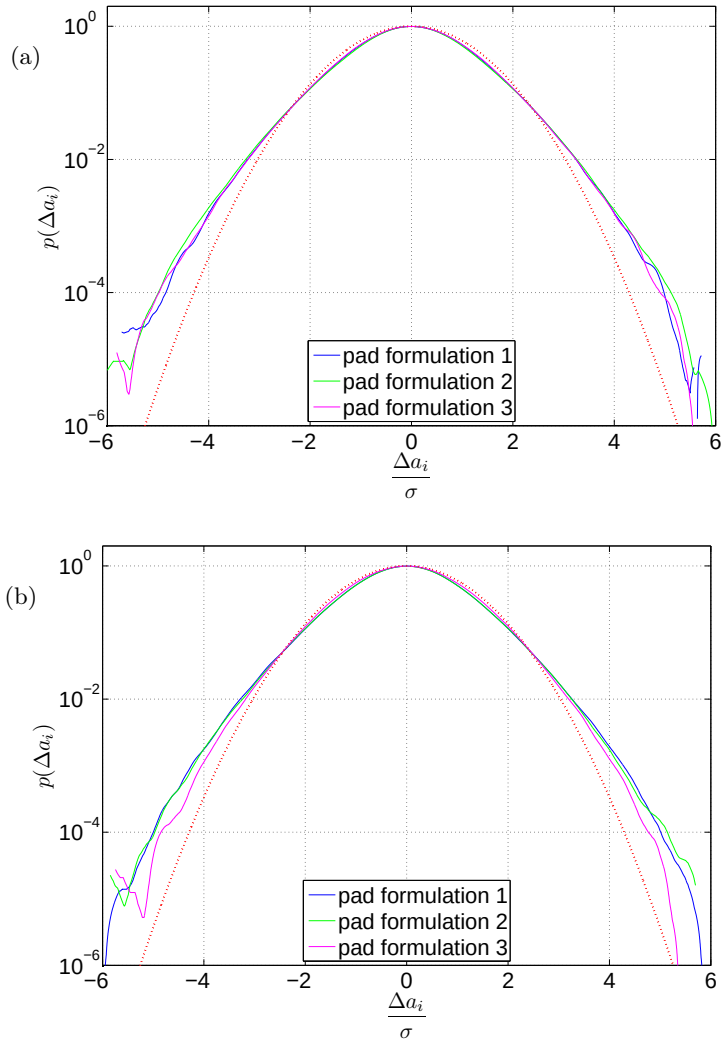

Figure 4.26: *Increment probability distribution at the initiation of the respective experiments, (a) step no.3, (b) step no.10, of three different pad formulations, (1) quiet, (2) moderate noisy, (3) noisy*

substantiate these findings. The distributions of three pad formulations at the beginning of a respective experiment are depicted in Figure 4.26. The upper graph holds the observations at brake application number 3 in Figure 4.26(a) and number 10 in Figure 4.26(b) [40] . While the increment distribution at the foremost point of time and less sliding distance is definitely not normally distributed, the magenta colored

[40] The numbers are consecutively numbered and refer to the international standard bench procedure SAE2521 [11] in which both brake application 3 and 10 are in the section *green* or *bedding* with decreasing appropriate vehicle velocity from $v = 80$ km/h to $v = 30$ km/h.

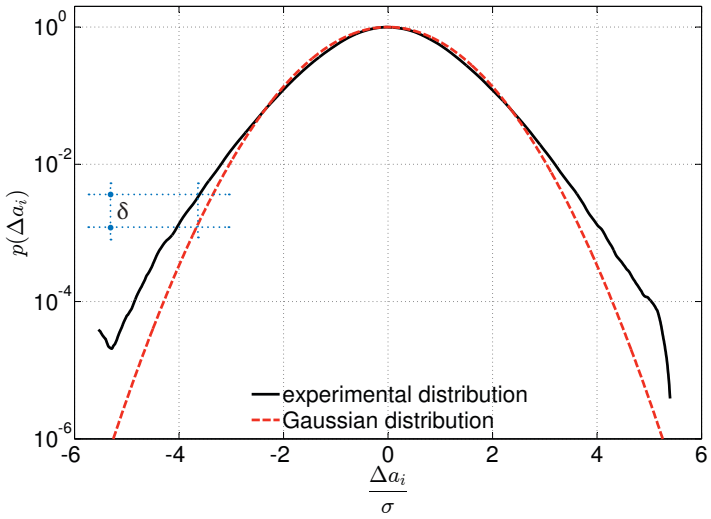

Figure 4.27: *Measure δ to indicate deviation between experimental data and Gaussian distribution*

curve in the lower picture, representing an instant of time with higher covered sliding distance, by contrast already tends towards the Gaussian curve. Not surprisingly, the magenta colored line represents a noisy pad formulation which mostly fits later in the experiment, and after a large sliding distance, the dotted red line. Thus, it becomes normal distributed.

In turbulence investigations fit functions are rather commonly used to describe and convert the discontinuous increment distributions into a continuous PDF. Whereas in case of the present data, the parameters that control the increment distribution and their quantification are unknown, another method has been applied in the current context. The measure δ was introduced which describes the deviation between the experimental data and the Gaussian curve at a fixed distance from the mean value. Therefore, the measured data were piecewise linearized and then simply the absolute value of the deviation to the normal distribution has been calculated by

$$\delta = \left| \frac{1}{\sigma\sqrt{2\pi}} \exp -\frac{1}{2} \left(\frac{x-\mu}{\sigma} \right)^2 - y_{lin}(t) \right|, \tag{4.20}$$

where σ is the *standard deviation*, μ the *mean* or *expectation*, y_{lin} the *linearized data*, t the *threshold* and δ the introduced measure. The principle is illustrated in Figure 4.27. The measure is useful for describing the friction interface conditions through a singular value, either for entire brake applications (averaging) or for data fragments. To characterize the development of the deviation during a brake application,

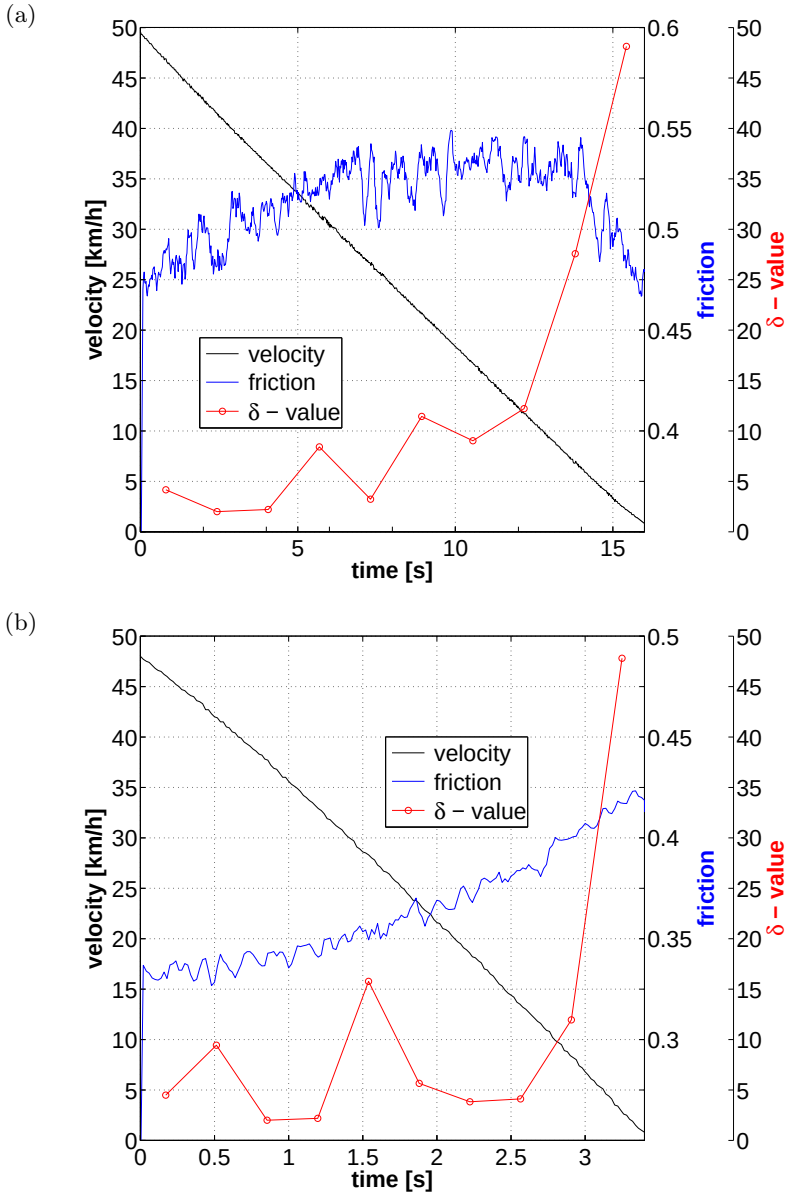

Figure 4.28: *Stop brake application examples (a) and (b), measure σ (red), friction coefficient (blue) and velocity (black) over time, velocity as corresponding vehicle speed*

segmentally calculated δ - values were applied to two different brake applications, depicted in Figure 4.28. In both the upper and the lower figure stop brake applications were examined, initial corresponding vehicle velocity (black curve) was 50 km/h, decreasing during braking to near 0 km/h. The blue line gives each the global friction coefficient, respectively. Figure 4.28(b) confirms as generally expected a moderately rising friction with decreasing velocity. Figure 4.28(a) in contrast displays a rather

uncommon behavior. The friction value initially increases at the beginning of the brake application but later, after some seconds and a corresponding sliding distance, decreases with the turnaround at a velocity of approximately 7 km/h.
Notwithstanding this difference concerning the global friction, the δ - value shows in either instance a similar characteristic. In a first approximation the curves exhibit a rather exponential progression, but much more meaningful is the strong increase above about 10 km/h. This velocity value is considered to somehow prove a threshold [41] at which a brake system is supposed to substantially ramp up its noise propensity. It appears that, the introduced value δ is a direct attribute linked to the probability of the friction interface to promote the system in transitioning to an instability. Even more remarkable is the fact that this is seemingly separate from the development of the friction value. Obviously, the foregoing evaluation suggests, that the intermittent behavior of the friction contact mechanics, which is indirectly expressed by the attribute δ, is correlated with the friction dynamics tendency to trigger brake squeal.

[41] The given vehicle velocity threshold is somewhat weak in terms of the actual sliding speed of the brake pad which depends on the brake system geometry. But it reflect a good approximation of the velocity at which brake systems typically exhibit a behavior turnaround. Brake squeal at higher velocities is almost never an issue.

Chapter 5

Conclusion and Perspective

In the preceding chapters, friction interface dynamics with specific regard to brake squeal generation has been analyzed. The initial point was the implementation of experiments, whereby the object of study, the friction contact mechanics, has been a mechanical subsystem of a commercial vehicle brake, assembled on a dynamometer. The following investigations have been accomplished:

- friction surface examination
  - visual inspection
  - topographical imaging
  - roughness estimation
  - friction film investigations
- vibration data
  - linear spectral analyses
  - nonlinear time series analyses
    - estimation of dimension
    - Lyapunov exponent estimation
    - recurrence analyses
    - recurrence quantification analyses
  - probability density distributions

At the beginning, analyses of the brake pad and disk surfaces revealed the importance of vibration sampling rates in the ultrasonic range to cover the friction interface dynamics, which evidently belong to a microscale. Additionally, physical and chemical transformations of the friction interface during the experiments have been discovered, showing clearly that even when the alteration is quite smooth from one brake

application to the next however, all of the brake applications have been unique concerning the surface topologies and the friction film coating on the disk. This picture was also supported by the spectral analyses of the vibration data in non-squealing condition which illustrated the conversion over time and from one brake application to subsequent brake applications, even though the spectral distribution seems to be quite steady on time scales of seconds. By means of zooming time-wise into the mechanics through increasing the time resolution of the vibration data and on the basis of recurrence analyses, an *intermittent* behavior on smaller time scales has become obvious. The intermittency was in particular represented by longer *laminar phases* which have been seemingly randomly and abruptly disrupted by vibration bursts, whereby the bursts themselves proved a general short duration and afterwards were again replaced by laminar phases, and so forth. This is in contradiction to the widespread assumption, that the sliding motion without squeal ought to be a stable equilibrium point and thus would be stationary [55, 43]. Instead, the estimation of the largest Lyapunov exponent has shown signatures of chaos also during seemingly steady sliding, definitely without squeal occurrence or other large scale periodic motion. In contrast to the generally idea that a (squealing) limit-cycle appears due to an instability of a steady sliding state [24], i.e. a fixed point in terms of dynamical systems, the present analysis rather suggests a different point of departure: the state that is assumed to equal steady sliding shows characteristics of chaotic dynamics, and further, that the transition between quiet steady sliding and audible squeal is the generation of a limit-cycle from a state bearing strong characteristics of chaos. Other just recently submitted investigations dealing with brake dynamics during non-squealing condition and brake squeal, following the traditional thinking, have been suggested by Oberst and Lai [46]. Based on experimental data they have proposed that the analyzed steady sliding results as a static equilibrium solution. This is not in contradiction to the findings of the present work. Several experiments as part of this study have proven that the deterministic chaotic behavior of the friction interface dynamics becomes hidden when the information of the microscale structures is neglected. This has been mainly the case in the considered previous studies, experimental records obviously have not been expanded in the ultrasonic range.

In contrast, the present findings rather suggest that small and smallest scale mechanics of the friction interface, formed, among others, by wear particles of indeterminable quantity and unknown passive and active degrees of freedom, move in non-squealing condition in sum as a chaotic deterministic mechanical system. This definitely does not equal an equilibrium or steady sliding. In a more far sense this observation corre-

sponds with other findings in the context of surface dynamics in steady sliding [6, 52].

Regarding the squealing state conversely, in the present study irregular, chaotic squealing has not been detected. The suggestion of Oberst and Lai [47], that the squealing state itself inherits chaotic behavior, is not supported by the present evaluations. Whilst the scaling region pointing to a positive Lyapunov exponent became markedly smaller when transitioning from chaotic non-squealing vibration to the onset of squeal, and then, when squeal has set in, the scaling range disappeared. When analyzing this 'come within reach of squeal' for several transitions, evidently, the length of the scaling range continuously decreased when the system came closer to the squealing state. Squealing and non-squealing states thus differ extensively regarding their largest Lyapunov exponents: the non-squealing state has a positive exponent pointing towards underlying chaotic dynamics, while the squealing state does not exhibit positive exponents. The seeming contradiction can again be derived from the difference of the underlying data. The present conclusions have been obtained from records with high detailed temporal (thus spatial) resolutions, clearly pointing out the necessity of including microscales to discover the small-scale dynamics. The Lyapunov coefficient estimation and also other investigations of the present work, even with much different approaches and techniques, have revealed the same fact: the assignment of a sufficient large enough sample rate is crucial. The attempt of a phase space reconstruction with a sampling rate too low has therefore failed. Additionally, the estimated largest Lapunov exponent is only positive for firstly, a significant duration within the time series and secondly, for a record frequency considerably above 100 kHz, below no clear scaling range appears.
Beyond a squeal regime with chaotic characteristics, Oberst and Lai [46] have additionally found that squeal is also possible without presence of chaos. But simultaneously they admit, that this estimation might also be the consequence of too fast processes which their experimental equipment would not have allowed to observe. This does rather not provide a satisfying answer to harmonize the findings, instead it outlines again the impact of small scales. As undersized acquisition resolution tends to mask phenomena at the involved scales, further investigations with possibly even higher sampling rates ought definitely to shed more light on open inconsistencies and to promote defining a minimum sufficient scale.

While the phase space reconstruction and the Lyapunov coefficient characteristics of non-squealing states indicate the presence of a strange attractor in phase space, the

estimation of a suitable embedding dimension has revealed that the attractor features only low dimensionality. Seemingly, parts of the friction interface, e.g. wear particles that are connected with each other in a specific way, may couple synchronous and form the entire mechanical system. This leads then obviously to a low number of active dimensions regarding the complete friction interface system on the macroscopic scale. Analogous to these results, patch synchronization mechanisms of friction interface patches have been already suggest by Dombek and Ostermeyer [15]. However, their concept has been mainly specified for the initiation of the squealing mechanism which emerges from the dynamical interaction of the friction partners.
Furthermore, the phase space reconstruction of a friction couple that exhibited a generally high squeal propensity, has demonstrated an additional decrease of the estimated active dimensions. The smaller number of active dimensions thus obviously leads, when viewed in a stochastic light, to a higher propensity that the system transitions from (quiet) low-dimensional chaotic dynamics to a limit cycle. Apparently, the condition of the friction contact and the alternation of the friction interface influences the characteristics of the friction dynamics, e. g. changes the dimension of the underlying mechanical system. In any case, it remains a system with a remarkable low number of dimensions. Concerning the estimation of dimensionality, it has been seen from the results that the deterministic approach works surprisingly well, stochastic processes seem to play only a tangential role. Therefore, the incorporation of stochastic aspects in the phase space reconstruction has remained open for possible future studies.

In recognition of the results regarding the recurrence in phase space and the intermittent behavior of the *laminar sliding*, the analyses have been extended on the basis of further time series data characterization with attributes of the *recurrence quantification analysis* (RQA). At this, the investigations in particular have been based on well established measures: the *laminarity* and the *trapping time* [1] [41]. Therefore, three different experiments on a relatively large time scale of a couple of hours or approximately 250 brake applications have been executed. Three distinct pad formulations have been applied, different in particular regarding their squeal propensities. The evaluation has made evident that the laminarity significantly corresponds to the

[1] The laminarity corresponds with the amount of laminar phases, characterized by only minor phase changes below a certain threshold and the trapping time measures the average duration of the laminar phases, i. e. how long the system remains in a specific state.

squeal propensity in the way that the larger the laminarity, the less squeal occurs. Surprisingly, this has been already observed from the very beginning of the experiments, respectively. Even on smaller time scales of seconds, a decreasing laminarity and trapping time during a brake application matched with an upcoming noise event. This denotes in other words that the small scale friction interface dynamics controls the noise behavior of the overall system, and is, what is new so far, measurable.
Furthermore and rather remarkable in this context is the fact that the laminarity appears to be independent from the overall friction value. Generally suggestions (e.g. [26]) that have claimed that the friction level (of the entire friction surfaces, thus the complete pad contour, not local friction) is the main trigger for friction induced vibrations because mode-coupling occurs beyond a certain threshold. Obviously, this expectation has to be extended. Certainly, as a basic principle, higher friction coefficients lead to higher noise propensity, but, as shown in the present work, the small scale dynamics definitely have to be taken into account as well.

Regarding the intermittent behavior of the vibration during sliding, identified by the investigations so far, a further and different approach to substantiate the findings has proven to be appropriate. Firstly, as a non-Gaussian probability density distribution is an indication of intermittency [13], the time series data should manifest a deviation from the normal distribution. Secondly, since the statistics of velocity increments in (wind-) turbulence (as an example) is found not to be Gaussian as well [57, 13], the dynamics in the friction interface were supposed to exhibit similarities with turbulent flows. Consequently, the increment distributions of the time series vibration data of the sliding pad have been analyzed with respect to the Gaussian distribution on different scales, respectively. It has turned out that basically, the increment distributions deviate from the normal probability curve. This is a hint to the intermittent character of motion. In more detail, the deviation on small scales is negative which means that small increments and events are underrepresented in the experimental data, with respect to white noise, and large increments are much more often observable.

But moreover and rather surprisingly, the deviation between experimental distribution and the bell-shaped curve seems to be a measure for the trend of the noise propensity of the pad formulation. Since formulations known to be rather noisy possess an increment distribution which is nearly congruent with a white noise distribution curve, in contrast, quiet formulations demonstrate characteristics significantly dissimilar in comparison with the Gaussian curve. Even when it does not look like complying with previous results, it actually is in congruence with the findings of the

RQA, namely, that small increments refer rather to laminar phases and large increments correspond with the intermittent bursts or disruptions of motion in the friction interface. In this context, it must be taken into consideration that the concept of the laminarity is unlike the idea of counting and classifying increments: the laminarity counts the number or ratio of laminar phases in which the distance in phase space stays below a certain threshold. This certainly says nothing about the magnitude of possible bursts in between. In other words, the presence of extreme disruptions which form the tails of the increment distribution curves does not contradict the characteristic of laminar phases of motion. Surprisingly, the presence of disruptions obviously retards the system in generating self-induced vibrations. The mechanism probably inherits similarities to well known inhibitors applied in the same matter but with a different technique: squealing brake pads which are exposed in an appropriate way to narrow-banded structure-born noise, become quiet [66]. Obviously, this is analogues to the present study in which extreme but short events within a rather laminar movement impede the dynamics to transit from chaotic motion to limit cycles, and thus squeal.
In conformance with the remarks regarding the independence between the laminarity and the overall friction coefficient, the deviation from the Gaussian distribution and the friction is also not linked. Contrariwise, to a greater degree and rather remarkably, the relative value of deviation is almost directly following the general noise propensity regarding the velocity dependence. Since the typical noise emitting vehicle velocity range is known to be, very roughly and based on experience only, below 10 km/h, the deviation from the normal distribution behaves proportional on this and increases exponentially, similar to the rather 'universal' noise tendency. This is in that sense new that noise propensity has not been measurable yet. Consequently, the possibility of determining noise propensities of brakes even in non-squealing condition shows potential and might promote brake noise refinement and instability prediction. Additionally, it might help to accelerate the development of noise free brakes in the automotive industry and possibly could assist to overcome today's practice: the principle of trial and error, beside heuristic knowledge, has still remained rather common.

In summary, the discussed approaches ought firstly to provide a further fragment to the general understanding of friction mechanics and are supposed to give some new answers to the fundamental questions. And secondly, with a more in particular focused view on friction induced vibrations and noise propensity, tools for characterizing and identifying the friction mechanics and their tendency to lead to instabilities,

have been presented. Even though the experimental elaborations cover a particular brake application and therefore might not be generalized in a too comprehensive sense, nevertheless these first findings in the field of deterministic friction vibration seem to be quite promising. Further investigations on this path that are capable to close the above discussed uncertainties and knowledge gaps, would definitely be meaningful.

Bibliography

[1] H. Abendroth and B. A. Wernitz. The integrated test concept: Dyno - vehicle, performance - noise. *SAE Technical Paper*, page 2774, 2000.

[2] A. Akay. Acoustics of friction. *Journal of the Acoustical Society of America*, 111:1525–1548, 2002.

[3] R. Allgaier, L. Gaul, W. Keiper, and K. Willner. Mode-lock-in and friction modelling. *Computational Methods in Contact Mechanics IV. Southampton: WIT Press*, pages 35–47, 1999.

[4] I. Baillet, V. Linck, S. D'Errico, B. Laulagnet, and Y. Berthier. Finite element simulation of dynamic instabilities in frictional sliding contact. *Journal of Tribology*, 127:652–658, 2005.

[5] I. Balogh. The formation of spherical particles under abrasive conditions. *Periodica Polytechnica Mechanical Engineering*, 46:29–35, 2002.

[6] J. Behrendt, C. Weiss, and N. P. Hoffmann. A numerical study on stick-slip motion of a brake pad in steady sliding. *Journal of Sound and Vibration*, 330:636–651, 2010.

[7] O. Ben-David, G. Cohen, and J. Fineberg. The dynamics of the onset of frictional slip. *Science*, 330:211–214, 2010.

[8] F. Böttcher, S. Barth, and J. Peinke. Small and large scale fluctuations in atmospheric wind speeds. *eprint arXiv:nlin/0408005*, 2004.

[9] F.P. Bowden and D. Tabor. *The Friction and Lubrication of Solids*. Number Bd. 1. Clarendon Press, 2001.

[10] F. Chen. Automotive disk brake squeal: an overview. *International Journal of Vehicle Design*, 51:39–72, 2009.

[11] SAE Brake NVH Standards Committee. SAE2521 - Disc and drum brake dynamometer squeal noise matrix standard. *Society of Automotive Engineers (SAE)*.

[12] A. Culla and F. Massi. Uncertainty model for contact instability prediction. *Journal of the Acoustical Society of America*, 126:1111–1119, 2009.

[13] P. D. Ditlevsen. *Turbulence and Shell Models*. Cambridge University Press, 2010.

[14] A. I. Dmitriev, W. Österle, H. Klošs, and G. Orts-Gil. A study of third body behaviour under dry sliding conditions. comparison of nanoscale modelling with experiment. *Estonian Journal of Engineering*, 18(3):270–278, 2012.

[15] D. Dombek and G.P. Ostermeyer. Modelling of lateral oscillations in the interface of brake systems. *PAMM*, 9(1):293–294, 2009.

[16] J. P. Eckmann, S. Kamphorst, Oliffson, D. Ruelle, and S. Ciliberto. Lyapunov exponents from time series. *Physical Review A*, 34:4971–4979, 1986.

[17] J. P. Eckmann, S. O. Kamphorst, and D. Ruelle. Recurrence plots of dynamical systems. *Europhysics Letters*, 4:973–977, 1987.

[18] M. Eriksson and S. Jacobson. Tribological surfaces of organic brake pads. *Tribology International*, 12:817–827, 2000.

[19] M. Eriksson, J. Lord, and S. Jacobson. Wear and contact of brake pads: Dynamical in-situ studies of pad on glass. *Wear*, 249:272–278, 2001.

[20] B. F. Feeny and J. W. Liang. Parametric identification of chaotic systems. *Journal of Vibration and Control*, 4:405, 1998.

[21] A. M. Fraser and H. L. Swinney. Independent coordinates for strange attractors from mutual information. *Phys.*, Rev. A 33, 1986.

[22] M. Graf and G. P. Ostermeyer. Instabilities in the sliding of continua with surface inertias: An initiation mechanism for brake noise. *Journal of Sound and Vibration*, 330:5269, 2011.

[23] R. Hegger, H. Kantz, and T. Schreiber. Practical implementation of nonlinear time series methods: The tisean package. *CHAOS*, 9:413–435, 1999.

[24] H. Hetzler, D. Schwarzer, and W. Seemann. Analytical investigation of steady-state stability and hopf-bifurcations occurring in sliding friction oscillators with application to low-frequency disc brake noise. *Communications in Nonlinear Science and Numerical Simulation*, 12(1):83–99, 2007.

[25] N. P. Hoffmann and L. Gaul. Friction induced vibrations of brakes - research fields and activities. In *SAE 2008-01-2579*, 2008.

[26] J. Huang, C. Krousgrill, and A. Bajaj. An efficient approach to estimate critical value of friction coefficient in brake squeal analysis. *Journal of Applied Mechanics*, 74 (3):534–541, 2006.

[27] R. A. Ibrahim. Friction-induced vibration, chatter, squeal, and chaos - part i: Mechanics of contact and friction. *Applied Mechanics Reviews*, 47:209, 1994.

[28] R. A. Ibrahim. Friction-induced vibration, chatter, squeal, and chaos - part ii: Dynamics and modeling. *Applied Mechanics Reviews*, 47:227, 1994.

[29] S. Jiang and Y. Zheng. A contact stiffness model of machined plane joint based on fractal theory. *Journal of Tribology*, 132:011401, 2010.

[30] C. L. Webber Jr. and J. P. Zbilut. Recurrence quantification analysis of nonlinear dynamical systems. In *Tutorials in contemporary nonlinear methods for the behavioral sciences, 26-94*. M. A. Riley and G. C. Van Orden (Eds.) Retrieved from http://www.nsf.gov/sbe/bcs/pac/nmbs/nmbs.jsp, 2005.

[31] H. Kantz and T. Schreiber. *Nonlinear Time Series Analysis*. Cambridge University Press, 2004.

[32] M. E. Kartal, D. M. Mulvihill, D. Nowell, and D. A. Hills. Measurement of tangential contact stiffness in frictional contacts: The effect of normal pressure. *Applied Mechanics and Materials*, 70:321–326, 2011.

[33] M. B. Kennel, R. Brown, and H. D. I. Abarbanel. Determining embedding dimensions for phase-space reconstruction using a geometrical construction. *Physical Review A*, 45:3403–3411, 1992.

[34] N. M. Kinkaid, O.M. O'Reilly, and P. Papadopoulos. Automotive disc brake squeal: A review. *Journal of Sound and Vibration*, 267 (1):105–166, 2003.

[35] Fuyuan Liao and Yih-Kuen Jan. A recurrence network approach for the analysis of skin blood flow dynamics in response to loading pressure. *Journal of Biomedical Graphics and Computing*, Vol 2 (1), 2012.

[36] P. Manshour, S. Saberi, Muhammad Sahimi, J. Peinke, Amalio F. Pacheco, and M. Reza Rahimi Tabar. Turbulencelike behavior of seismic time series. *Physical Review Letters*, 102:014101, 2009.

[37] N. Marwan. A historical review of recurrence plots. *European Physical Journal*, 164:3–12, 2008.

[38] N. Marwan, J. F. Donges, Y. Zou, R. V. Donner, and J. Kurths. Complex network approach for recurrence analysis of time series. *Physics Letters A*, 373(46):4246–4254, 2009.

[39] N. Marwan, A. Facchini, M. Thiel, J. P. Zbilut, and H. Kantz. 20 years of recurrence plots: Perspectives for a multi-purpose tool of nonlinear data analysis. *European Physical Journal: Special Topics*, 164:1–2, 2008.

[40] N. Marwan, M. C. Romano, M. Thiel, and J. Kurths. Recurrence plots for the analysis of complex systems. *Physics Reports*, 438:237–329, 2007.

[41] N. Marwan, N. Wessel, U. Meyerfeldt, A. Schirdewan, and J. Kurths. Recurrence-plot-based measures of complexity and their application to heart-rate-variability data. *Physical Review E*, 66:026702, 2002.

[42] F. Massi, L. Baillet, O. Giannini, and A. Sestieri. Brake squeal: Linear and nonlinear numerical approaches. *Mechanical Systems and Signal Processing*, 21:2374–2393, 2007.

[43] F. Moirot and Q. S. Nguyen. Brake squeal: a problem of flutter instability of the steady sliding solution. *Archives of Mechanics*, 52 (4-5):645 – 661, 2000.

[44] M. Müller and G.P. Ostermeyer. Cellular automata method for macroscopic surface and friction dynamics in brake systems. *Tribology International*, 40:942–952, 2007.

[45] S. Oberst and J.C.S. Lai. New approaches for understanding the mechanisms of brake squeal. *Acoustics 2008, Geelong, Australia*, 2008.

[46] S. Oberst and J.C.S. Lai. Chaos in brake squeal noise. *Journal of Sound and Vibration*, 330:955–975, 2011.

[47] S. Oberst and J.C.S. Lai. Statistical analysis of brake squeal noise. *Journal of Sound and Vibration*, 330:2978–2994, 2011.

[48] W. Österle, , H. Kloss, I. Urban, and A. I. Dmitriev. Towards a better understanding of brake friction materials. *Wear*, 263(7-12):1189–1201, 2007.

[49] W. Österle and A.I. Dmitriev. Functionality of conventional brake friction materials - perceptions from findings observed at different length scales. *Wear*, 271:2198, 2011.

[50] W. Österle, C. Prietzel, and A. I. Dmitriev. Investigation of surface film nanostructure and assessment of its impact on friction force stabilization during automotive braking. *International Journal of Materials Research*, 101:669–675, 2010.

[51] W. Österle and I. Urban. Third body formation on brake pads and rotors. *Proceedings of the 22nd SAE Brake Colloquium*, 2004-01-2767:17–23, 2004.

[52] G. P. Ostermeyer and M. Müller. Dynamic interaction of friction and surface topography in brake systems. *Tribology International*, Volume 39 (5):370–380, 2006.

[53] G. P. Ostermeyer and M. Müller. New insights into the tribology of brake systems. *Proceedings of the Institution of Mechanical Engineers, Part D: Journal of Automobile Engineering*, 222:1167–1200, 2008.

[54] G. P. Ostermeyer, M. Müller, H. Abendroth, and B. Wernitz. Surface topography and wear dynamics of brake pads. *Proceedings of the 24th SAE Brake Colloquium and Exhibition*, SAE Paper 2006-01-3202:145–159, 2006.

[55] Huajiang Ouyang, Wayne Nack, Yongbin Yuan, and Frank Chen. Numerical analysis of automotive disc brake squeal: a review. *International Journal of Vehicle Noise and Vibration*, 1, 2005.

[56] Antti Papinniemi, Joseph C.S. Lai, Jiye Zhao, and Lyndon Loader. Brake squeal: a literature review. *Applied Acoustics*, 63:391–400, 2002.

[57] J. Peinke, S. Barth, F. B"ottcher, D. Heinemann, and B. Lange. Turbulence, a challenging problem for wind energy. *Physica A*, 338:187–193, 2004.

[58] Yves Pomeau and Paul Manneville. Intermittent transition to turbulence in dissipative dynamical systems. *Communications in Mathematical Physics*, 74:189–197, 1980.

[59] S.M. Rubinstein, G. Cohen, and J. Fineberg. Detachment fronts and the onset of dynamic friction. *Nature*, 430:1005–1009, 2004.

[60] T. Sauer, J. A. Yorke, and M. Casdagli. Embedology. *Journal of Statistical Physics*, 65(33):579– 616, 1991.

[61] R. Schroth, N. Hoffmann, and R. Swift. Mechanism of brake squeal - from theory to experimentally measured mode coupling. In *XXII IMAC*, 2004.

[62] F. Takens. Detecting strange attractors in turbulence. *Lecture Notes in Mathematics*, 898:366–381, 1981.

[63] M. Thiel, M.C. Romano, and J. Kurths. Spurious structures in recurrence plots induced by embedding. *Nonlinear Dynamics*, 44(1-4):299–305, 2006.

[64] A. Tuchinda, N.P. Hoffmann, D.J.Ewins, and W. Keiper. Mode lock-in characteristics and instability study of the pin-on-disc system. In *XIX IMAC, 2001.*, 2001.

[65] A. Vanossi, N. Manini, M. Urbakh, S. Zapperi, and E. Tosatti. Modeling friction: From nano to meso scales. *ArXiv e-prints - Rev. Mod. Phys. Colloquium*, 2011arXiv1112.3234V:26, December 2012.

[66] U. von Wagner, D. Hochlenert, T. Jearsiripongkul, and P. Hagedorn. Active control of break squeal via smart pads. Oktober 2004. Also published in 'SAE Transactions, J. of Passenger Cars: Mechanical Systems, 1186-1192 (2004)'.

[67] B. A. Wernitz and N. P. Hoffmann. Linear and non-linear time series analysis. In *Proceedings of the 8th World Congress on Computational Mechanics (WCCM8) 2008*, 2008.

[68] B. A. Wernitz and N. P. Hoffmann. New approaches to signal analysis of friction noise and vibration. In *Proceedings of the IMechE International Conference of Braking 2009, York*, 2009.

[69] B. A. Wernitz and N. P. Hoffmann. Non-linear signal analysis of friction induced vibrations. In *Proceedings of the SAE Brake Colloquium 2010*, 2010.

[70] B. A. Wernitz and N. P. Hoffmann. Recurrence analysis and phase space reconstruction of irregular vibration in friction brakes: Signatures of chaos in steady sliding. *Journal of Sound and Vibration*, 331(16), 6, 2012.

[71] B. A. Wernitz and N. P. Hoffmann. Statistical analysis of structural vibrations with respect to brake squeal. In *EuroBrake 2012 conference*, 2012.

[72] S. Yang and R. F. Gibson. Brake vibration and noise: reviews, comments, and proposals. *Int. J. of Materials and Product Technology*, 12:496–513, 1997.

[73] C.M. Yuan and B.F. Feeny. Parametric identification of chaotic systems. *Journal of Vibration and Control*, 4:405, 1998.

[74] J. P. Zbilut and C. L. Webber Jr. Embeddings and delays as derived from quantification of recurrence plots. *Physics Letters A*, 171:199–203, 1992.

Acknowledgements

Firstly, I wish to express my gratitude to Prof. Norbert Hoffmann who has encouraged this study and has inspired me with new ideas and with fruitful discussions and suggestions. Furthermore I would like to thank Harald Abendroth who had stimulated the kick-off of this PhD. And not at least I have received help from students in supporting especially the experimental tasks; my thanks go to Sebastian Gramstat, Martin Gomse and Nikolai Köllisch; especially to Niko for his helpful unusual ideas. And I particularly would like to thank Philippa Bennett for her language support services. Finally, I sincerely thank Prof. Michael Hanss for acting as second assessor.

This work has been supported comprehensively by Honeywell Friction Materials GmbH, Glinde, near Hamburg.

Irregular friction brake vibration data have been collected with sampling rates above 200 kHz. Recurrence analyses of the measured time series indicated that irregular vibration states of friction brakes in non-squealing condition are strongly dominated by intermittency phenomena.

Hereby, space reconstructions suggest that this intermittency is predominantly controlled by low-dimensional irregular chaotic dynamics than by high-dimensional stochastic processes. Correlations between the brake squeal propensity and measures of recurrence quantification analysis and probability density distribution of acceleration increments have been revealed.

urn:nbn:de:gbv:830-tubdok-12462
TUBdok der Universitätsbibliothek
der TU Hamburg-Harburg